NTNU – Trondheim
Norwegian University of
Science and Technology

The effect of cuttings on annular pressure loss

An analysis of field data in the North Sea

Håvard Tarjei Kummen
Andreas Anderssønn Wold

Petroleum Geoscience and Engineering
Submission date: June 2015
Supervisor: Sigve Hovda, IPT
Co-supervisor: Pål Skalle, IPT

Norwegian University of Science and Technology
Department of Petroleum Engineering and Applied Geophysics

Preface

This thesis is written as part of the MSc programme in Petroleum Technology, at the Department of Petroleum Engineering and Applied Geophysics at the Norwegian University of Science and Technology (NTNU) in Trondheim, Norway.

We would like to thank our supervisors, associate professor Sigve Hovda and associate professor Pål Skalle, for their guidance and support throughout the work with this thesis. Their theoretical and technical knowledge within drilling and data analysis has been essential to the outcome of our work. Their enthusiasm has been inspiring and encouraging.

Finally, we would like to thank each other for the collaboration and great fun during the final semester.

Håvard Tarjei Kummen and Andreas Anderssønn Wold

Trondheim, June 2015

Abstract

This master's thesis studies the correlation between rapid alterations in cuttings concentration and the corresponding change in pressure loss, using the standpipe pressure as pressure indicator. Drilling data from two wells in the North Sea is used when analysing the pressure effect from cuttings concentration. Intervals where there is a change in rate of penetration and standpipe pressure simultaneously, while all other relevant parameters are kept constant, are identified. Difference in standpipe pressure and rate of penetration is represented graphically in order to identify trends between the two parameters.

A correlation between change in rate of penetration and the response in standpipe pressure was found for all sections. Calculations indicate that the change in pressure loss cannot solely be explained by cuttings bedding, viscosity and density changes or weight of suspended cuttings in the wellbore. Some other effect is therefore likely to be present.

Empirical equations from curve fitting were obtained for each section, describing the relation between change in standpipe pressure and change in rate of penetration. The number of cases evaluated is, however, not sufficient for the empirical equations to accurately predict changes in standpipe pressure beyond the evaluated sections. A correlation between the slope of the fitted curves and the properties of each section was not identified.

Sammendrag

Denne masteroppgaven undersøker sammenhengen mellom endringer i kakskonsentrasjon og korresponderende endringer i standpipe-trykket. Sanntidsdata fra to brønner i Nordsjøen er brukt for å analysere effekten av endringer i kakskonsentrasjonen. Dette er gjennomført ved å se på endringer i boreraten og standpipe-trykket, uten forstyrrelse fra andre påvirkende parametere. Endringer i borerate og standpipe-trykk er fremstilt grafisk, i den hensikt å avdekke eventuelle trender.

For alle de analyserte seksjonene ble det funnet en korrelasjon mellom endringer i borerate og trykkrespons. De observerte trykkendringene kan, i følge våre beregninger, ikke alene skyldes økt viskositet og densitet som følge av endret kakskonsentrasjon. Et annet, ukjent kaksrelatert forhold synes derfor å være til stede.

Empiriske likninger for hver seksjon ble generert ved hjelp av kurvetilpasning av datapunktene. Grunnet antallet datapunkter funnet gjennom analyse av boredataene, kan ikke disse likningene nøyaktig beregne endringer i standpipe-trykk utover de analyserte seksjonene. Det ble ikke funnet en klar korrelasjon mellom stigningstallet i de empiriske ligningene og brønnparametre fra hver seksjon.

Contents

List of Figures

List of Tables

1 Introduction

Oil and gas wells are becoming more complex with tighter mud windows, requiring more accurate methods for controlling the pressure in the well. An important part of well control is understanding how changes in drilling parameters affect the pressure profile downhole. One of the factors that affect the bottom hole pressure (BHP) is the transport of cuttings from the drill bit to surface. Transportation and accumulation of cuttings yields an additional pressure loss in the well. Being able to estimate the pressure loss due to cuttings is important whenever downhole pressure measurement during drilling is not installed. If the rate of penetration (ROP) is too high, cuttings may accumulate in the annulus causing pressure to build up. Losses to the formation as a result of fracturing must be avoided, while still maintaining an optimized ROP. To achieve such control, the pressure effect from cuttings can be estimated in order to predict changes in pressure during drilling.

Other studies [Cayeux et al., 2013] have taken a modelling approach where pressure changes related to cuttings transport and operational parameters are calculated from heavy theoretical and data-intensive models. This thesis takes a more practical approach in order to estimate rapid pressure effects caused by cuttings generation and transport. A baseline in standpipe pressure (SPP) is identified where critical parameters have been stable over a certain period of time. By investigating the deviation in SPP from the baseline caused by a change in ROP, the effect of stable parameters become less important, as they are already accounted for in the baseline. Such parameters may include fluid rheology, wellbore geometry, BHA setup, formation properties, cuttings size and flow patterns. A major challenge of our approach is interpretation of the drilling parameters.

In this thesis, drilling data from two wells in the North Sea was analysed. In order to distinguish a pressure change as a result of change in cuttings concentration, a thorough understanding of what affects the SPP is needed. Only when other effects from change in drilling parameters are understood, the effect of cuttings in SPP can be distinguished. Theory describing effects from parameters such as flow rate, rotation, surge and swab, cuttings and fluid properties is presented.

In order to identify a relationship between cuttings concentration and standpipe pressure,

cases where a pressure effect is assumed caused by cuttings, were manually selected. The change in SPP was plotted against a corresponding change in ROP for each case, and grouped by section. Curve fit on the form $\Delta\text{SPP} = a\Delta\text{ROP}$ was performed for each section. A strong correlation between change in SPP and change in ROP was observed within each section. The results from curve fitting were attempted replicated by using theoretical models, but without success, yielding too low simulated pressure losses. Possible explanations to this are suggested and discussed by the authors.

2 Friction pressure loss in the circulating system, "baseline" of SPP

The "baseline" of the standpipe pressure, SPP, is defined as the pressure during the interval where SPP and all affecting parameters are stable. In order to analyse pressure changes from this baseline, it is necessary to understand the different contributions to the total friction loss under normal conditions.

SPP is the sum of all pressure losses along the path of the mud. As the drilling fluid is pumped through the circulating system, friction pressure loss occurs as a result of change in kinetic energy and shear forces between the fluid, drill string and borehole walls. The SPP is measured in the standpipe at surface. **Figure 1** illustrates the flow path of the mud and the sections and components where major pressure losses occur. In this section, a brief introduction to these components and sections will be presented along with basic equations needed to calculate the pressure losses under stationary conditions.

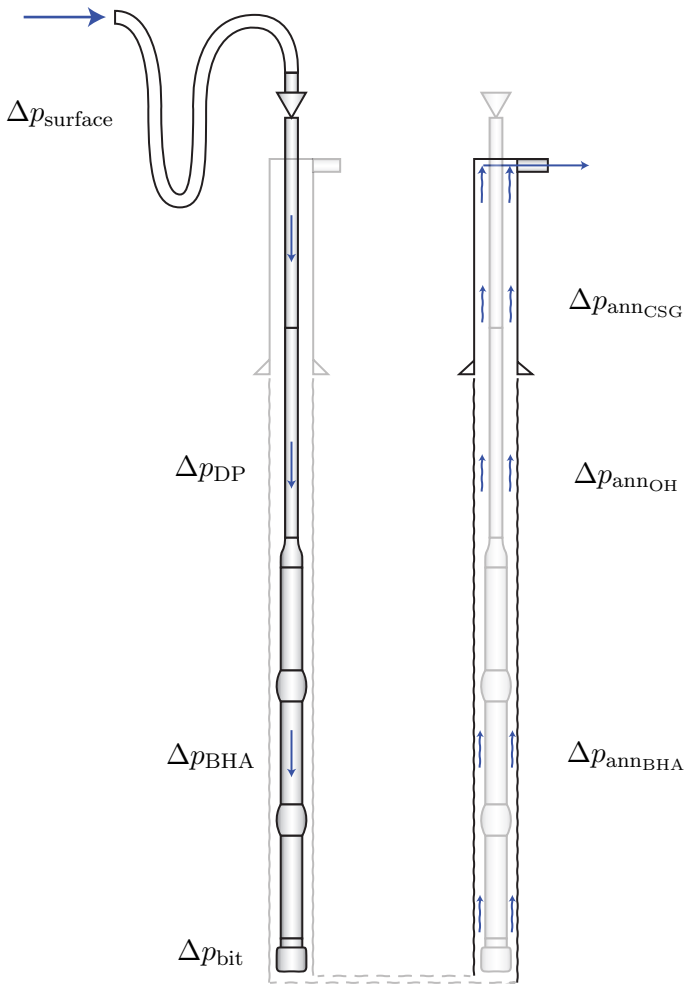

Figure 1: Fluid flow path through the goose neck, top drive, drill string and the annulus. Blue arrows indicate fluid flow. Δp_{DP}, Δp_{BHA} and Δp_{bit} represent the pressure loss through drillpipe, BHA and the drill bit respectively. $\Delta p_{\text{ann}_{\text{BHA}}}$, $\Delta p_{\text{ann}_{\text{OH}}}$ and $\Delta p_{\text{ann}_{\text{CSG}}}$ represent the annular pressure loss over BHA, and over drill string in open and cased hole respectively. $\Delta p_{\text{surface}}$ represents the pressure loss through surface pipes, goose neck and topdrive.

2.1 Fluid rheology

Drilling fluids are designed to have several functions during circulation, such as cooling, lubrication and transport of cuttings. Drilling fluids can be a complex mix of different components in order to obtain the desired properties and qualities needed for a specific operation. The behaviour of fluids during flow can be described by different flow models such as Newtonian, Bingham Plastic, Power Law and Herschel-Bulkley. The equations describing the relation between shear stress and shear rate for each model are given by equations 1, 2, 3 and 4 below.

Newtonian model: τ is the shear stress, μ the fluid viscosity, and $\dot{\gamma}$ the shear rate:

$$\tau = \mu\dot{\gamma}, \tag{1}$$

Bingham plastic model: τ_y is the yield point which defines the minimum shear stress needed to enable flow, while μ_{pl} is the plastic viscosity.

$$\tau = \tau_y + \mu_{pl}\dot{\gamma}, \tag{2}$$

Power law model: K is the consistency index and n is the flow behaviour index ($n < 1$ for drilling fluids).

$$\tau = K\dot{\gamma}^n, \tag{3}$$

A Herschel-Bulkley fluid, also referred to as a yield power law fluid (YPL), has a yield point below which the fluid will not flow. This yield point, or shear stress is theoretically equal to the yield point in the Bingham Plastic model, but has a different calculated value [Hemphill et al., 1993]. Model parameters n and K can be derived from the plastic viscosity (PL), yield point (YP), and yield stress (τ_y).

$$\tau = \tau_y + K\dot{\gamma}^n \tag{4}$$

These four flow models are displayed graphically in **figure 2**, curve fitted for fluid rheology data provided in the data set.

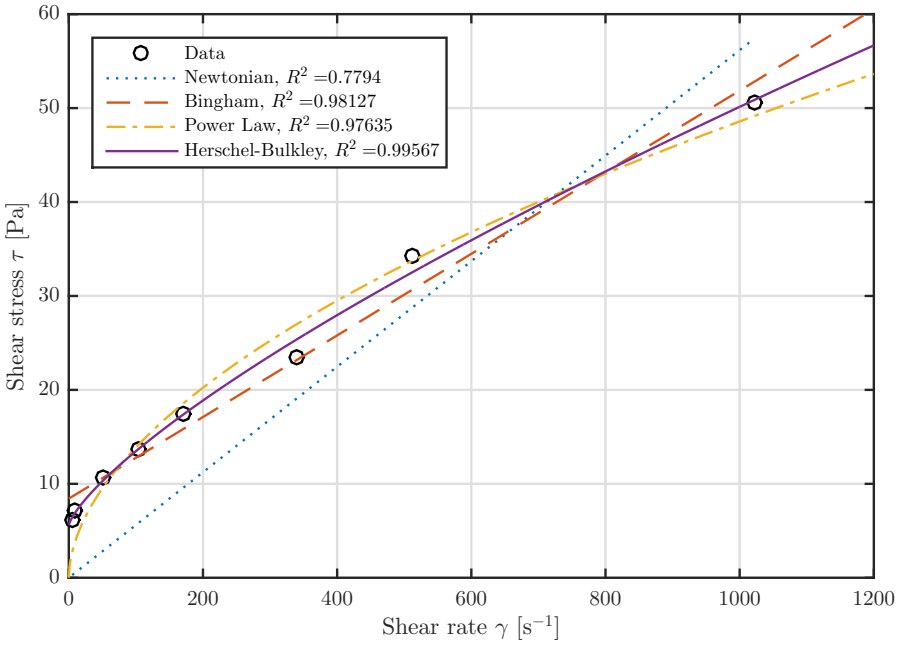

Figure 2: Shear stress τ vs. shear rate $\dot{\gamma}$ for rheology models Newtonian, Bingham Plastic, Power law and Herschel-Bulkley (Yield Power law). Rheology measurements are taken from one of the sections in the data set used for analysis.

Drilling fluids are usually non-Newtonian fluids with shear-thinning properties. This causes the viscosity of the drilling fluid to decrease as the shear forces acting on the fluid are increasing. Herschel-Bulkley is usually chosen as the most applicable model to most drilling fluid, since it is based on both Power Law and Bingham Plastic fluid behaviour. However, Chowdhury et al. [2009] found examples of the Bingham plastic model matching measured drilling data better than the other three models.

Viscosity at a specific shear rate, $\dot{\gamma}$, is defined as the derivative of the shear stress with respect to shear rate, as shown in equation 5 below.

$$\mu(\dot{\gamma}) = \frac{\partial \tau}{\partial \dot{\gamma}} \tag{5}$$

The pressure drop from friction when a fluid flows through a pipe or annulus depends on the flow regime. In a laminar flow regime, the friction loss is caused by shear forces between the fluid and pipe wall. At a specific velocity, the flow regime turns transient, which means that both shear forces and kinematic forces in the fluid system contributes

to the friction pressure loss. At even higher flow velocities, the flow regime becomes turbulent, meaning that most of the friction loss is due to kinematic forces in the fluid, as the complex flow pattern in this regime causes the fluid to change direction constantly during flow.

Whether the flow regime is laminar, transitional or turbulent is defined by the general Reynolds number, given in equation 6. ρ is fluid density, v is fluid velocity, d is diameter, and μ is fluid viscosity. Since the different rheology models describe fluid behaviour differently, the limits between the flow regimes will also differ between the models. The flow regime during drilling is difficult to determine, as parameters, such as string rotation, pipe vibration, pipe eccentricity, tool joints come into play. Traditionally, laminar flow is defined as a flow with Reynold's number below 2000, and turbulent flow above 4000. However, turbulence may occur at lower Reynold's numbers, due to the complexity of the flow during drilling.

$$Re = \frac{\rho v d}{\mu} \tag{6}$$

2.2 Pressure loss through the drill pipe

As drilling fluid is pumped down the drill string, a friction pressure loss occurs due to the shear forces between the fluid and the pipe wall and kinematic forces in the fluid. The friction pressure loss over a pipe segment with length L and inner diameter d_i can be calculated by using the Darcy-Weisbach equation

$$\Delta p_f = \frac{f}{2}\frac{L}{d}\rho v^2, \tag{7}$$

where ρ is the fluid density and v is the fluid velocity. The friction factor f can be calculated by using the Haaland equation:

$$\frac{1}{\sqrt{f}} = -1.8\log_{10}\left[\left(\frac{\epsilon/d}{3.7}\right)^{1.11} + \frac{6.9}{\mathrm{Re}}\right] \tag{8}$$

ϵ is the absolute roughness of the pipe wall, and Re is the Reynolds. d is the inner diameter for flow in pipe, or hydraulic diameter for flow through annulus. The relative roughness ϵ_{rel} equals the absolute roughness divided by the diameter of the pipe.

$$\epsilon_{\text{rel}} = \frac{\epsilon}{d} \tag{9}$$

The inside of the drill string can be considered as relatively smooth and geometrically consistent from surface to BHA. There is little variation of the steel surface roughness inside of the pipe, compared to the outside of the drill pipe, where tool joints and the borehole walls have a rougher surface.

2.3 Pressure loss through BHA and bit

Pressure loss through the BHA

The pressure drop caused by flow resistance through the bottom hole assembly (BHA) must be calculated separately, as the inner diameter of each BHA component varies. In addition, turbines and steering systems are driven by the mud flow, causing additional pressure losses. An example of such losses can be the loss over the rotary steerable system (RSS). RSS can be driven by a mud flow being diverted as it enters the steering tool. This causes an additional pressure loss, and will contribute to an increase in SPP. The pressure loss over such a tool is given as

$$\Delta p_{\text{RSS}} = \frac{\rho_m q_m^2}{C_{\text{RSS}}}, \tag{10}$$

where ρ_m is the mud weight, q_m is the flow rate, and C_{RSS} is a constant specified by the producer [Schlumberger, 2010].

Positive displacement motor

A positive displacement motor (PDM), often referred to as a downhole mud motor, is a mechanism used for rotating the bit without rotating the drill string. By letting a part of the mud flow pass through a chamber with an eccentric rotor shaft, rotation is generated. Approximately 2-15% of the mud flow is used to rotate the bit. The motor causes a pressure loss, which depends on the flow rate and the force needed to rotate the bit. The pressure loss is a function of torque, which is weight on bit (WOB) dependent. A general equation for the pressure loss over the PDM is proposed in equation 11.

$$\Delta p_{\text{PDM}} = \Delta p_{\text{NL}} + (\Delta p_{\text{max}} - \Delta p_{\text{NL}}) \frac{\text{WOB}}{\text{WOB}_{\text{max}}} C_{\text{TF}}, \tag{11}$$

Δp_{NL} is the pressure loss with zero WOB, Δp_{max} is the pressure loss at maximum recommended WOB, and C_{TF} is a tool factor. These parameters are specified by the producer [Skalle, 2013].

Pressure loss over bit

As the drilling fluid passes through the nozzle pipes and nozzles in the bit, the flow velocity increases. This leads to a change in kinematic energy as well as a friction pressure loss through the nozzle pipes. To evaluate the pressure loss over the bit, the Bernoulli equation can be used (13). Subscript $_1$ and $_2$ signify a point before and inside the nozzles respectively.

$$p_1 + \rho g z_1 + \frac{1}{2}\rho \bar{v}_1^2 = p_2 + \rho g z_2 + \frac{1}{2}\rho \bar{v}_2^2 + \Delta p_{\text{loss}} \tag{12}$$

p is the pressure at the chosen point, ρ is the fluid density, g is the gravity of Earth, z is the vertical height, and $\bar{v}$ is the average fluid velocity. Δp_{loss} is the friction loss through the nozzle pipes. The hydrostatic pressure difference over the bit is negligible due to the small difference between z_1 and z_2. Rearranging equation 12 in order to find the difference in pressure over the bit gives

$$\Delta p_{\text{bit}} = p_1 - p_2 = \frac{1}{2}\rho \bar{v}_2^2 - \frac{1}{2}\rho \bar{v}_1^2 + \Delta p_{\text{loss}} \tag{13}$$

The velocity through the nozzles is assumed to be much higher than the velocity before the nozzle pipes. The loss through the nozzle pipes, Δp_{loss}, as well as entrance and end effects are compensated for by a nozzle loss coefficient, K_{bit}, typically given in the literature with a value of 1.11 [Skalle, 2013]. Using these simplifications, equation 13 reduces to

$$\Delta p_{\text{bit}} = K_{\text{bit}} \frac{1}{2} \rho \bar{v}^2_{\text{nozzle}}, \tag{14}$$

where $\bar{v}_{\text{nozzle}}$ is the average velocity of the fluid through the nozzles expressed as

$$\bar{v}_{\text{nozzle}} = \frac{q_m}{N \frac{\pi}{4} d^2_{\text{nozzle}}}, \tag{15}$$

where N is the number of nozzles in the bit and d_{nozzle} is the inside diameter of the nozzle. Additional pressure loss may occur if clay is blocking the nozzles of the bit while drilling. This is referred to as "bit balling".

2.4 Pressure loss through annulus

Similar to fluid flow through a pipe, there is a friction pressure loss as fluid is circulated through annulus. During annular flow, shear forces will act between the fluid and the outside of the pipe and borehole wall. A hydraulic diameter, d_{hyd}, must be used when calculating friction pressure loss. The hydraulic diameter is given as

$$d_{\text{hyd}} = \frac{4\, A_{\text{ann}}}{S_{\text{ann}}}, \tag{16}$$

where A_{ann} is the cross sectional area of the annulus and S_{ann} is the wetted perimeter of the annulus. By setting in for the cross sectional area and the wetted perimeter of the annulus and expanding the expression for A_{ann}, the equation for d_{hyd} reduces to

$$d_{\text{hyd}} = 4 \frac{\frac{\pi}{4}(d_o^2 - d_i^2)}{\pi(d_o + d_i)} = 4 \frac{\frac{\pi}{4}(d_o + d_i)(d_o - d_i)}{\pi(d_o + d_i)} = d_o - d_i, \tag{17}$$

where d_o and d_i are the outer and inner diameter of the annulus respectively. In a drilling situation, this will typically correspond to the diameter of the borehole and outer diameter of the drill pipe or BHA.

A relative roughness of 0.05 is usually used as an estimate in the open hole part of the well, but the smoothness of the borehole wall depends on the formation [Woods et al., 1966]. Above the open hole section, the relative roughness will be defined by the roughness of the casing and drill pipe.

2.5 Correlation between SPP and ECD

In drilling operations, increases in well pressure as a result of friction pressure loss must be considered and planned for in order to prevent fracturing and losses to the formation. As previously mentioned, SPP represents the total pressure loss through the circulation system. The friction pressure loss through the drill string, BHA and bit does not affect the bottom hole pressure (BHP), as they occur before the drilling fluid enters the annulus. They are therefore irrelevant to the pressure profile exposed to the formation. The pressure loss through the annulus, on the other hand, causes an increase in BHP.

Equivalent circulating density

In order to obtain a unit of measure on the total pressure acting on the bottom of the wellbore, the equivalent circulating density (ECD) is used. ECD is the sum of the static mud density and the annular friction loss, back pressure, pipe movement and other sources of pressure contribution, converted to an equivalent density contribution, as expressed in equation 18.

$$\text{ECD} = \rho_m + \frac{\sum_i \Delta p_i}{gz} \tag{18}$$

$\sum_i \Delta p_i$ is the sum of the annular pressure losses caused by friction, cuttings transportation, rotation, acceleration, surge and swab, denoted as Δp_f, Δp_c, Δp_{rot}, Δp_{acc} and $\Delta p_{s\&s}$ respectively. These pressure losses are further described in chapter 3.

ECD is an important parameter when controlling the pressure profile in the annulus. It can, however, not be measured directly from surface, and downhole pressure gauges must be included in the BHA in order to obtain correct measurements. This adds complexity and costs to the drilling operation, but offers true measurements of the annular pressure drop and therefore the true ECD. ECD is a better indicator of the bottom hole pressure during drilling than SPP. However, in this thesis, pressure losses are analysed using SPP due to inaccurate estimations of the annular pressure losses.

In cases where a pressure gauge is not installed in the BHA, estimations of pressure losses must be made when downhole conditions or drilling parameters are changed. Knowing how such parameters affect the annular pressure loss is crucial in drilling operations.

3 Important parameters affecting the baseline of SPP, theoretical evaluation

Several parameters affect the pressure loss through the annulus. The effect of cuttings in SPP can first be distinguished when the other effects from change in drilling parameters are understood. In this section, parameters that have a large impact on SPP are evaluated.

3.1 Flow rate

As seen in the previous section, the pressure loss through the drill string, bit, RSS and annulus are proportional to the flow rate squared, q_m^2. Alterations in the flow rate has a large impact on SPP and ECD. When the flow rate is altered, the change in pressure will occur immediately. It is reasonable to assume that intervals with constant flow rate will be unaffected by any previous alterations in flow rate. However, a short delay in SPP can be observed when changing the flow rate. This can be explained by the compressibility of the mud and bore hole, where the length of this delay depends on the length of the well. A measuring error in the flow rate may also be the cause of this delay.

3.2 String rotation

When the drill string is rotated, the annular flow patterns will differ from those when there is no rotation. Rotation yields a tangential velocity in addition to the axial velocity from circulation. Because of the shear forces between the pipe and drilling fluid, a helical flow pattern may form in the annulus as a result of the tangential and axial velocity as illustrated in the left part of **figure 3**. The altered velocity from rotation can affect the friction pressure loss in different ways.

Laboratory studies on the effect of pipe rotation on friction pressure loss show that rotation can cause a decrease in friction pressure [Ahmed and Miska, 2008]. Drilling fluids are usually non-Newtonian fluids with shear-thinning properties. Rotation of the drill string causes the viscosity of the drilling fluid to decrease, as the shear rate is increased.

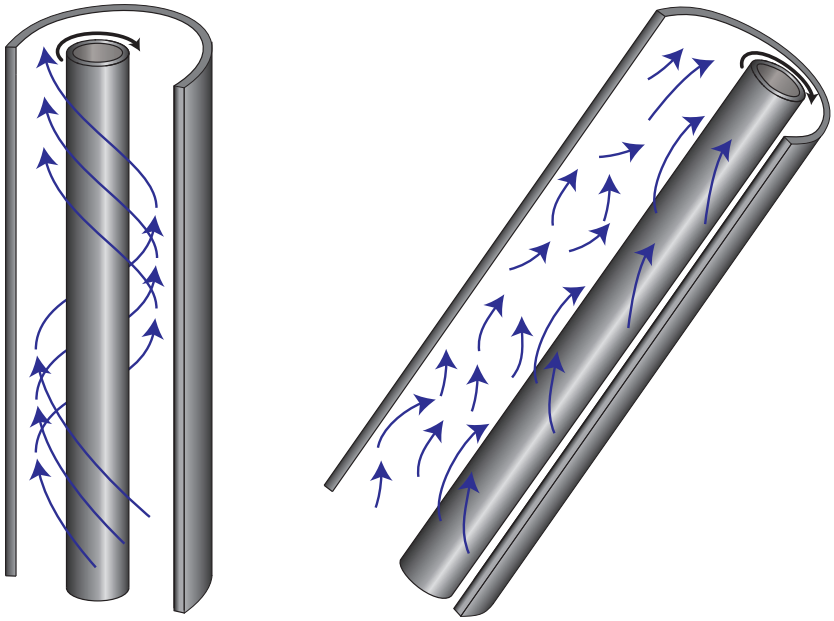

Figure 3: Left: Helical flow patterns generated by annular flow and rotation of the drill string in a concentric annulus. **Right:** Eccentric annulus where the drill string is located of centre in the annular cross section. This contributes to changing the direction and acceleration of the annular flow, causing turbulence and reducing the shear thinning effect.

The apparent viscosity μ for a Herschel-Bulkley fluid can be derived from equation 4, yielding

$$\mu = \frac{\tau_0}{\dot{\gamma}} + K\dot{\gamma}^{n-1}. \tag{19}$$

As seen from equation 19, viscosity μ decreases with an increasing shear rate $\dot{\gamma}$. The shear rate, $\dot{\gamma}$, which is the case during rotation [Ahmed and Miska, 2008]. A decreasing viscosity yields a higher Reynolds number, resulting in a lower friction factor and friction pressure loss. Following this, a higher rotation yields a lower annular pressure loss. However, in this case it is assumed that the annulus is concentric, giving a helical flow pattern in the annulus.

The assumption of a concentric annulus is often not realistic. The drill string is elastic and has the possibility to wobble in the hole. It can be positioned differently in the wellbore cross section at different depths, depending on inclination and hook load. Because of eccentricity, wobbling and geometrical irregularities in the well, turbulence can occur, as illustrated in figure 3 (right). This contributes to an increase in annular pressure loss, as seen in most field cases, where the effect of the eccentricity dominates the shear-thinning effect [Ahmed and Miska, 2008].

3.3 Surge and swab

When running the drill string into the borehole, mud is displaced by the drill string. The displaced mud causes a change in annular flow velocity around the pipe, leading to an increased friction pressure loss. This additional contribution to the BHP is referred to as surge pressure. If the pipe is pulled out of the hole, the drilling fluid will flow to replace the volume of drill pipe removed from the hole. This will cause a decrease in annular velocity, and therefore a decrease in friction pressure loss. The following reduction in SPP caused by this, is referred to as swab. Annular flow caused by pipe movement is illustrated in **figure 4**. When calculating pressure changes from either surge or swab, it is necessary to make simplifying assumptions.

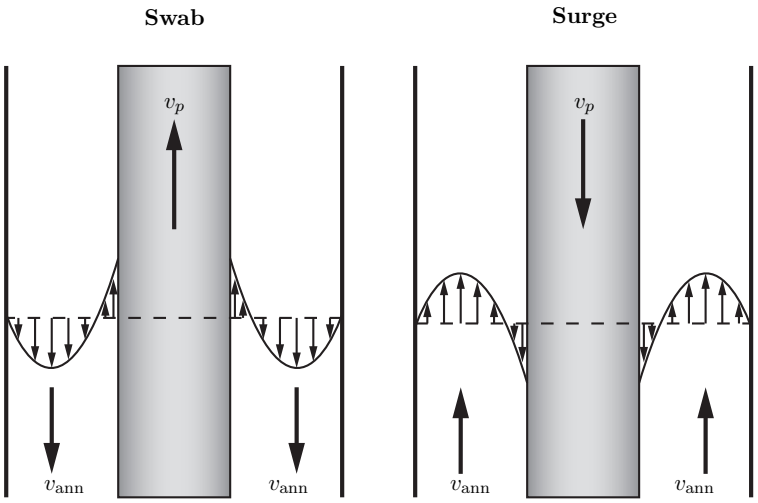

Figure 4: Annular flow caused by pulling and running the pipe.

When performing calculations on surge and swab pressures, the drill string is usually assumed to be close-ended at the bottom. By assuming this, the added volume either occupied during surge or removed during swab, can be calculated. Equation 20 shows the total flow rate as a function of pipe movement, pump rate and hole size.

$$q_{tot}^{\text{ann}} = q_m + \dot{V} = q_m + v_p A_p + q_{\text{cling}} \tag{20}$$

q_m is the pump rate of the drilling fluid, $\dot{V}$ is the volume rate being removed or displaced by the drill string during swab or surge respectively. v_p is the tripping velocity, i.e. the velocity of the drill string when being run in or out of the hole. Running the pipe into the pipe is defined as the positive direction, giving an increased fluid flow rate when tripping in, and a decreased flow when tripping out. q_{cling} accounts for the mud that clings to the string when pulling or running the pipe. A_p is the cross sectional area of the closed drill pipe.

By dividing the total flow rate by the annular cross section, the annular velocity caused by circulation and drill string movement can be expressed:

$$v_{tot}^{\text{ann}} = \frac{q_{tot}^{\text{ann}}}{A_{\text{ann}}} = \frac{q_m + v_p \frac{\pi}{4} {d_p}^2 + q_{\text{cling}}}{\frac{\pi}{4}(d_o^2 - d_p^2)} \tag{21}$$

d_o is the diameter of the borehole or casing and d_p is the outer diameter of the drill pipe.

Steady state flow conditions are usually assumed, meaning no alterations in flow rate while the section is being evaluated. In order for the flow pattern to remain constant over the evaluated section, the annular geometry is assumed to be concentric, although this is usually not the case in a realistic situation. Experimental results show that the pressure change caused by surge and swab can be reduced by up to 40 % due to eccentricity [Crespo et al., 2012].

Pressure changes due to surge and swab is experienced during pulling or running of pipe in hole, such as during trip out or in. This thesis focuses on pressure changes related to drilling and reaming. The highest pipe velocity relevant to analysed intervals in this thesis, will be experienced during reaming. The pressure changes caused by this must be taken into consideration when identifying key contributions to SPP. The pressure change experienced during surge and swab is given by equation 22 [Crespo et al., 2012].

$$\Delta p_{\text{s\&s}} = \frac{f}{2} \frac{\rho(v_{\text{ann}} + \frac{v_p}{2})^2}{g(d_o - d_p)} L \tag{22}$$

f is the fanning friction factor, v_{ann} is the annular velosity from the mud pumps, d_o is the diameter of the bore hole and L is the measured depth from surface to bit. The friction factor can be calculated by using the Haaland equation given in equation 8.

3.4 Cuttings effects

In the following subsections, theory regarding the influence of cuttings on SPP will be presented in order to evaluate what theoretically can result in a change in SPP. Example calculations will be provided along with theory.

Cuttings generally have a higher mass density than most drilling fluids. When heavy cuttings are suspended in the mud and transported by the drilling fluid, additional energy

is used. Increased cuttings concentration contributes to an increased fluid density and viscosity, and acts out as a pressure loss that must be overcome by the mud pumps. Cuttings tend to be transported with a lower velocity than the mud, which leads to cuttings accumulation and cuttings bedding, which increases the pressure loss further. In some cases, the well can pack off completely, causing stuck pipe or no circulation.

In this thesis we divide the annulus into two main sections: A vertical section, where the inclination of the borehole is below 45° from the vertical line, and an inclined section, where the borehole inclination is above 45°. By doing so, simplifications can be made regarding hole cleaning and cuttings transport. This is illustrated in an example wellpath in **figure 5**. Cuttings beds are generally formed in boreholes with inclination above 30°. However, in sections between 30° and 45°, beds may not be continuous or stable, and tend to slide downwards when pumps are shut off, causing cuttings avalanches. Cuttings in this interval are easily stirred into suspension by rotation of the pipe. For simplicity, no cuttings beds are therefore assumed to form in the vertical section, *i.e.* at inclinations below 45°.

The first two of the following subsections will look at the pressure increase due to increased mud density. Theory regarding viscosity increase due to cuttings will be presented in the third subsection. The fourth subsection will look at the additional pressure effect of bedded cuttings in the inclined section.

3.4.1 Cuttings concentration in the inclined section

When drilling new formation, the concentration at the bit can be expressed as the volume ratio of the cuttings influx, q_c, and the total influx of cuttings and mud, $q_c + q_m$:

$$c_{\text{bit}} = \frac{q_c}{q_c + q_m} \tag{23}$$

Typical values for cuttings concentration observed in the analysed data sets are $c_{\text{bit}} = 0.5-1\%$ in the 12 ¼" and 8 ½" sections, and as high as 2% in the 17 ½" section. The mass density of the cuttings and mud mixture, as a function of the cuttings concentration, is given by equation 24. c is the cuttings concentration, ρ_m and ρ_c are the mud and

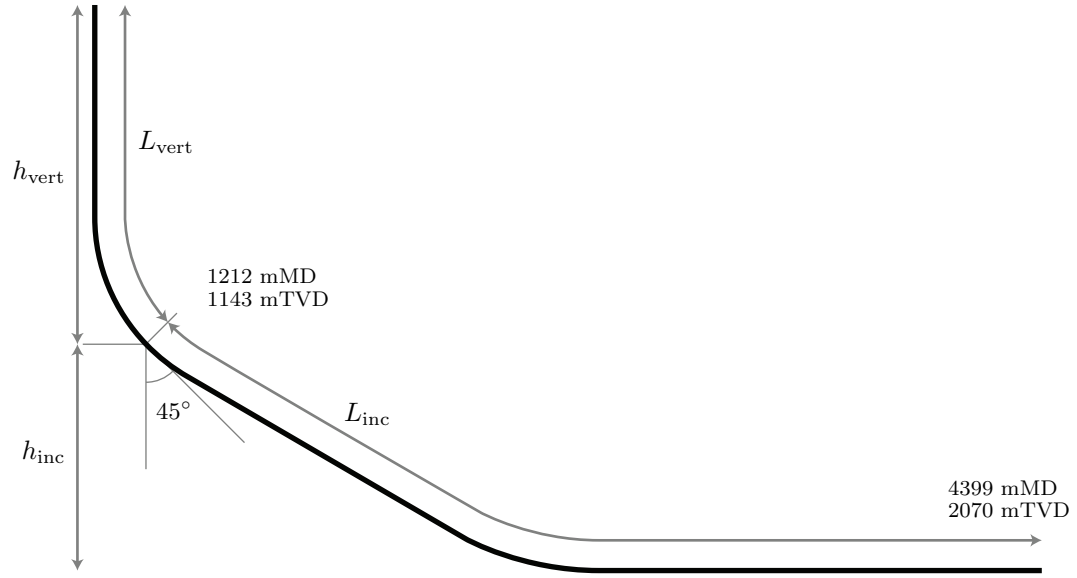

Figure 5: Example wellpath with a vertical section with inclination below 45° and an inclined section with inclination above 45°. h_{vert} and h_{inc} represent vertical height of the vertical and horizontal section respectively. L_{vert} and L_{inc} represent axial length along the wellbore in the vertical and horizontal section.

cuttings density, respectively.

$$\rho(c) = \rho_m + c(\rho_c - \rho_m) \tag{24}$$

As the fluid density increases, both the hydraulic friction pressure loss and the hydrostatic pressure increase. The friction factor f, as a function of the Reynold's number Re (6), is affected by fluid density. By calculating the ratio between pressure loss with and without suspended cuttings, the cuttings effect on pressure can be investigated. Equations 25 and 26 represent relative hydrostatic and friction pressure loss p^*_{hyd} and Δp^*_f, respectively. The friction factor f is given in equation 8. Superscript * indicates relative pressure, while superscript ^{0} indicates a reference value without suspended cuttings.

$$p^*_{\text{hyd}} = \frac{p_{\text{hyd}}(c)}{p^0_{\text{hyd}}} = \frac{\rho(c)gh_{\text{inc}}}{\rho^0 gh_{\text{inc}}} = \frac{\rho_m + c(\rho_c - \rho_m)}{\rho_m} \tag{25}$$

$$\Delta p^*_f = \frac{\Delta p_f(c)}{\Delta p^0_f} = \frac{\frac{f(c)}{2}\frac{L}{d_{\text{hyd}}}\rho(c)v^2}{\frac{f^0}{2}\frac{L}{d_{\text{hyd}}}\rho^0 v^2} = \frac{f(c)\rho(c)}{f^0\rho^0} = \frac{f(c)}{f^0}\frac{\rho_m + c(\rho_c - \rho_m)}{\rho_m} \tag{26}$$

A pump rate $q_m = 2100$ lpm and ROP = 30 m/h in the 8 ½" section gives a cuttings concentration $c_{\text{bit}} = 0.86\%$. With $\rho_m = 1700$ kg/m^3 and $\rho_c = 2200$ kg/m^3, equations 25 and 26 both yield 1.0025. The change in hydrostatic and friction pressure loss are equal, which indicates that friction factor f is little affected at this cuttings concentration.

In a 17 ½" hole with pump rate $q_m = 5000$ lpm, ROP = 30 m/h and $c_{\text{bit}} = 1.5\%$, the equations yield 1.0045 and 1.0043. Pressure increases of this magnitude could theoretically be seen in SPP. However, the effect takes place gradually as the fluid with different cuttings concentration is displaced. With the above mentioned parameter values for the 8 ½" section, and the wellbore geometry in figure 5, the cuttings front travels with a velocity of 90 m/min around a drill pipe with diameter 5". With this velocity, it takes approximately 30 minutes before the front reaches the vertical section after drilling is commenced.

Because the fluid velocity is lower closer to the walls due to friction, the cuttings will be transported faster in the centre of the flow area, dispersing the cuttings front. This phenomenon is referred to as axial dispersion, and is illustrated in **figure 6**. After an ROP change, the cuttings concentration at a stationary point along the wellbore will start to increase when the cuttings front arrives, and will continue to increase until the "tail", *i.e.* the cuttings travelling along the wall, arrives.

The fluid velocity profile as a function of radius r in figure 6 is given as $v(r) = v_{\text{wall}} + (v_{\max} - v_{\text{wall}})(1 - \frac{r^2}{R^2})$, with average velocity $\bar{v} = 1.5$ m/s, $v_{\text{wall}} = \frac{1}{2}\bar{v}$ and $v_{\max} = \frac{3}{2}\bar{v}$. R is the outer radius. Turbulence due to rotation, vibration, and wall roughness is assumed, hence wall velocity $v_{\text{wall}} \neq 0$. Although the model in figure 6 is a simplification, axial dispersion will contribute to elongate a potential pressure effect.

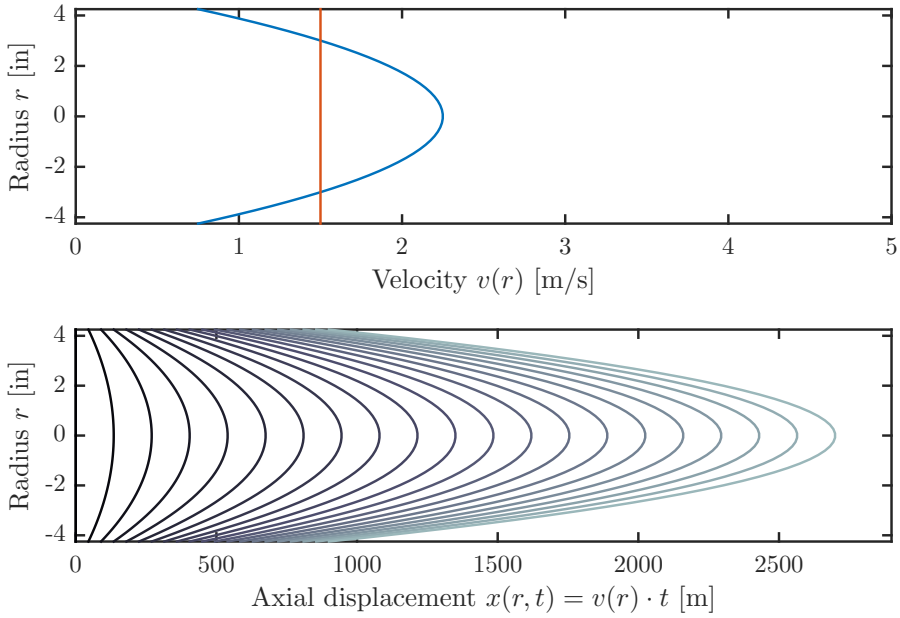

Figure 6: The upper plot shows an example of fluid velocity as a function of the radius. The orange vertical line is the average volumetric velocity. The lower plot shows the position of the cuttings front as a function of the radius for a time t, from 0 to 20 minutes.

3.4.2 Cuttings concentration in the vertical section

When cuttings are transported through the vertical section of a well, the lifting force has to act against the gravitational force acting on the cuttings particles. If the cuttings particles are large and heavy in comparison to the drilling mud, and the mud has a low viscosity, the gravitational force may exceed the friction forces, and the particles will sink in the mud with a slip velocity v_{slip}. The slip velocity of a perfect sphere can be expressed as

$$v_{\text{slip}} = \frac{d_c^2 g\,(\rho_c - \rho_m)}{6\pi\mu_{\text{eff}}} f_c(c), \tag{27}$$

where d_c is the diameter of the cuttings particle, g is the gravity of Earth. ρ_c and ρ_m are the mass density of cuttings and mud respectively, and μ_{eff} is the effective viscosity. $f_c(c)$ is a flow resisting-factor and is a function of cuttings concentration, taking particle interaction into account, reducing the slip velocity of the particles. $f_c(c)$ can be given

as $f_c(c) = 1 - 5.1c$ [Skalle, 2013].

Based on the cuttings concentration in the inclined section and a transport ratio for the vertical section, the cuttings concentration in the vertical section can be found:

$$c_{\text{vert}} = \frac{c_{\text{inc}}}{R_t} \tag{28}$$

The transport ratio R_t is defined as the ratio of the transport velocity, $v_{\text{ann}} - v_{\text{slip}}$, to the average mud velocity. R_t is less than or equal to 0 when no cuttings are transported, and 1 when all cuttings are transported to surface.

$$R_t = \frac{v_{\text{ann}} - v_{\text{slip}}}{v_{\text{ann}}} = 1 - \frac{v_{\text{slip}}}{v_{\text{ann}}} \tag{29}$$

Note that with a cuttings slip velocity of 40% of the average annular velocity, the transport velocity is 60% of the annular velocity. The retention time of the cuttings becomes 67% longer than that of the mud, resulting in a 67% higher cuttings concentration in the vertical section than in the inclined section. Based on the cuttings concentration in the vertical section and the mass density of the mud and cuttings, the average density of the cuttings and mud in the vertical section is found:

$$\rho_{\text{vert}} = \rho_m + c_{\text{vert}}(\rho_c - \rho_m) \tag{30}$$

The ratio of the hydrostatic pressure with and without cuttings in the vertical section is given by equation 31. The same ratio for the friction pressure is given by equation 32:

$$p^*_{\text{hyd}}(c_{\text{vert}}) = \frac{p_{\text{hyd}}(c_{\text{vert}})}{p^0_{\text{hyd}}} = \frac{\rho_{\text{vert}} g h_{\text{vert}}}{\rho^0 g h_{\text{vert}}} = \frac{\rho_m + c_{\text{vert}}(\rho_c - \rho_m)}{\rho_m} \tag{31}$$

$$\Delta p^*_f(c_{\text{vert}}) = \frac{\Delta p_f(c_{\text{vert}})}{\Delta p^0_f} = \frac{f(c_{\text{vert}})\rho(c_{\text{vert}})}{f^0\rho^0} = \frac{f(c_{\text{vert}})}{f^0}\frac{\rho_m + c_{\text{vert}}(\rho_c - \rho_m)}{\rho_m} \tag{32}$$

With $q_m = 2100$ lpm and ROP = 30 m/h in the 8 ½" section, and a concentration in the inclined section $c_{\text{inc}} = c_{\text{bit}} = 0.86\%$, a transport ratio $R_t = 0.92$ yields a vertical cuttings concentration $c_{\text{vert}} = 0.94\%$. With mud density of 1700 kg/m^3 and a cuttings density of 2200 kg/m^3, the relative pressure increase in hydrostatic and friction pressure loss due to cuttings in the vertical section is $p^*_{\text{hyd}} = 1.0028$ and $\Delta p^*_f = 1.0027$. As with the inclined section, the pressure increase due to cuttings is low, however slightly higher than 1.0025 in the horizontal section. This is due to a higher concentration in the vertical section.

In the 17 ½" section, with pump rate $q_m = 5000$ lpm, ROP = 30 m/h, $c_{\text{bit}} = 1.5\%$ and a transport ratio $R_t = 0.81$, the cuttings concentration in the vertical section becomes $c_{\text{vert}} = 1.9\%$. Equations 31 and 32 yield 1.0055 and 1.0052 respectively.

3.4.3 Viscosity change due to cuttings

An increase in suspended cuttings and particles in the drilling mud will result in increased particle interaction. This interaction between the particles can act out as an increase in internal friction and an increase in effective viscosity of the mud. An increase in effective viscosity results in a decrease in the Reynold's number. As seen from the moody chart in Appendix F, or directly from the Haaland equation (8), a decrease in Re results in an increase in friction factor f in the Darcy-Weisbach equation (7) and a higher friction pressure loss. An expression for the effective viscosity in a mix of fluid and solids is Einstein's viscosity equation for a slurry, is given as

$$\mu_{\text{eff}} = \mu_m(1 + 2.5c). \tag{33}$$

For a cuttings concentration of 1%, the relative increase in viscosity $\frac{\mu_{\text{eff}}}{\mu_m} = 1 + 2.5 \cdot 0.01 = 1.025$. When accounting for the effective viscosity as a function of cuttings concentration in equations 25 - 26, an increase in pressure loss is seen. **Table 1** shows relative pressure losses for ROP=30 m/h for 8 ½" and 17 ½" sections with and without viscosity increase from cuttings. The pump rate in the 8 ½" section is 2100 lpm, and 5000 lpm in the 17 ½" section. As seen from the table, viscosity increase gives a small increase in friction pressure loss, from 1.0027 to 1.0032 and from 1.0052 to 1.0072 in 8 ½" and

17 ½" vertical section respectively. A higher effective viscosity of the mud will also decrease the slip velocity of cuttings in the vertical section, and theoretically reduce cuttings concentration, giving a lower hydrostatic pressure. This effect is, however, too small to be seen in the table.

Table 1: Relative pressure losses for 8 ½" and 17 ½" sections, with and without viscosity increase from cuttings. μ_m indicates original mud viscosity, and μ_{eff} indicates effective viscosity for the mud-cuttings suspension. Note that hydrostatic pressure is not affected by the additional viscosity increase from cuttings. All numbers are based on an ROP of 30 m/h.

		8 ½"		17 ½"	
		μ_m	μ_{eff}	μ_m	μ_{eff}
Inclined	p^*_{hyd}	1.0025	1.0025	1.0045	1.0045
	Δp^*_f	1.0025	1.0030	1.0043	1.0062
Vertical	p^*_{hyd}	1.0028	1.0028	1.0055	1.0055
	Δp^*_f	1.0027	1.0032	1.0052	1.0072

The increase in viscosity for the mud-cuttings suspension will be immediate after generation, as cuttings are suspended in the drilling mud at the bit. However, the effect could be gradual on a larger scale, due to axial dispersion and fluid displacement. In addition to increased viscosity due to particle interaction, some clays and shales may alter the composition and rheology of the mud, and further increase the viscosity.

3.4.4 Cuttings beds

Most of the cuttings produced will sooner or later be transported up to surface. However, a constant amount of cuttings will remain in the wellbore as bedded cuttings during stable drilling and reaming. Skalle [2013] suggests that tentatively 5% of the wellbore volume in the inclined section is occupied by bedded cuttings around the drill string. Simulations by Cayeux et al. [2013] have shown that no cuttings are bedded around the BHA, due to the narrow annulus and a high fluid velocity.

As seen from the Darcy-Weisbach equation (7), a reduction in hydraulic diameter d_{hyd} and flow area A_{ann} increases the friction pressure loss, as the average velocity is given as

$v = \frac{q_m}{A_{\text{ann}}}$. In order to investigate the pressure increase due to bedded cuttings, a relative cuttings bed height x is introduced, defined as

$$x = \frac{h_c}{d_o}. \tag{34}$$

h_c is the cuttings bed height, and d_o is the borehole diameter. A relative bed height $x = 0$ indicates no bedded cuttings present in the wellbore, whereas $x = 1$ indicates a wellbore completely filled with cuttings.

As cuttings are deposited on the low side of the wellbore, the hydraulic diameter is unevenly increased around the wellbore perimeter. A new expression for hydraulic diameter as a function of x is therefore introduced (35). A_h (36) is the area of the homogeneous phase, *i.e.* cross sectional area of the mud-cuttings suspension, and S_h (37) is the perimeter of the homogeneous phase, illustrated in **figure 7**. A is the cross sectional area of the wellbore, while A_p and A_b are the cross sectional area of the drill pipe and cuttings bed layer respectively. S is the perimeter of the wellbore without cuttings, s is the arc length of the cuttings bed layer, c is the chord length of the cuttings bed layer, and S_p is the perimeter of the drill pipe.

$$d_{\text{hyd}}(x) = \frac{4A_h(x)}{S_h(x)} \tag{35}$$

$$A_h(x) = A - A_p - A_b(x) \tag{36}$$

$$S_h(x) = S - s(x) + c(x) + S_p \tag{37}$$

A_b, c and s as functions of x are given in equations 38, 40 and 41, where r_o is the radius of the wellbore, h_c is the cuttings bed height, and θ is the central angle, given in equation 39. The drill pipe is assumed to be located on top of the bed.

$$A_b(x) = \frac{r_o^2}{2}\Big(\theta(x) - \sin\theta(x)\Big) \tag{38}$$

$$\theta(x) = 2\arccos\frac{r_o - h_c}{r_o} = 2\arccos(1-2x) \tag{39}$$

$$c(x) = 2r_o \sin\frac{\theta(x)}{2} = 4r_o\sqrt{x(1-x)} \tag{40}$$

$$s(x) = r_o\theta(x) = 2r_o\arccos(1-2x) \tag{41}$$

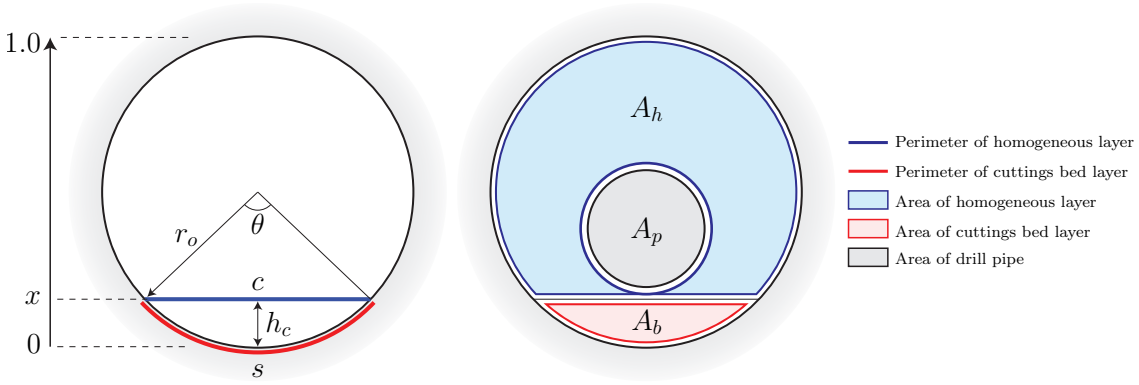

Figure 7: Geometry of the borehole with a layer of bedded cuttings. x is the relative bed height, A_h is the cross sectional area of homogeneous layer, A_p is the cross sectional area of drill pipe, A_b is the cross sectional area of cuttings bed layer, S_h is the wetted perimeter of the homogeneous layer, S is the perimeter of wellbore, s is the arc length of cuttings bed layer, c is the chord length of cuttings bed layer and S_p is the perimeter of drill pipe

The annular friction pressure loss over a wellbore segment ΔL_b with a relative bed height x is given by

$$\Delta p_f(x) = \frac{f(x)}{2}\frac{\Delta L_b}{d_{\text{hyd}}(x)}\,\rho\, v(x)^2, \tag{42}$$

where the hydraulic diameter d_{hyd}, average velocity v and friction factor f are all functions of the amount of bedded cuttings in the wellbore, represented by the cuttings bed

height x.

In order to analyse how each factor in equation 42 affects the hydraulic pressure loss at various amounts of bedded cuttings, relative variables for friction factor, hydraulic diameter, velocity and pressure loss are introduced. By increasing the relative bed height, thus decreasing the hydraulic diameter and the cross sectional flow area, the effect of cuttings bedding on the friction pressure loss can be investigated. An increase in mass density of the wellbore fluid due to suspended cuttings is ignored in this analysis. Equations 43 - 46 below describe relative friction factor, relative hydraulic diameter, relative fluid velocity and relative pressure loss respectively.

$$f^* = \frac{f(x)}{f^0} \tag{43}$$

$$d^*_{\text{hyd}} = \frac{d_{\text{hyd}}(x)}{d^0_{\text{hyd}}} = \frac{d_{\text{hyd}}(x)}{d_o - d_p} \tag{44}$$

$$v^* = \frac{v(x)}{v^0} = \frac{A^0_{\text{ann}}}{A_h(x)} \tag{45}$$

$$\Delta p^*_f = \frac{\Delta p_f(x)}{\Delta p^0_f} = f^* \left(d^*_{\text{hyd}}\right)^{-1} (v^*)^2 \tag{46}$$

$f(x)$ is the friction factor given by equation 8 as a function of $v(x)$ and $d_{\text{hyd}}(x)$. $\Delta p_f(x)$ is the hydraulic friction pressure loss over the cuttings bed, defined in equation 42. Superscript * indicates a relative parameter and ^{0} indicates a reference value without any bedded cuttings. The relative parameters are all equal to 1 for a wellbore without bedded cuttings.

The relative parameters pressure loss Δp^*_f, velocity v^*, hydraulic diameter d^*_{hyd} and friction factor f^*, were calculated for relative bed heights $x \in [0, 0.20]$ in a wellbore with outer diameter $d_o = 8\ ½$" and a drill pipe diameter $d_p = 5$". A cuttings bed length of 400 meters, flow rate of 2000 lpm and a specific gravity of 1.7 was used, although not affecting the relative parameters.

By plotting relative pressure losses Δp^*_f, velocity squared $(v^*)^2$, the inverse of the relative hydraulic diameter $(d^*_{\text{hyd}})^{-1}$ and relative friction factor f^* against the relative cuttings

bed height x, **figure 8** was generated. Note that the lower x-axis represents relative bed height x, while the upper x-axis shows the relative hydraulic diameter d^*_{hyd}. A relative bed height of 10% corresponds to a relative hydraulic diameter of 93%, while a relative bed height of 20% corresponds to a hydraulic diameter of 80%.

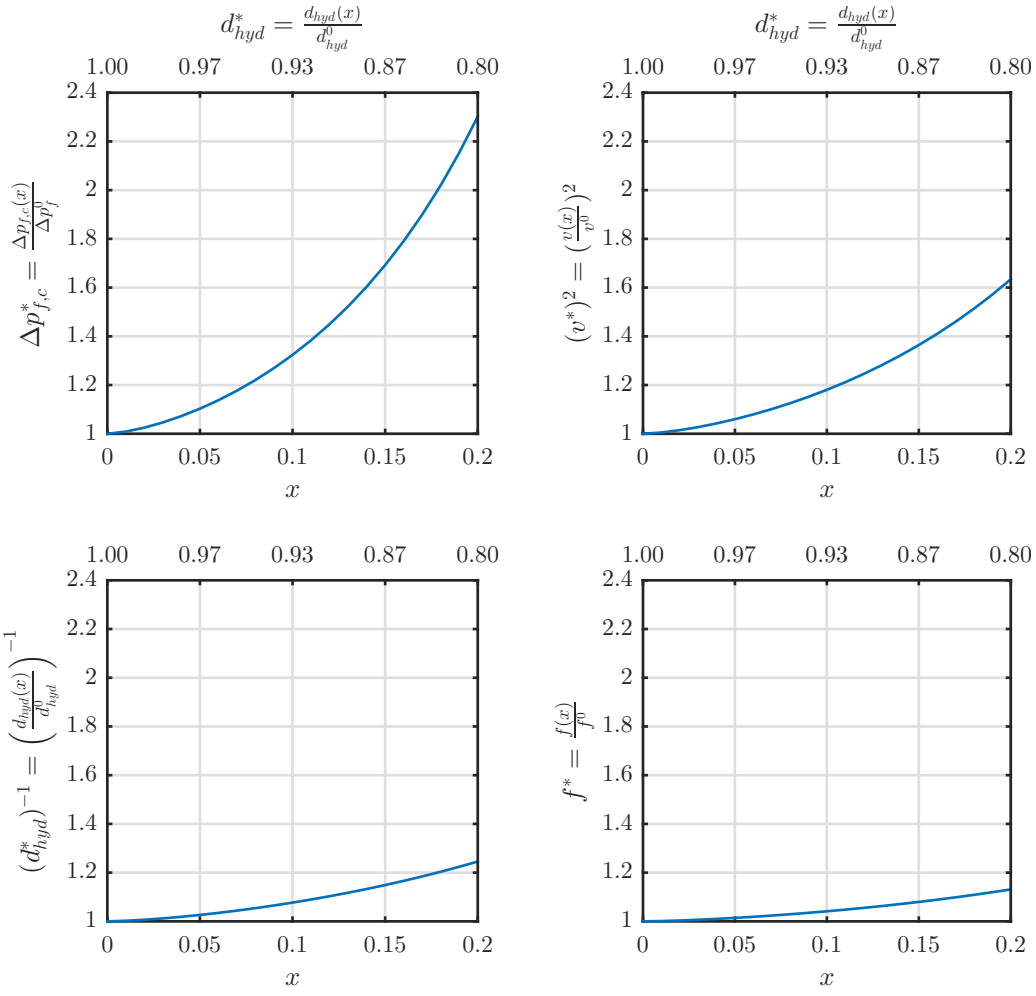

Figure 8: Upper left graph shows the relative hydraulic pressure loss $\Delta p^*_f = \frac{\Delta p_f(x)}{\Delta p^0_f}$ vs. relative bed height, $x = \frac{h_c}{2r_o}$ over the cuttings bed. The x-axis on top presents the corresponding relative hydraulic diameter $d^*_{\text{hyd}} = \frac{d_{\text{hyd}}(x)}{d^0_{\text{hyd}}}$. The remaining graphs represent relative velocity squared $(v^*)^2$, inverse relative hydraulic diameter $(d^*_{\text{hyd}})^{-1}$, and relative friciton factor f^* vs. relative bed height over the cuttings bed. Note that the product of graph 2, 3 and 4 equals graph 1, $f^*(d^*_{\text{hyd}})^{-1}(v^*)^2 = \Delta p^*_f$, as equation 46 states.

The annular pressure loss over the cuttings bed increases with 32% for $x = 0.1$, while

the pressure loss increases with a factor 2.3 for $x = 0.2$. The three factors in Equation 42 that are influenced by bedded cuttings are f, $(d_{\text{hyd}})^{-1}$ and v^2, and are plotted in figure 8. Velocity squared increases with a factor 1.18 and 1.63 for $x = 0.1$ and 0.2 respectively, while inverse hydraulic diameter increases with a factor 1.08 and 1.25. The friction factor increases with a factor 1.04 and 1.13 correspondingly.

As mentioned earlier, a plausible amount of bedded cuttings is 5% of the cross sectional area of the wellbore, $F_b = \frac{A_b}{A} = 0.05$. By using equations 35 - 41, a relative bed height x that fulfils the statement $F_b = \frac{A_b}{A} = 0.05$ can be found. Rearranging equation 38 gives

$$2\frac{A_b}{r_o^2} = 2\frac{F_b\,\pi r_o^2}{r_o^2} = 2\pi F_b = \theta(x) - \sin\theta(x). \tag{47}$$

When solving equation 47 for θ by using Newton's method with $F_b = 0.05$, x can be found by rearranging equation 39:

$$x = \frac{1}{2}\left(1 - \cos\frac{\theta}{2}\right) = 9.73\% \tag{48}$$

A relative cuttings bed height $x = 0.0973$ corresponds to a bed height $h_c = 2.1$ cm in a 8 ½" hole. As calculated earlier, a cuttings bed of 10% of the borehole diameter will increase the friction pressure loss over the cuttings bed with more than 30%.

The packing efficiency of a cuttings bed is around 50% [Cho et al., 2001], which means the volume of settled solids is half the bulk volume of the cuttings bed. If 5% of the cross sectional borehole area is occupied with cuttings, 2.5% of the suspended cuttings were settled. As new formation is drilled, new wellbore surface behind the BHA is continuously being exposed to cuttings being bedded. This results in a cuttings concentration of 97.5% of c_{bit} behind the BHA:

$$c = (1 - 0.05 \cdot 0.5)\, c_{\text{bit}} = 0.975 \cdot c_{\text{bit}} \tag{49}$$

A study by Cayeux et al. [2013], where a cement plug was drilled out with a 8 ½" bit, showed little cuttings returns compared to the amount of cuttings produced when drilling for 14 hours. The inclination of the hole was 65°, and drilled with a flow rate of 1900 lpm,

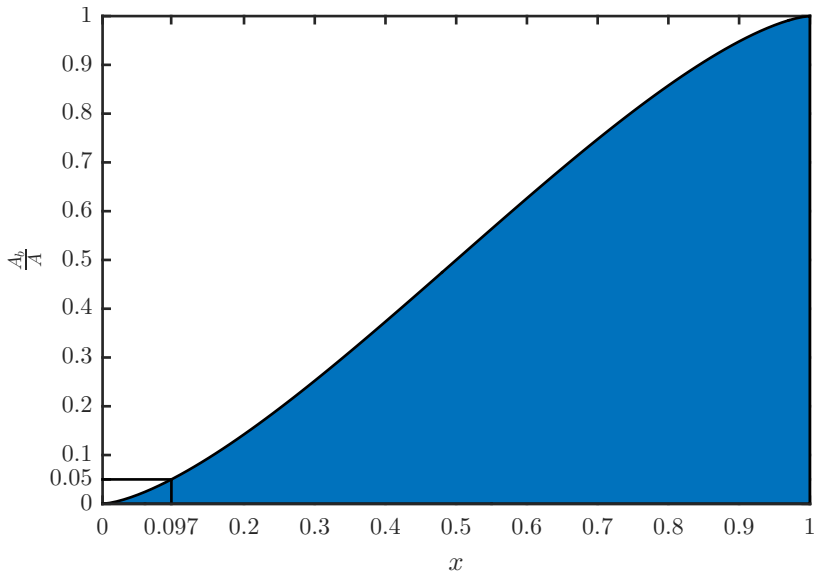

Figure 9: Relative cuttings bed area $\frac{A_b}{A}$ vs. relative bed height x. A cross sectional bed area of 5% of the cross sectional borehole area corresponds to a relative bed height $x = 9.73\%$

string rotation 80 RPM, and an average rate of penetration of 15 m/h. When simulating the cuttings transport for the similar scenario, no cuttings returns were shown. In both the drilling case and its simulation, large cuttings beds were formed in the borehole, causing a cuttings avalanche and a stuck pipe incident. As the case of the study was drilling a cement plug inside a casing, it is reasonable to believe that no cuttings beds were present inside the casing before drilling started. Whenever starting to drill after a casing or a liner has been set, a proper clean out run has been performed. It is therefore assumed that a large amount cuttings will be bedded, before a significant amount of cuttings reaches the vertical section. However, when the equilibrium bed height has been reached, all suspended cuttings will be transported to the surface.

Experiments by Cho et al. [2001] indicate that a fraction of the fluid flow passes *through* the cuttings bed, rather than 100% of the flow passing above the bed. When taking into account pressure loss *through* the cuttings bed rather than only *above*, the total annular friction pressure loss can increase with up to 20% at 60° inclination (or approximately one bar additional per 100 m for a nominal annular velocity of 3 ft/s). This effect increases with increasing inclination, and shows that there is a significant effect of bedded cuttings on the annular friction pressure loss.

Critical flow rate is defined as the flow rate at which cuttings beds start to form. Cuttings are easily deposited in a horizontal well with low annular velocity and string rotation speed. Likewise, bedded cuttings can be suspended when increasing either the flow rate or rotation speed. Critical flow rate is also affected by rate of penetration, as a high generation of cuttings requires a higher flow rate in order to prevent cuttings deposition. The cuttings bed height is therefore a function of flow rate, string rotation speed and rate of penetration.

If the flow rate is below critical flow rate in the annulus, cuttings beds will form until reaching an equilibrium bed height decided by the fluid velocity, rotation speed and ROP. For bed heights greater than equilibrium bed height, the cross sectional flow area will decrease, resulting in an increased fluid velocity and ultimately erosion of the bed. Continuous erosion and deposition of cuttings in the bed is assumed, and the deposition rate is equal to the erosion rate when equilibrium has been reached.

When cuttings beds are formed, the concentration of suspended cuttings will decrease, postponing a considerable cuttings concentration in the vertical section. This reduction in cuttings concentration is illustrated in **figure 10**. The postponed pressure effect may, however, in some degree be compensated by the pressure increase due to cuttings beds.

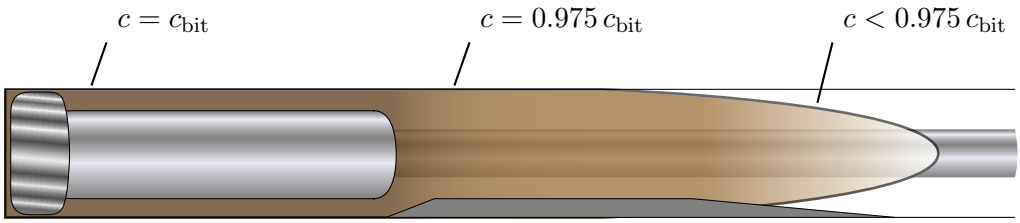

Figure 10: Cuttings bed (grey) and cuttings concentration in the annulus (brown). Cuttings concentration arround BHA is assumed equal to c_{bit}. Concentration is reduced (light brown gradient) as cuttings go out of suspension, forming beds.

3.4.5 Example calculations of pressure loss due to cuttings

In this section, pressure losses from increased density and viscosity in hydrostatic and friction pressure loss are calculated. In addition, the expected increase in pressure loss

over a cuttings bed is presented. The values used in the calculations are given in **table 2** at the end of this section, and represent typhical values observed in the data.

Density and viscosity increase

Difference in *hydrostatic* pressure loss due to suspended cuttings is calculated by summing the pressure loss *with* cuttings in both the vertical and inclined section, and subtracting the pressure loss over the whole well *without* suspended cuttings:

$$\begin{aligned} p_{\text{hyd}}^{\text{vert}} + p_{\text{hyd}}^{\text{inc}} - p_{\text{hyd}}^{0} &= \rho_{\text{vert}} g h_{\text{vert}} + \rho_{\text{inc}} g h_{\text{inc}} - \rho_m g h \\ &= 191.1 + 155.0 - 345.2 \\ &= 0.9 \text{ bar} \end{aligned}$$

ρ_{vert} and ρ_{inc} represent density of the mud-cuttings suspension in the vertical and inclined section. The total vertical height is given as $h = h_{\text{vert}} + h_{\text{inc}}$.

The difference in *friction* pressure loss due to suspended cuttings is calculated by summing the friction pressure loss *with* cuttings in the vertical and inclined section and subtracting the friction pressure loss over the whole well *without* suspended cuttings:

$$\begin{aligned} \Delta p_f^{\text{vert}} + \Delta p_f^{\text{inc}} - \Delta p_f^{0} &= \frac{f_{\text{vert}}}{2} \frac{L_{\text{vert}}}{d_{\text{hyd}}} \rho_{\text{vert}} v^2 \\ &\quad + \frac{f_{\text{hor}}}{2} \frac{L_{\text{hor}}}{d_{\text{hyd}}} \rho_{\text{hor}} v^2 \\ &\quad - \frac{f}{2} \frac{L}{d_{\text{hyd}}} \rho_m v^2 \\ &= 27.8 + 73.0 - 100.5 \\ &= 0.3 \text{ bar} \end{aligned}$$

Total pressure loss due to increased mud density and viscosity caused by cuttings is $0.9 + 0.3 = 1.2$ bar, given that the whole wellbore contains mud with suspended cuttings. Although an effect of this magnitude is noticeable in SPP, the pressure increase is

gradual, due to fluid displacement, axial dispersion and formation of cuttings beds. In this example, the cuttings front passes the BHA after approximately one minute after commencement of drilling, enters the vertical section after 36 minutes, and reaches the top after approximately 51 minutes.

$$
\begin{aligned}
t_{\text{inc}} &= \frac{L_{\text{inc}}}{v} = 36.3 \\
t_{\text{vert}} &= \frac{L_{\text{vert}}}{v - v_{\text{slip}}} = 15.0 \\
t_{\text{tot}} &= t_{\text{inc}} + t_{\text{vert}} = 51.3
\end{aligned}
$$

Cuttings beds

The difference in friction pressure loss due to bedded cuttings is calculated by subtracting the pressure loss over a wellbore segment *without* bedded cuttings from the pressure loss over the same segment *with* bedded cuttings:

$$
\begin{aligned}
\Delta p_f^{\text{bed}} - \Delta p_f^0 = &\frac{f(x)}{2}\frac{L_b}{d_{\text{hyd}}(x)}\rho_m v(x)^2 \\
&- \frac{f^0}{2}\frac{L_b}{d_{\text{hyd}}^0}\rho_m (v^0)^2 \\
&= 5.98 - 4.57 = 1.41 \text{ bar}
\end{aligned}
$$

Over a 200 m long segment with relative bed height $x = 9.73\%$, the difference in pressure loss is 1 bar.

Table 2: Input data used in example calculations

Length of wellbore	L	4399 mMD
Depth of wellbore	h	2070 mTVD
Length of vertical section	L_{vert}	1212 mMD
Length of inclined section	L_{inc}	3187 mMD
Height of vertical section	h_{vert}	1143 mTVD
Height of inclined section	h_{inc}	927 mTVD

Continued on next page

Table 2 – *Continued from previous page*

Mud density	ρ_m	1700 kg/m3
Cuttings density	ρ_c	2200 kg/m3
Mud viscosity	μ_m	35 cp
Rate of penetration	ROP	30 m/h
Flow rate	q	2100 lpm
Diameter bit	d_{bit}	8.5 in
Diameter drill pipe	d_p	5 in
Diameter cuttings	d_c	4 mm
Absolute roughness	e_{abs}	0.01 m
Cuttings concentration	c	0.0086
Effective viscosity	μ_{eff}	35.8 cp
Fluid velocity	v	1.46 m/s
Reynolds number w/o cuttings	Re^0	6312
friction factor w/o cuttings	f^0	0.1118
Fluid density inclined section	ρ_{inc}	1704 kg/m3
Reynolds number inclined section	Re_{inc}	6195
Friction factor inclined section	f_{inc}	0.1118
Slip velocity	v_{slip}	0.1113 m/s
Transport ration	R_t	0.92
Cuttings concentration vertical section	c_{vert}	0.0094
Effective viscosity vertical section	$\mu_{\text{eff,vert}}$	35.8 cp
Fluid density vertical section	rho_{vert}	1705 kg/m3
Reynolds Number vertical section	Re_{vert}	6196
Friction factor vertical section	f_{vert}	0.1118

3.5 Change in mud properties

Change in temperature has a large impact on SPP [Rommetveit and Bjørkevoll, 1997], as the viscosity and density of the drilling fluid are both functions of temperature. A general rule is that viscosity decreases with increasing temperatures. Formation temperature increases with vertical depth, heating cold drilling mud when pumped down from the rig or platform. When the mud passes the bit and travels upwards, the mud will at some point have a higher temperature than the formation temperature, leading to cooling of the mud. Both short term and long term effects in SPP can occur due to changes in temperature. After a period of no pumping and minimal circulation of the mud, the mud temperature approaches the temperature of the formation. When resuming pumping, hot mud will be displaced by colder mud, causing rapid pressure changes. As mud is heated by the formation during circulation, the temperature of the mud in the pits on the rig will increase, affecting the mud properties and SPP on longer term.

Drilling mud is a compressible fluid, and mass density of the fluid is a function of both pressure and temperature. An increase in pressure will compress the fluid, and result in a higher density, while a decrease in pressure will cause the fluid to expand. Increasing temperature will also cause a decrease in density, while the density increases by cooling of the mud. Inside the drill pipe the pressure is high and the temperature relatively low, resulting in a high density. The lowest mass density occurs after passing the bit, where the mud has been heated by the surroundings, and pressure is relatively low after a large pressure drop over the bit. The density then increases upwards through the annulus due to cooling, even though pressure is decreasing [Cayeux et al., 2013].

An other phenomenon that may affect SPP is gelling of the mud, *i.e.* increase in viscosity after a longer absence of shear forces applied on the drilling fluid. After a period without rotation or circulation, such as during connections, a higher SPP can be observed when starting the mud pumps. The SPP goes back to normal after a couple of minutes if the connection time is short. However, higher SPP as a result of gelling can be observed for several hours depending on the shear history of the mud, according to Rommetveit and Bjørkevoll [1997].

High viscosity pills, *i.e.* pumping high viscosity mud for a limited time to improve hole cleaning, may also affect the SPP. When drilling into a formation containing gas, the

gas follows the mud up to surface, decreasing the viscosity of the mud. This may lead to a decrease in SPP.

The changes in mud properties mentioned above are hard to correct for as there are many unknown parameters, limited published theory and uncertain and varying down-hole conditions. Our approach in this theses is therefore to avoid data intervals where above mentioned effects may occur, and rather look at changes in SPP between stable periods.

4 Approach

4.1 Description of the data sets

A total of four sections from two different wells in the North sea have been used in analysis. In well K 470, a 17 ½", 12 ¼" and an 8 ½" section has been analysed, while an 8 ½" section has been available for analysis in well K 480. All sections are presented further in appendix D, where illustrations of the well path are included. In addition to key information and well data, important events during drilling from the "End of Well" report are summarized for each section.

4.2 Analysing data

As described in the previous section, there are several parameters that affect the pressure loss in the annulus. Because of the impact both flow rate and string rotation can have on the pressure, they are defined as *critical parameters*. Stable critical parameters, in addition to a stable pressure, defines a baseline of SPP. This is an absolute criteria for an interval to be qualified for further analysis.

ROP is an important parameter when analysing the changes in the concentration of cuttings suspended in the mud. ROP gives an estimate on the volume of cuttings added to the mud flow over a period of time. The concentration of suspended cuttings is found from the flow rate and the rate of penetration. When analysing drilling data, ROP is calculated and plotted along with other parameters of interest, such as standpipe pressure, flow rate, block height, weight on bit, rotation and torque. In order to reduce noise from small variations in the measured depth, the ROP is estimated by the centre derivative of the measured depth with respect to time, given in equation 50. L_i is the measured depth at time t_i.

$$\text{ROP} = \frac{L_{i+1} - L_{i-1}}{t_{i+1} - t_{i-1}}, \tag{50}$$

In order to investigate the effect of ROP on SPP, the changes over time are calculated and evaluated. $\Delta\overline{\text{ROP}}$ and $\Delta\overline{\text{SPP}}$ are defined as the difference between the average of two intervals, where the values appear stable. These intervals are manually selected,

based on a significant change in both parameters where no other cause of the pressure change seems reasonable. The change in average ROP and SPP is given as

$$\Delta\overline{\mathrm{ROP}} = \frac{1}{M}\sum_{i=1}^{M}\mathrm{ROP}_i - \frac{1}{N}\sum_{j=1}^{N}\mathrm{ROP}_j \quad \text{and} \tag{51}$$

$$\Delta\overline{\mathrm{SPP}} = \frac{1}{M}\sum_{i=1}^{M}\mathrm{SPP}_i - \frac{1}{N}\sum_{j=1}^{N}\mathrm{SPP}_j \tag{52}$$

respectively, where i and j represent data points within two non-overlapping time intervals with M and N number of measurements respectively. The length of each interval can be as short as a couple of minutes where the effect is brief, such as when drilling through a thin stringer. In some cases, there is a small delay between an observed pressure effect and the causative change in ROP. If the duration of the intervals of investigation is brief, the time delay is accounted for. Such a time shift is done provided that critical parameters remain stable and no other reasonable cause of the pressure change is found.

Both drilling and reaming contribute to generation and suspension of cuttings. During drilling, new cuttings are generated at the bit and transported along the drill string. A change in ROP will therefore result in a change in cuttings concentration. A limited amount of new cuttings are generated during backreaming, but bedded cuttings can be eroded or removed as the drill string with a large diameter BHA is pulled out of hole. Both drilling and backreaming intervals are analysed when investigating the effects of cuttings concentration.

By plotting the observed changes in SPP and ROP, potential trends can be identified within and between sections. By curve fitting the data points in MATLAB, empirical equations involving $\Delta\overline{\mathrm{SPP}}$ and $\Delta\overline{\mathrm{ROP}}$ can be found.

5 Results and evaluation

The most important findings from analysis of drilling data are presented in this section. Consistent results were not found in the reaming intervals, and findings from the back-reaming analysis are further described in appendix B. Observed effects from change in flow rate, rotation speed and weight on bit are presented in appendix A.

Observed changes in SPP were plotted against change in ROP and grouped by section. Empirical equations were obtained for each section by curve fitting in MATLAB. Data from all sections were plotted together, along with the fitted curves, in order to find correlations between sections.

Simulations of effects from viscosity and density caused by cuttings over the BHA were performed in an attempt to replicate the observed pressure responses. The intention with these simulations was to investigate whether the observed pressure effects from the drilling data could be explained by already known cuttings effects, or if some other and unknown effect is present. The results of the simulations are presented graphically together with the observed effects from the data.

5.1 Observed pressure responses caused by change in ROP

The following correlations between the change in standpipe pressure and the change in rate of penetration were observed in several different cases:

- SPP decrease related to an ROP decrease when hitting a harder formation
- SPP increase related to an ROP increase when drilling into a softer formation
- SPP decrease related to an intentional ROP decrease
- SPP increase related to an intentional ROP increase

The parameters ROP and WOB determine whether the change in ROP is formation hardness induced or operator induced. When drilling into a harder formation, the ROP is significantly reduced, even though an equal WOB is maintained, or even increased. In the opposite case, when hitting a soft formation, the ROP is increased, even though an equal WOB is maintained, or even decreased. A hard stringer, some times referred to as just “stringer”, is defined as a thin bed that is harder than the surrounding formation,

and a significantly higher WOB is required in order to drill past the stringer with a maintained ROP. A change in ROP caused by drilling into a stringer or a soft formation is referred to as formation related ROP change.

When setting more weight onto the formation, the bit goes deeper into the rock and crushes the formation with greater force. In a formation with constant hardness, an increase in WOB will increase ROP, whereas a decreased WOB decreases the ROP. A change in ROP as a result of an operator induced change in WOB is in this thesis referred to as an intentional ROP change. A summary of the formation related and the intentional ROP changes is presented in **table 3**, along with the corresponding qualitative changes in SPP, ROP and WOB. The cause of the ROP change is referred to as a "phenomenon" in this thesis.

Table 3: Observed phenomena and the effect on the parameters SPP, ROP and WOB. A plus "+" indicates an increase in the given parameter, whereas a minus "−" indicates a decrease. The combination of ΔROP and ΔWOB indicates whether the ROP change is formation induced, *i.e.* drilling into harder or softer formation, or operator induced, called intentional ROP change.

ΔSPP	**ΔROP**	**ΔWOB**	**Phenomenon**
+	+	−	Soft formation
−	−	+	Hard formation
+	+	+	Intentional ROP increase
−	−	−	Intentional ROP decrease

A significant decrease in ROP and SPP was observed in cases when drilling into a hard stringer, along with an increase in WOB. When drilling though the stringer, meeting softer formation, the opposite effect is seen. A manually drawn example of a typical relationship between ROP and SPP when drilling into a stringer is shown in **figure 11**.

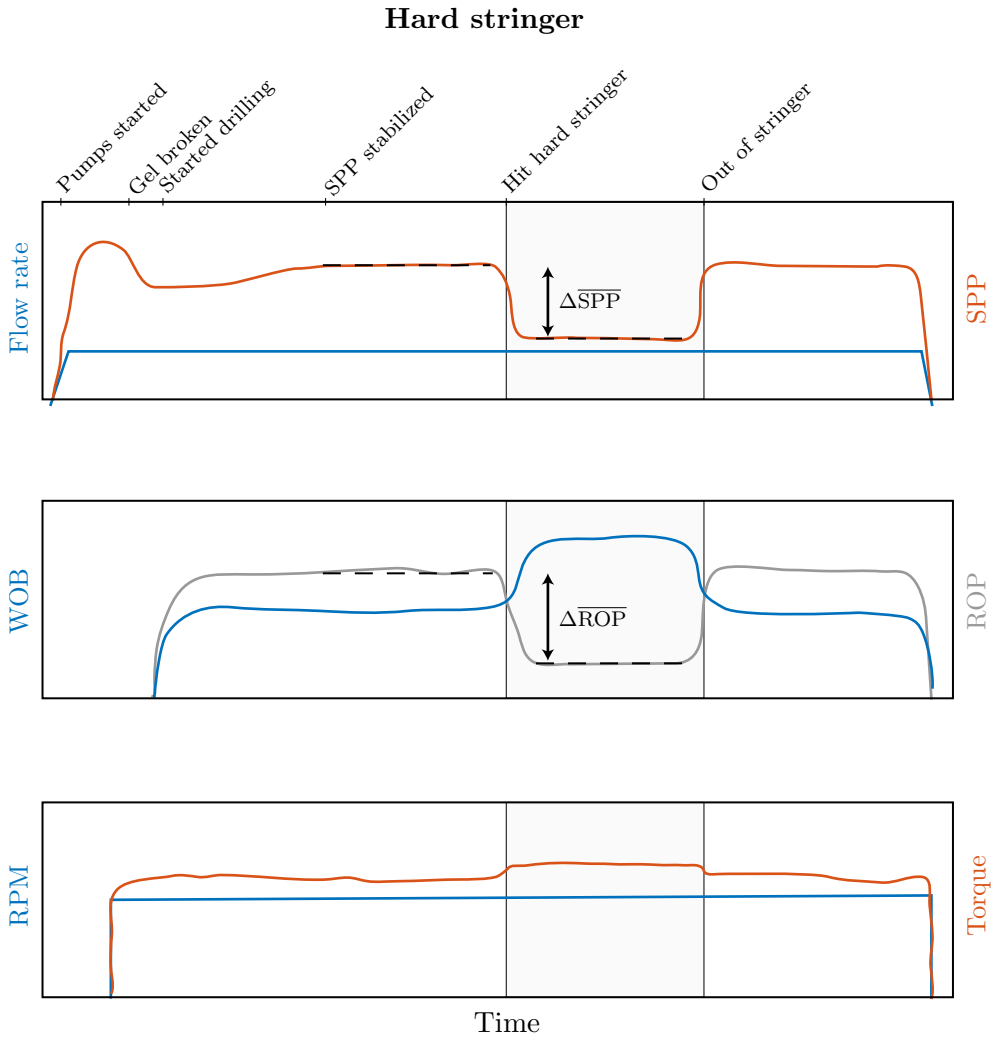

Figure 11: Manually drawn example of an ideal SPP decrease in a hard stringer. SPP (orange, upper) increases immediately when pumps are turned on, and a small pressure decrease is seen when gel is broken. The pressure increases as cuttings are being produced, until it stabilises. When the hard stringer is hit, the SPP and ROP (grey, middle) decrease, while WOB (blue, middle) increases. When drilling through the stringer and into softer formation, the opposite effects are seen. A small change in torque is sometimes observed, but seems to be affected more by the WOB, than the ROP.

A close relationship between WOB and ROP was discovered, where an increase in WOB is seen together with and increase in ROP and SPP and vice versa. This effect seems to be especially distinct in soft formations. It seems, however, to be a closer relation

between SPP and ROP than SPP and WOB. A typical relationship between SPP, ROP and WOB in soft formation is illustrated by a drawing in **figure 12**, where an increase in ROP results in an increase in SPP.

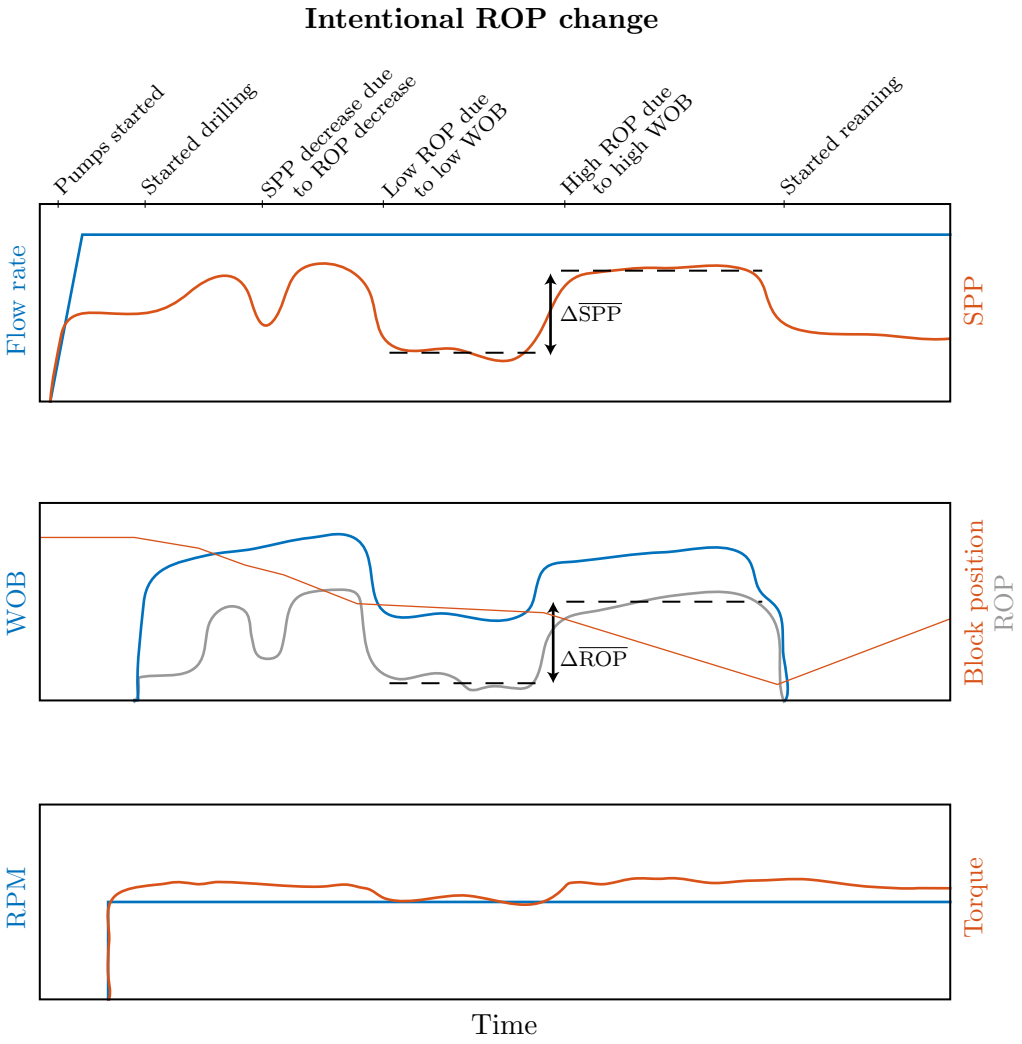

Figure 12: Manually drawn example of SPP vs. ROP and WOB in soft formation. WOB and ROP seem to follow each other closely in formations with homogeneous properties. SPP seems to have a closer relation to ROP than WOB. In a formation with little variation in hardness, an increase in WOB usually results in an increase in ROP. However, a decrease in ROP with constant WOB tends to result in a decreased SPP. A change in ROP caused by a changed WOB is referred to as an intentional ROP change.

Figure 13 shows drilling data from the 8 ½" section in well K 480. When hitting a hard stringer, the ROP decreases from approximately 26 to 7 m/h, with a decrease in SPP of 2.24 bar. The WOB increases accordingly. The change in SPP and ROP takes place within a couple of minutes.

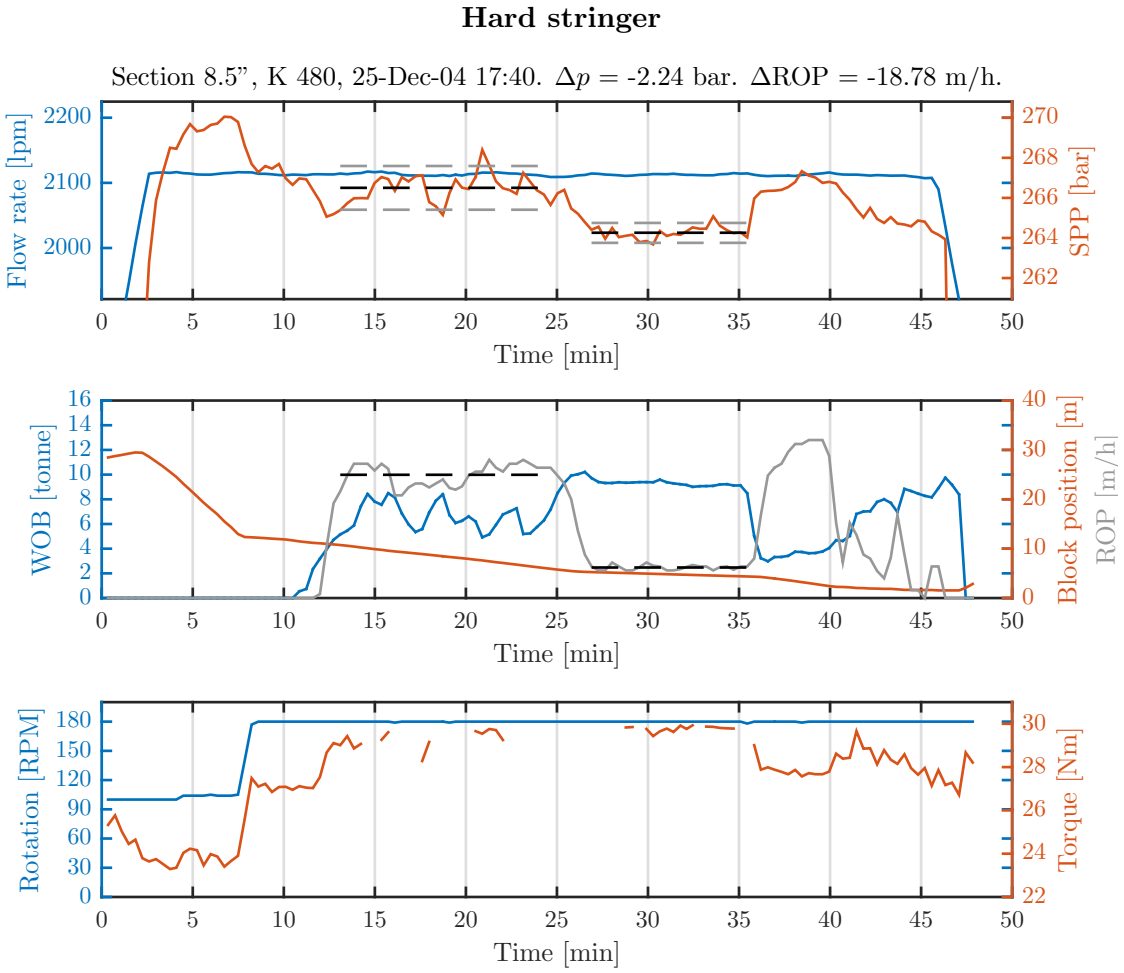

Figure 13: SPP decreases when hitting a hard stringer in section K 480 8 ½". In the interval 13 - 24 min, the average ROP (grey, middle) is approximately 25 m/h. At 25 min the ROP decreases to 7 m/h and WOB (blue, middle) increases, indicating a hard stringer. A decrease in SPP (orange, upper) of 2.24 bar is seen between the two intervals. The black dashed lines in the upper plot indicate the mean pressures over each interval, while the grey dashed lines represent the 5th and 95th percentile. Both flow rate (blue, upper) and RPM (blue, lower) are constant over the intervals of interest. SPP increases equally at 36 min when hitting softer formation, and again decreases when hitting a harder stringer at 41 min.

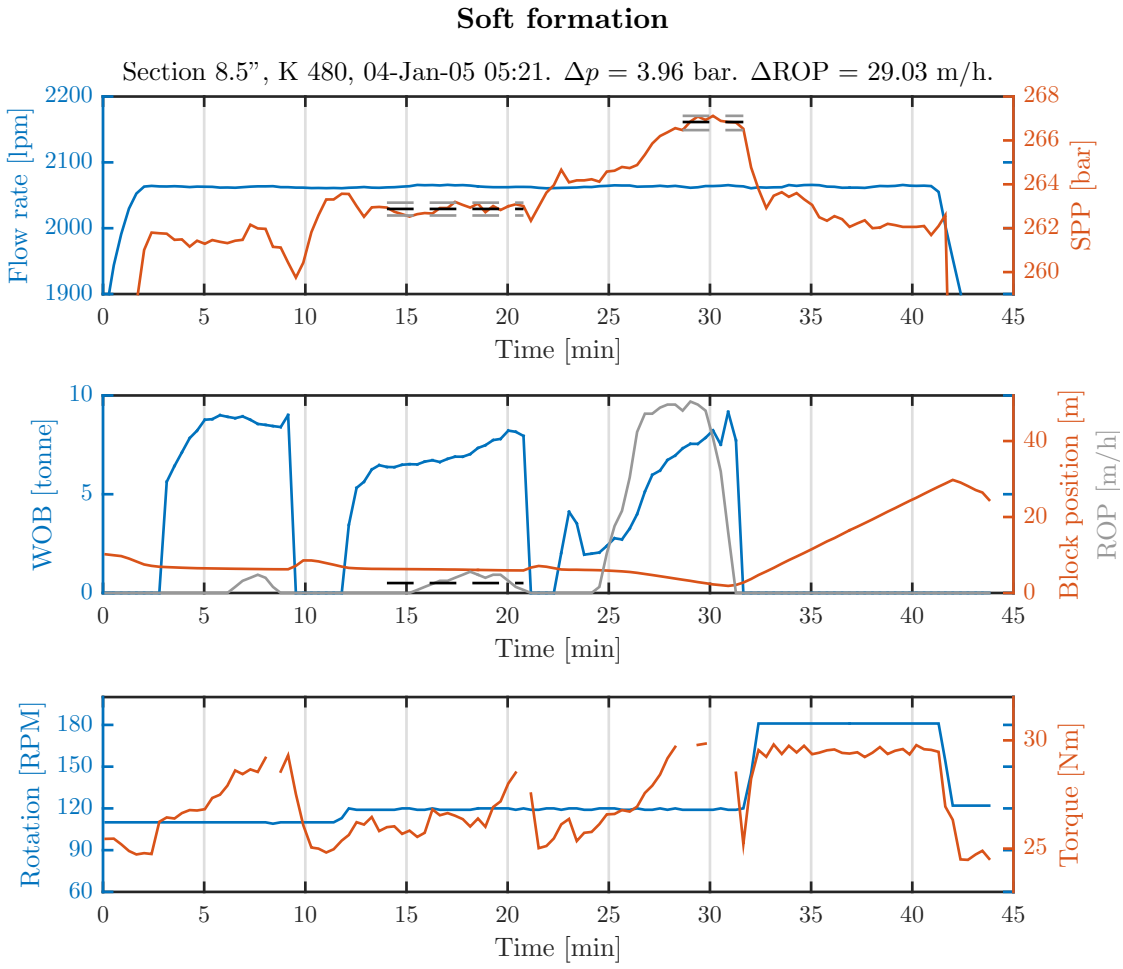

Figure 14: SPP increases when hitting soft formation in K 480 8 ½". Between 14 - 21 min the ROP (grey, middle) is approximately 5 m/h and WOB (blue, middle) 7 tonnes. At 25 min the ROP increases to 50 m/h, with a WOB lower than the previous interval. This indicates the end of a hard formation. The increase in SPP (orange, upper) is 3.96 bar between the two intervals.

Figure 14 shows drilling data from section K 480 8 ½", where a soft formation is encountered at 25 minutes. Between 13 and 21 minutes, the WOB is between 6 and 8 tonne, with ROP below 5 m/h and SPP of approximately 263 bar. At 23 minutes the WOB increases from 0 to 4 tonne although ROP is zero, and SPP increases with 1.2 bar. At 25 minutes the ROP increases to 49 m/h, where it remains high for 5 minutes, although the WOB is less than or equal to WOB in the preceding interval between 13 and 21 min. The sudden increase in ROP, with the lack of an increase in WOB, indicates drilling into a soft formation. SPP increases further to 267 bar when ROP is high. The

low SPP and ROP combined with a high WOB in the interval between 13 and 21 minutes indicates that ROP may be the cause of the increase in SPP.

There is a small delay between the ROP increase and the SPP increase of approximately one minute. This may however be caused by incorrect calculation of WOB or ROP/bit position in the data.

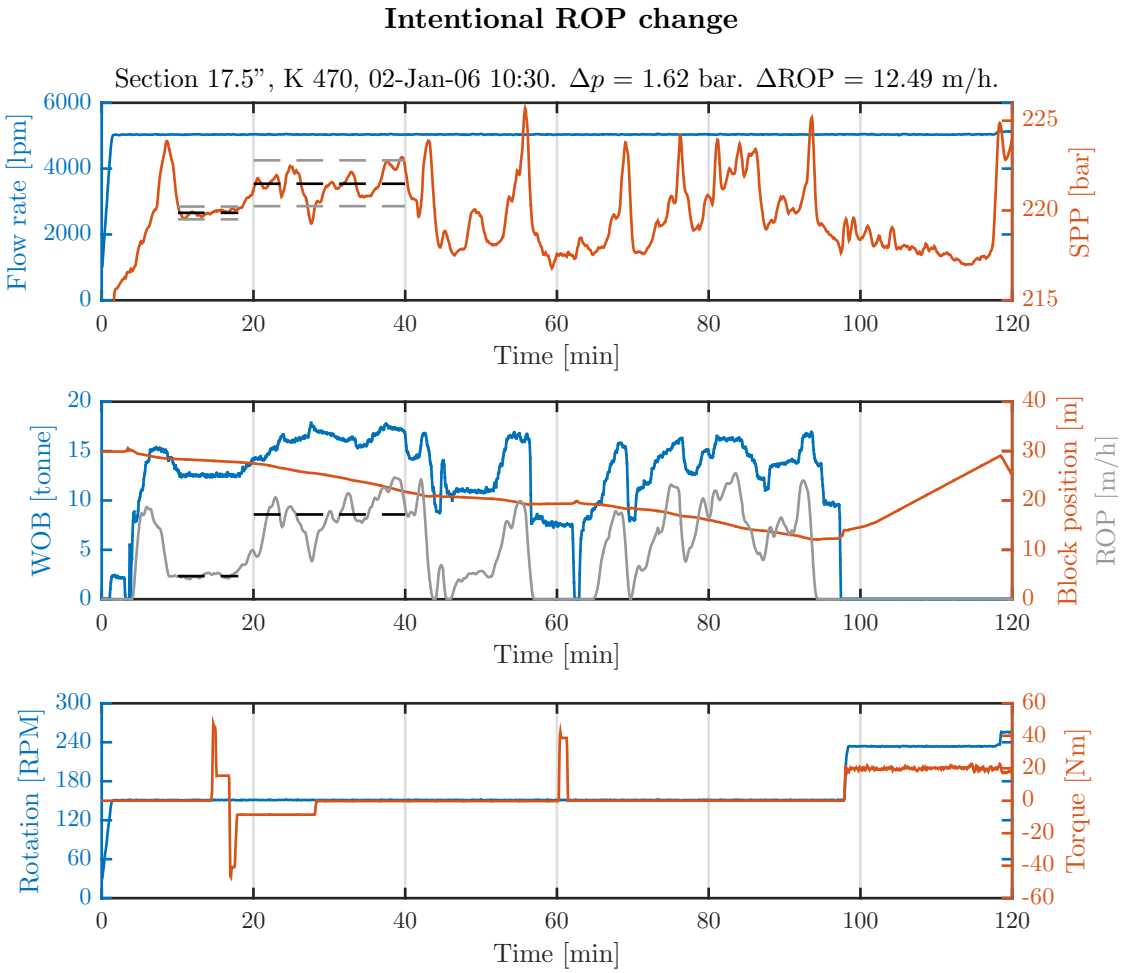

Figure 15: SPP increases from an intentional ROP increase in K 470 17 ½". ROP increases as WOB is increased. SPP seems to have a closer correlation to ROP than to WOB, as seen by the dip in SPP and ROP at approximately 27 minutes. No mud motor is used when drilling this section.

In the 17 ½" section in well K 470, a close correlation between SPP, ROP and WOB was seen in several cases. **Figure 15** shows an increase in WOB from 13 to approximately

17 tonne between the interval 10 - 18 and interval 22 - 42 minutes. The increase in ROP and SPP between the same intervals are 12.49 m/h and 1.62 bar respectively.

At approximately 27 minutes, a small decrease in ROP, instantaneously followed by an increase in SPP, is seen. This change is not seen in WOB. This may indicate encountering a harder bed, where WOB is maintained the same and the ROP decreases, with a decrease in SPP as a result of the ROP change. However, another explanation may be incorrectly calculated WOB in the data.

Cases deviating from general trends in data

During analysis, a few cases that deviates from the general trend in data are found. **Figure 16** shows an interval from the K 480 8 ½" section, where the SPP decreases as the ROP increases. There is an increase in WOB between 26 and 50 minutes that seems to correspond to the alteration in SPP. Exactly what is causing this effect is not known, but one possibility is an effect from WOB masking the expected SPP decrease from the change in ROP. A similar effect is observed in an interval where there is no ROP change. This is further described in appendix A, under subsection weight on bit.

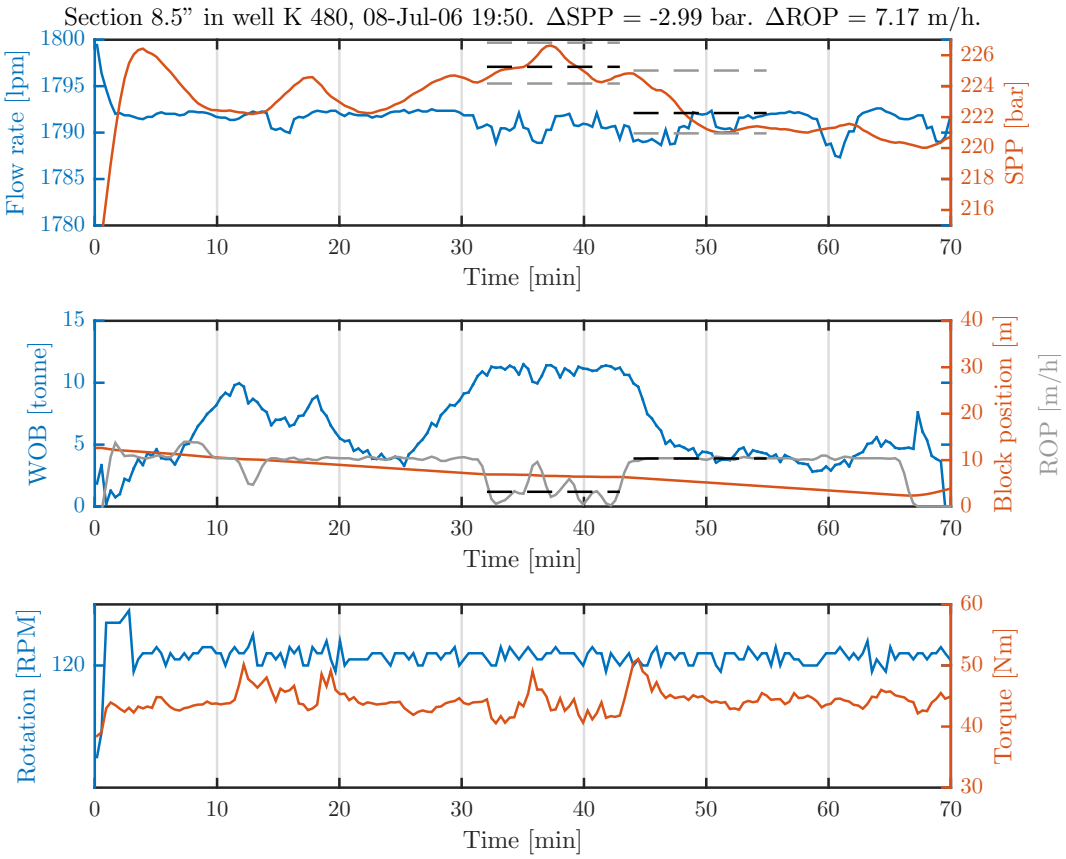

Figure 16: SPP decreases as the ROP increases at 44 minutes into the interval. WOB may explain this response in pressure.

5.2 Curve fit of pressure responses caused by change in ROP

In this section, pressure changes caused by change in ROP are analysed. Change in average rate of penetration, $\Delta\overline{\text{ROP}}$, is plotted against its respective pressure response, $\Delta\overline{\text{SPP}}$, grouped by phenomenon. By doing this, trends in SPP vs. ROP can be found. The different causes of ROP change during drilling, in addition to its definition, is listed in **table 4**.

Table 4: Causes of change in ROP and its definitions

Cause	Definition
Thin stringer	Hard, thin formation that is passed within a couple of minutes
Stringer	Hard formation that reduces the ROP for several minutes
Soft formation	A formation softer than the previous, causing an increase in ROP
Intentional ROP change	Change in ROP as a result of changing WOB

K 480 8 ½" section

Figure 17 shows different pressure and ROP changes from the 8 ½" section in well K 480. Four different causes to ROP change are identified through drilling data, and a total of 15 cases related to SPP and ROP change during drilling are found. A point inside the third quadrant of the plot indicates a *decrease* in both ROP and SPP, caused by either drilling into a hard stringer or by intentionally decreasing WOB. The cases within the first quadrant represent an *increase* in both ROP and SPP. Cases marked as stringers or thin stringers in this quadrant are cases with an ROP and SPP *increase* when drilling through the stringer and into softer formation.

In the third quadrant, the stringers appear to have the highest changes in both ROP and SPP compared to the thin stringers. Only two cases of intentional ROP change are identified in the K 480 8 ½" section, making it difficult to determine a trend.

The data points in figure 17 appear relatively linear in the plot. Using the curve fitting tool in MATLAB, a fitted curve on the form $y = ax$ has been included in the plot. No constant term is included in the curve fit, as zero change in ROP would yield zero change in SPP. The slope of the function is given as:

$a = 0.1017 \ \frac{\text{bar}}{\text{m/h}}$, with a coefficient of determination $R^2 = 0.9625$.

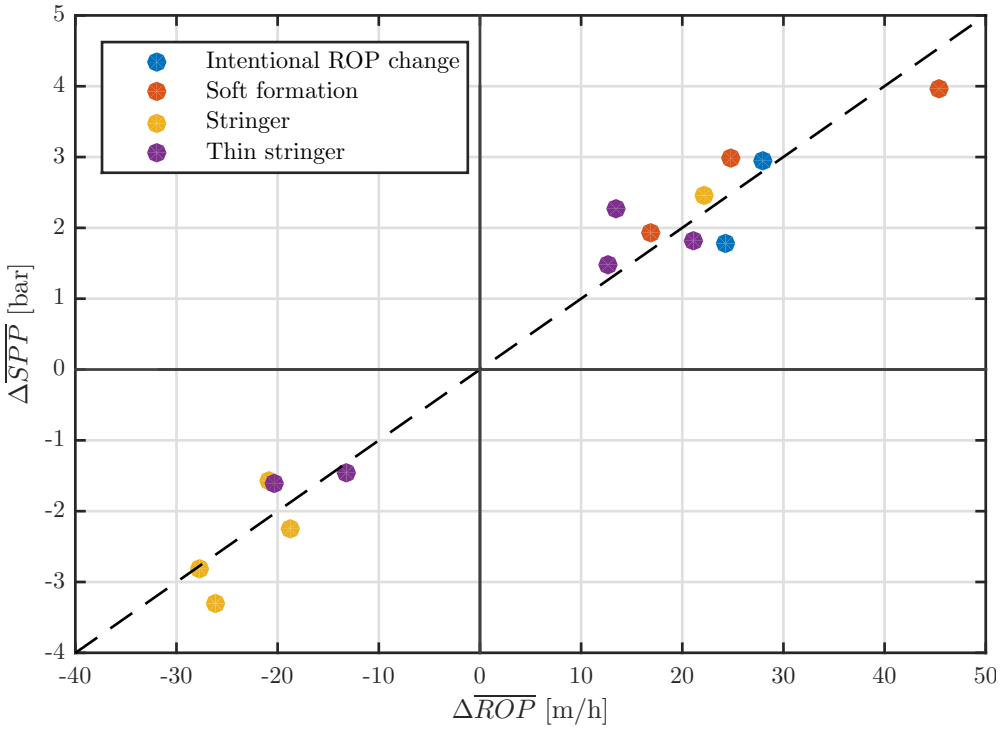

Figure 17: Change in SPP vs. change in ROP in K 480 8 ½" for the pressure phenomena stringer, thin stringer, intentional ROP change and soft formation. The curve fitted line has a slope $a = 0.1017$ $\frac{\text{bar}}{\text{m/h}}$, with $R^2 = 0.9625$.

No obvious difference between the cases representing intentional and soft formation ROP changes can be seen from figure 17. As an intentional ROP increase involves increasing the WOB in order to obtain a higher ROP, an additional increase in SPP, as shown in figure A-5, may be seen. When hitting a soft formation, the ROP increases despite of a reduction in WOB. Based on this, the intentional ROP change data points should express a larger pressure change than the soft formation data points. Such a difference is not observed in figure 17, indicating that the cause of ROP change has little impact on ΔSPP for these cases.

K 470 8 ½" section

In the 8½" section of well K 470, there were identified a total of 10 cases of stringers, thin stringers and soft formations. Similar to the 8 ½" section in well K 480, the ROP

and SPP changes appear to be higher in the stringers than the thin stringers. A fitted curve on the form $y = ax$ was also used for this section, and it can be observed from **figure 18** that the points are spread more than in the K 470 8 ½" section. Curve fitting gives a slope of

$a = 0.153 \ \frac{\text{bar}}{\text{m/h}}$, with $R^2 = 0.8784$

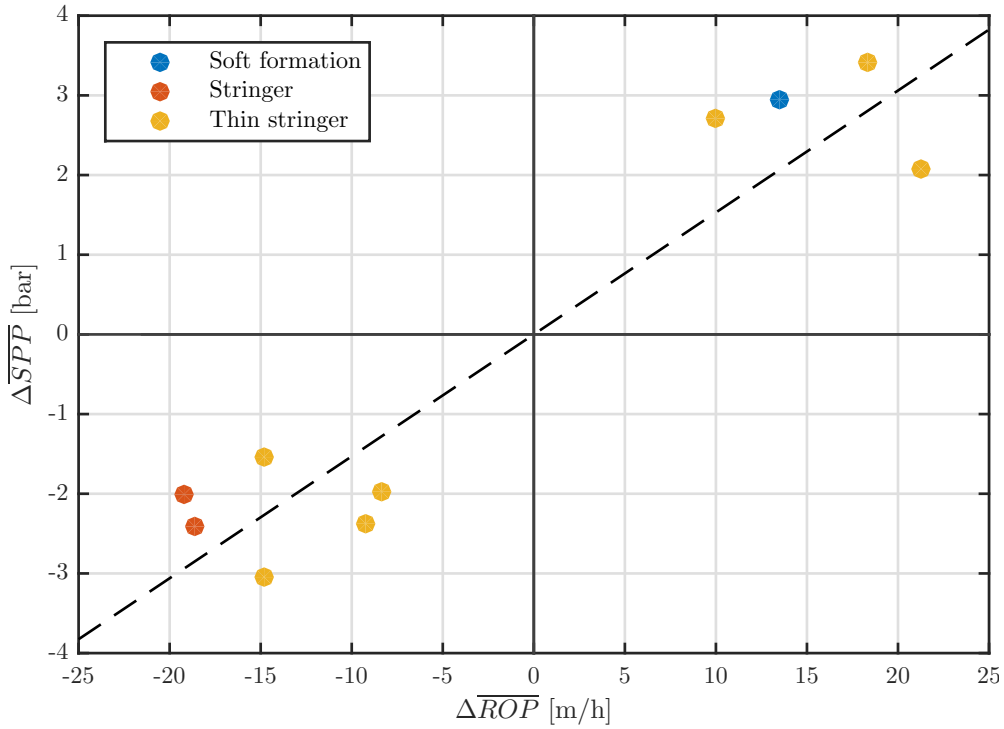

Figure 18: Change in SPP vs. change in ROP in K 470 8 ½" for the pressure phenomena stringer, thin stringer and soft formation. The fitted line has a slope $a = 0.153 \ \frac{\text{bar}}{\text{m/h}}$, with $R^2 = 0.8784$.

The number of data points from the phenomena stringer and thin stringer is not sufficient for a trend to be recognized, or to conclude that there is no difference in pressure response between these two. The difference between drilling through a thin stringer and a stringer is the period of time which the ROP remains low. The observed effect in the SPP is close to immediate when hitting both stringers and thin stringers. This indicates that the effect causing the change in SPP is a bit and/or BHA effect, and not caused by cuttings transportation higher up in the well. Figures 17 and 18 indicate that the cause of the change in ROP, *i.e.* stringer, soft formation or intentional change, does not affect

the extent of the resulting pressure response. The points are, seemingly, distributed along the curve fit line without there being any clear correlation between the category of ROP change and corresponding SPP.

K 470 12 ¼" section

The 12 ¼" section is drilled using Managed Pressure Drilling (MPD) with a positive displacement motor (PDM), an 8 ½" PDC bit and a 12 ¼" reamer wing. Three cases of intentional ROP change, and five cases related to formation hardness were found: two soft formation and three thin stringers. The cases from the 12 ¼" section are plotted in **figure 19**. Although the number of cases in this section is sparse, a trend between formation hardness related response and intentional ROP change can be observed.

Linear curve fitting of the the formation related and intentional cases respectively gives:

$a = 0.1666 \ \frac{\text{bar}}{\text{m/h}}$, $R^2 = 0.8446$, and

$a = 0.3842 \ \frac{\text{bar}}{\text{m/h}}$, $R^2 = 0.9062$.

The use of MPD, mud motor and reamer wing separates the section from the other evaluated sections in three major ways. First, the MPD technique involves using a back pressure pump, constantly adjusting the annular pressure. Changing the back pressure may affect the SPP, and can therefore disturb the drilling data in the intervals relevant for analysis. The number of intervals suitable for plotting and further analysis from this section is limited to 8 examples.

Mud flow with cuttings generated from the 8 ½" bit in front will have to flow past the reamer wing, which may result in an additional pressure loss. A second pressure loss can occur over the reamer wing, as it restricts the flow area between the bit and the rest of the BHA. This could give a larger ΔSPP per unit of ΔROP, since the mud and cuttings must flow through the reamer wing. Cuttings will also be generated at the reamer wing, which may contribute to restrict the flow area further.

As a mud motor is used for drilling the 12 ¼" section, a higher SPP may occur when the torque on the bit is high. Torque and weight on bit are closely related, as a higher WOB increases the friction forces between bit and the formation being drilled, resulting

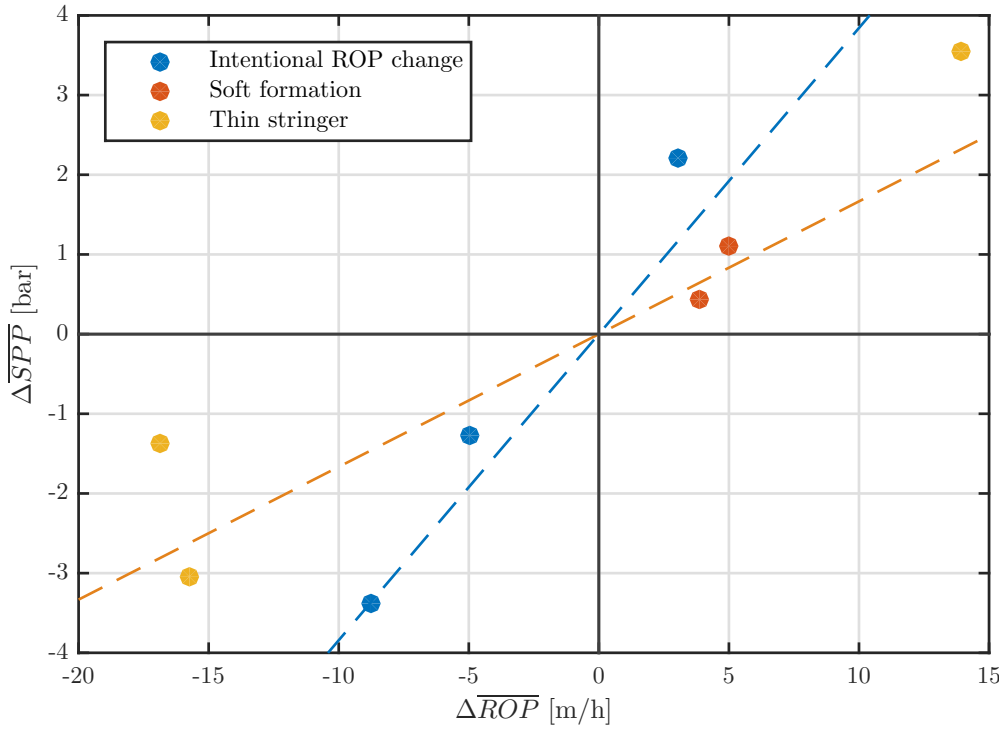

Figure 19: Change in SPP vs. change in ROP in K 470 12 ¼" for the phenomena intentional ROP change, thin stringer and soft formation. The fitted line for intentional ROP change has a slope $a = 0.3842\ \frac{\text{bar}}{\text{m/h}}$, with $R^2 = 0.9062$. The formation related ROP change has a fitted line with slope $a = 0.1666$ and $R^2 = 0.8446$.

in a higher torque. An increase in WOB in a homogeneous formation would result in an increase in ROP. High SPP changes from intentional ROP changes are therefore expected, as effects from both cuttings and the mud motor may appear. When hitting a hard stringer, the WOB and torque would increase while the ROP would decrease. A reduced amount of cuttings may cause a decrease in SPP, while an increase in WOB and torque acts out as a higher pressure increase, masking the effect of cuttings.

The pressure effect from the intentional ROP changes in figure 19 seems greater than those seen from soft formation and stringers. The slope of the intentional pressure response is over two times greater than the slope of the formation related pressure changes. This supports the expected effect from using a mud motor.

The curve fit model used does not take WOB into account, which may be a problem in cases where PDM is used: In two hypothetical cases where the ROP decrease is equal,

the increase in WOB can be different for the two cases, due to different hardness of the formations. In order to predict the pressure response when using PDM, a curve fit of the type $\Delta\text{SPP} = f(\Delta\overline{\text{ROP}}) + g(\Delta\overline{\text{WOB}})$ can be used, where f is a function of change in ROP and g is a function of change in WOB. In such an expression, the first term would represent the pressure response from alteration in cuttings concentration, while the second term would express the pressure effect from the PDM. The number of cases in this section is sparse, with tree and five cases only. As change in WOB is not included in our fitted curves for pressure responses from stringers and intentional ROP, the empirical equations obtained will not accurately predict the change in SPP from cuttings. It does, however, seem possible to distinguish between the data points where the PDM effect is present and where the pressure response is mainly caused by cuttings.

K 470 17 ½" section

Because of few intervals with stable critical parameters, only 6 examples were identified in the 17 ½" section. These examples were all classified as intentional ROP changes. Linear curve fit of the plotted data gives a line with slope:

$a = 0.1762 \ \frac{\text{bar}}{\text{m/h}}$, with $R^2 = 0.9215$.

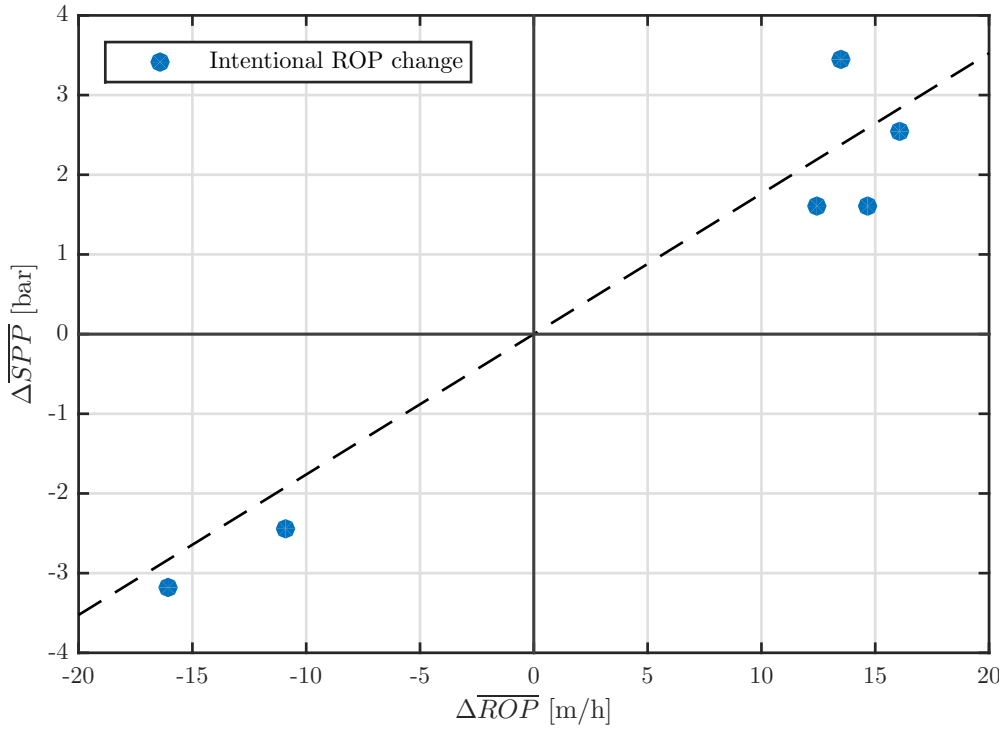

Figure 20: Change in SPP vs. change in ROP in K 470 17 ½" for the phenomenon intentional ROP change. The fitted line has a slope $a = 0.1762\ \frac{\text{bar}}{\text{m/h}}$, with $R^2 = 0.9215$.

Summarizing plot

It has not been observed a significant difference between the cause of ROP change and the pressure response in the 8 ½" sections, as seen in figures 17 and 18. The ROP cause is therefore ignored when comparing the sections with each other. The data points from the four analysed sections are plotted in **figure 21**. The points, with their respective fitted curves, are colour coded by section. Except for the 12 ¼" section, it is distinguished between the causes of the ROP change. The intentional ROP change from the 12 ¼" section has the steepest slope, followed by the 17 ½" section. The other points from the 12 ¼" section has the third highest slope, followed by the K 470 8 ½" section and the K 480 8 ½" section. The empirical parameters of all the analysed sections are summarized in **table 5**, including 95% confidence interval, coefficient of determination R^2, and number of cases N.

Table 5: Summary of empirical equations from curve fitting on the form $\Delta\overline{\text{SPP}} = a \cdot \Delta\overline{\text{ROP}}$. a is the slope of the curve, with 95% confidence intervals in $\frac{\text{bar}}{\text{m/h}}$. R^2 is the "coefficient of determination" and N is the number of data points.

Well	Section	a	Conf. int.	R^2	N
K 470	17 ½"	0.1762	(0.1188, 0.2336)	0.9215	6
	12 ¼" (intentional)	0.3842	(0.0315, 0.7370)	0.9062	3
	12 ¼" (stringers)	0.1666	(0.06764, 0.2656)	0.8446	5
	8 ½"	0.1530	(0.1103, 0.1958)	0.8784	10
K 480	8 ½"	0.1017	(0.08906, 0.1110)	0.9625	15

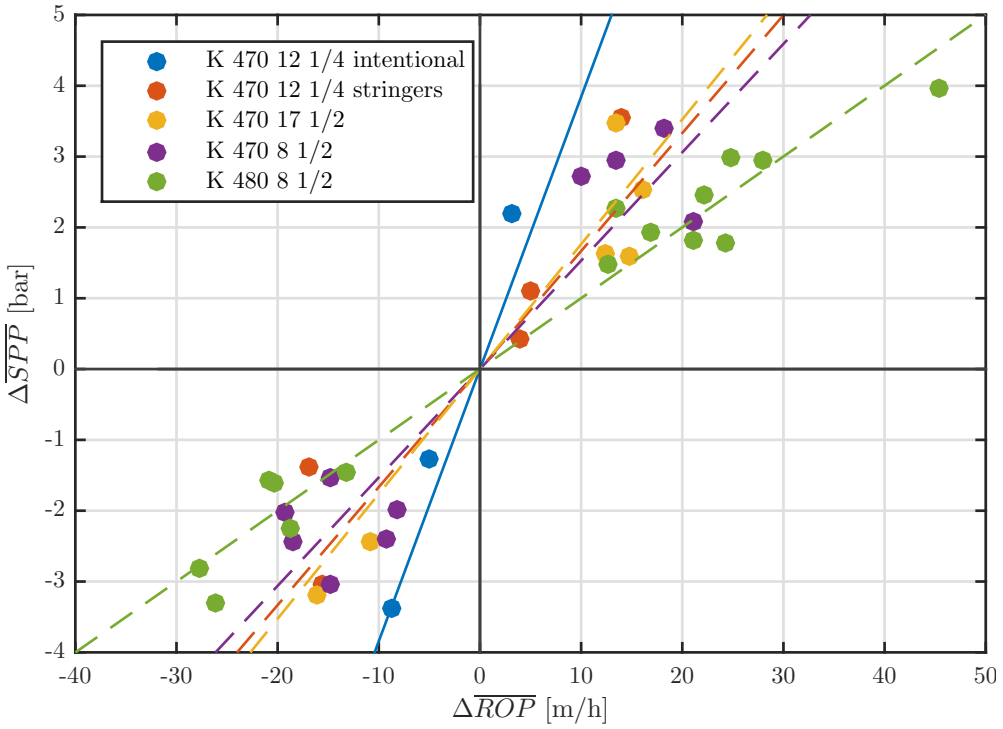

Figure 21: Change in SPP vs. change in ROP for all sections. The curve fit is grouped section without differentiating between causes of the SPP change, except from the 12 ¼" section. The slopes are summarized in table 5. The dashed orange line represents the fitted curve of thin stringers and soft formations in the 12 ¼" section, whereas the solid blue line represents the fit of the intentional ROP changes.

Section K 480 8 ½" has a lower slope than the K 470 8½" section. A possible explanation

may be the generally higher pumping rate used in the interval, compared to the K 470 8 ½" section. Seen from equation 23, an increase in flow rate q_m, will yield a lower concentration c_{bit}. Assuming the concentration of cuttings affects the SPP significantly, the over all lower c_{bit} caused by the generally higher q_m in K 480 8½" can be the reason for the low slope.

In **figure 22** the change in cuttings concentration has been calculated based on $\Delta\overline{\text{ROP}}$ and q_m, and plotted against $\Delta\overline{\text{SPP}}$. By plotting $\Delta\overline{\text{SPP}}$ against the calculated Δc_{bit}, the fitted curves for all sections have a more similar slope. The intentional ROP increases in the 12 ¼" section still differs from the rest of the sections.

The slope, confidence interval and coefficient of determination for the each curve fit from figure 22 are summarized in **table 6**. The coefficient of determination is slightly lower for the K 470 17 ½" and K 480 8 ½" sections in table 6 compared to the R^2 values from table 5, while it is slightly higher for the K 480 8 ½ in figure 21. There is no consequent difference in the goodness of fit for $\Delta\overline{\text{ROP}}$ or $\Delta\bar{c}$ vs. $\Delta\overline{\text{SPP}}$, as seen from R^2 in table 5 and table 6. This may be a consequence of few data points.

The amount of data is not large enough to clearly identify a correlation between the slope a and the specific parameters of each section. However, based on the data plotted in figure 22, a relationship between ΔSPP, $\Delta\overline{\text{ROP}}$, q_m and d_o can be suggested:

$$\Delta\text{SPP} = a\Delta\bar{c} \approx a\frac{\Delta\overline{\text{ROP}}}{q_m}\frac{\pi}{4}d_{\text{bit}}^2 \tag{53}$$

Table 6: Summary of empirical equations from curve fitting on the form $\Delta\overline{\text{SPP}} = a \cdot \Delta\bar{c}$. a in $\frac{\text{bar}}{\%\text{ cuttings}}$, with 95% confidence interval and R^2

Well	**Section**	a	**Conf. int.**	R^2	N
K 470	17 ½"	3.441	(2.329, 4.553)	0.9226	6
	12 ¼" (intentional)	8.609	(0.6752, 16.54)	0.9055	3
	12 ¼" (stringers)	3.675	(1.470, 5.880)	0.8420	5
	8 ½"	4.335	(3.140, 5.530)	0.8812	10
K 480	8 ½"	3.441	(3.062, 3.820)	0.9623	15

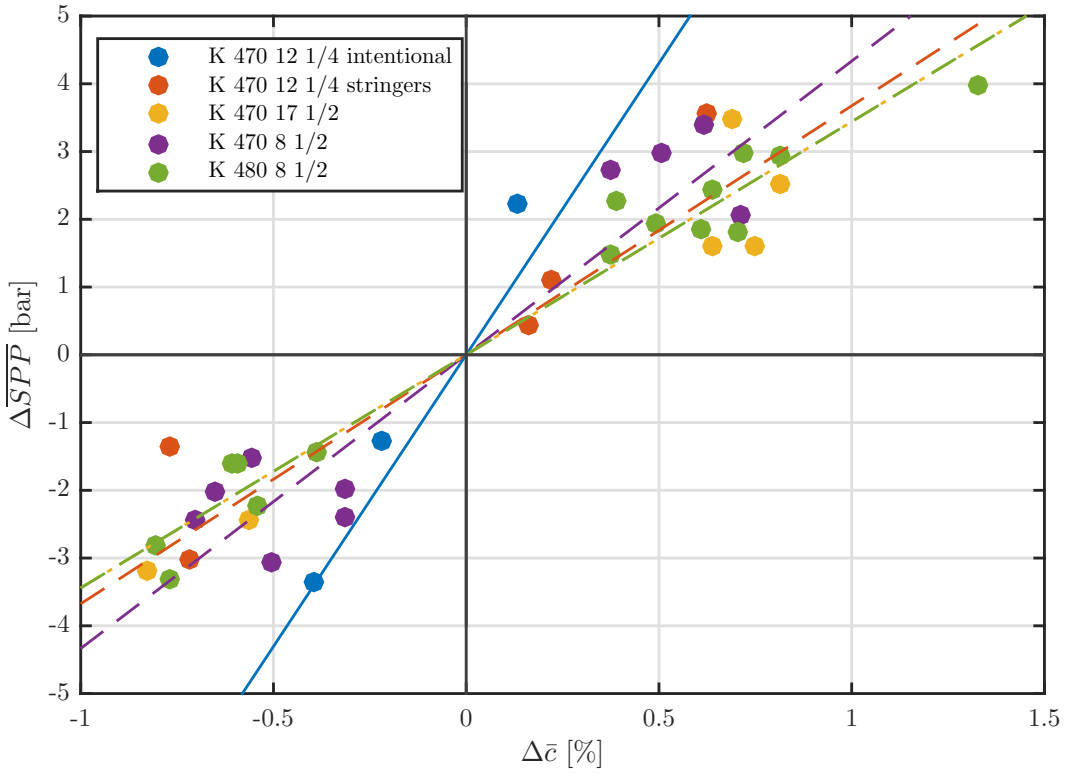

Figure 22: Change in SPP vs. change in cuttings concentration for all sections. The fitted curves are grouped by section, without differentiating between phenomena. Note that the fitted curve for section K 470 17 ½" and K 480 8 ½" have equal slopes. The slope of the fitted curves, along with the coefficients of determination R^2 are summarized in table 6.

More data is needed in order to verify and specify this equation. By including data from other sections, potential influencing parameters and effects can be identified, such as different formation types, BHA set-ups and well trajectories.

5.3 Simulation of pressure responses caused by change in ROP

The rapid response in SPP from a change in ROP indicates a cuttings effect around bit and/or BHA. In order to investigate if these pressure responses are caused by increased viscosity and density of the fluid through annulus around the BHA, the additional pressure loss due to suspended cuttings in the mud flow is simulated. By calculating a pressure loss over the BHA for different cuttings concentrations, the pressure effect of cuttings passing the BHA can be estimated. The friction pressure loss over the BHA,

Δp_{BHA} is calculated by summing the pressure loss over each component i in the BHA, as given in equation 54:

$$\Delta p_{\text{BHA}} = \sum_i \Delta p_f(f_i, L_i, d_{\text{hyd},i}, v_i) = \sum_i \frac{f_i}{2} \frac{L_i}{d_{\text{hyd},i}} \rho v_i^2 \tag{54}$$

f_i, L_i, $d_{\text{hyd},i}$ and v_i represent friction factor, length, hydraulic diameter and velocity of each component in the BHA. Information about length and outer diameter for each component is listed in table E-1 - E-4 in Appendix E. An outline of the BHA used to drill the K 470 17 ½" section is given in **figure 23**. The friction pressure loss over each BHA component in K 470 17 ½", $\Delta p_{f,i}$, including the hydraulic friction, here defined as $\frac{\Delta p_{f,i}}{L_i}$, is plotted in **figure 24**.

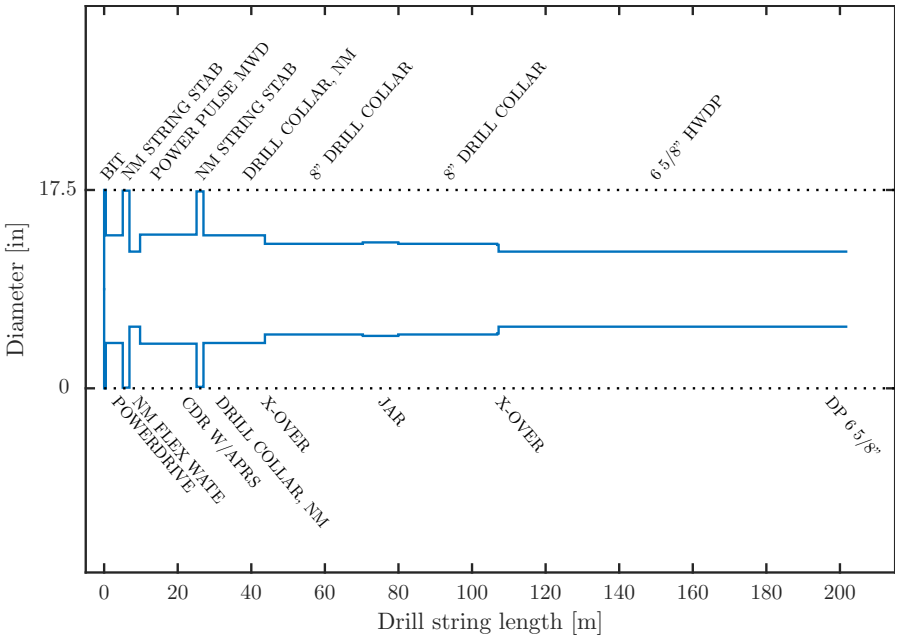

Figure 23: Outline of the BHA used in the 17 ½" section in K 470. The length of the BHA is approximately 110 m, followed by 85 m of heavyweight drill pipe.

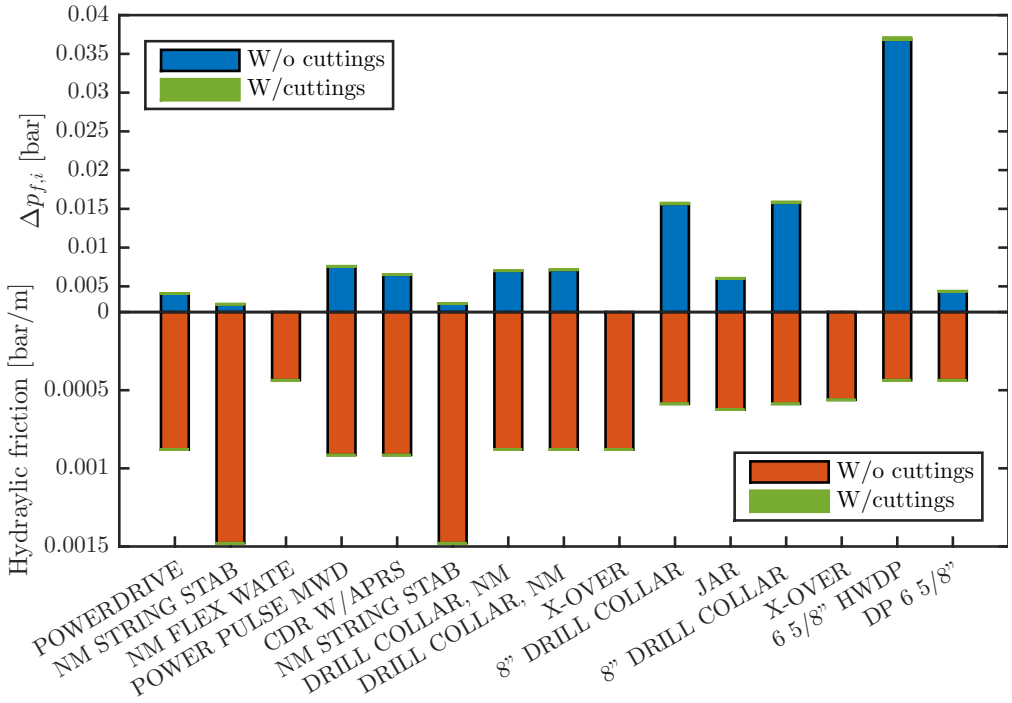

Figure 24: Pressure loss over each component and hydraulic friction in K 470 17 ½". Green colour indicates pressure loss and hydraulic friction with a cuttings concentration of 1%.

The total pressure loss over the 17 ½" BHA without cuttings is 0.0772 bar, while with 1% cuttings, the pressure loss is 0.0778 bar. This is based on a flow rate 5000 lpm and a mud weight 1300 kg/m^3. For section K 470 8 ½" the pressure loss over the BHA is calculated to 3.45 and 3.47 bar for 0% and 1% cuttings respectively, based on a flow rate of 2100 lpm and mud weight 1700 kg/m^3.

In order to simulate the observed ΔSPP found in figure 22 as a function of Δc, the friction pressure loss over the BHA is calculated with and without cuttings. Equation 55 expresses the difference in pressure loss over BHA between a cuttings concentration c and without cuttings.

$$\Delta p_{\text{BHA}}(c) - \Delta p^0_{\text{BHA}} = \sum_i \frac{f_i(c)}{2} \frac{L_i}{d_{\text{hyd},i}} \rho(c) v_i^2 - \sum_i \frac{f_i^0}{2} \frac{L_i}{d_{\text{hyd},i}} \rho^0 v_i^2 \tag{55}$$

$\Delta p_{\text{BHA}}(c)$ is the friction pressure loss over BHA at cuttings concentration c, while Δp^0_{BHA} expresses pressure loss over BHA without cuttings. Fluid density is a function of cuttings

concentration $\rho(c)$ and given by equation 24, while the friction factor $f(c)$ is a function of both density $\rho(c)$ and effective viscosity $\mu(c)$, given by equation 33.

When calculating the difference in pressure loss from cuttings over BHA for a cuttings concentration $c \in [0, 1]$ %, the calculated pressure response from equation 55 can be compared to the empirical equations from observed pressure responses, $\Delta\overline{\text{SPP}}$, found in figure 22. The calculated results are plotted in **figure 25**, including the observed pressure response for the 17 ½" section.

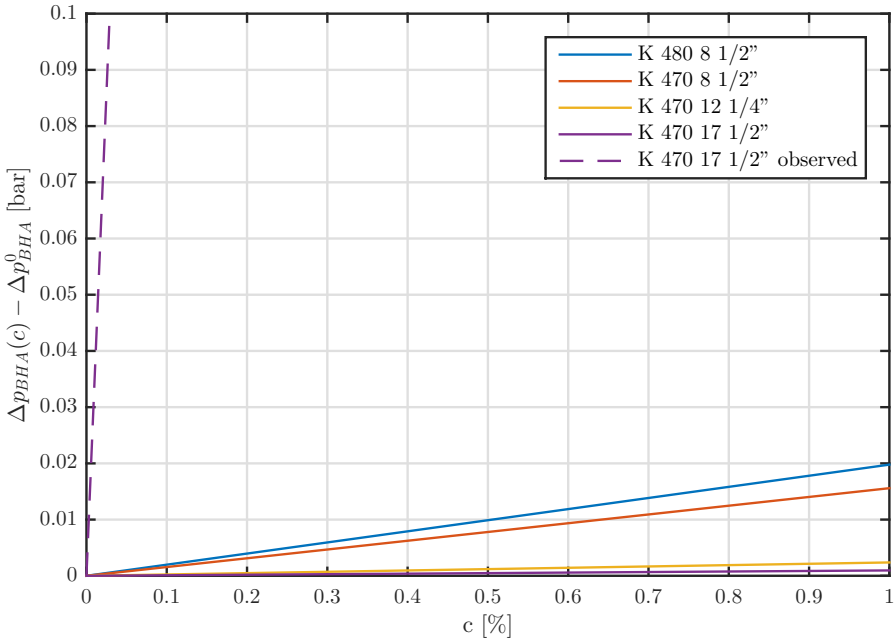

Figure 25: Difference in pressure loss over BHA as a function of ROP. The simulated pressure differences (solid lines) are highest in the tight 8 ½" sections, and decreases with increasing hole size. The calculated pressure effect for the 17 ½" section (solid purple line) is over 3600 times greater than the observed effect (dashed purple line).

The pressure responses calculated from equation 55 have a slope $a = 0.9555 \cdot 10^{-3}$ [bar/%] for section K 470 17 ½" and $a = 0.0198$ [bar/%] for section K 480 8 ½". In comparison, the empirical equations found in section 5.2 have both a slope $a = 3.441$ [bar/%]. The observed effects are 3600 and 174 times greater than the calculated pressure effects for sections K 470 17 ½" and K 480 8 ½" respectively. The highest calculated pressure responses are seen in the tight 8 ½" sections, where there is little space between the BHA and the borehole wall, whereas the smallest calculated effects are seen in the open

17 ½" section. The simulated pressure response from flow over BHA due to increased mud weight and viscosity is too small to explain the observed pressure responses alone. This may indicate that an additional effect is present.

6 Discussion

6.1 Quality of the data

Measurement errors may occur in all measured data. In some cases it is observed an increase in SPP just before a corresponding increase in flow rate. This may be explained by a measurement error in a flow meter, and causes the increase in flow to occur later than the SPP. The possibility of such errors and delays has been considered when evaluating the data.

Parameters calculated from measurements at surface describing down hole conditions may be incorrect. WOB, as given in the data set, is usually calculated from the hook load, corrected for the friction force between the drill string and outer annular wall. The part of the string weight being supported by friction is difficult to estimate accurately. It is therefore likely to believe that the calculated WOB in the data will deviate from the actual WOB acting on the formation.

The ROP is calculated from change in measured depth of the wellbore over time, which is given by the position of the bit. The position of the bit is calculated from block position and corrected for compression or extension of the drill string. As it is an calculated parameter, inaccuracies may be present.

Data for torque is missing for several cases. Although this parameter is not critical to the analysis, it may provide information about hole cleaning and pack-off tendencies. Cases with corrupt torque data can be incorrectly interpreted as effects from change in ROP. There is a possibility that such cases could be better interpreted by having complete torque data available.

6.2 Quality of the empirical equations

The cases used for analysis in this thesis are manually selected based on our observation. An objective approach has been a strived for while analysing the data. Confirmation bias can, however, be a source of error whenever data is selected manually. Only cases that has a change in SPP that fits our hypothesis are included in order to investigate the effect of cuttings on SPP. Although there are few cases where the cause of the change

in SPP is not understood, important aspects of the correlation between change in SPP and ROP could be overseen by not analysing these. The consequences of this could be both inaccurate empirical equations and less to obtained insight and knowledge.

There is a limited amount of intervals suitable for analysis, due to frequent changing of critical parameters by the drilling operator. Few cases within each section reduces the accuracy of the empirical equations. The confidence interval of the fitted parameters, in this case the slope a, becomes too large. The number of cases within each phenomenon of ROP change, such as stringers and soft formations, is low. More cases within each group could further highlight the group's effect on SPP.

In this thesis, data from four sections from two different wells is analysed. The low number of sections may prevent trends in the slope, a, between the different sections to be discovered. Correlations between parameters such as rheology, hole size and BHA design could give further insight in what is affecting the slope of the fitted curves. Both the analysed wells are from the same oil field and company. By including data from other fields, operators and contractors, further correlations and deeper understanding could be obtained.

The empirical equations are not tested on other wells and sections. Although the fit is good for data within each section, the accuracy of predicting the pressure response in cases from different wells is unknown. It can therefore only be concluded within the analysed data sets.

6.3 Possible explanations to the SPP response to change in ROP

An empirical correlation between SPP and ROP is observed, and change in cuttings concentration is believed to be the cause of the pressure effect. The exact cause of the change in SPP cannot be determined with certainty from the data itself, as both parameters are observed phenomena. The data does not describe in what way the generation of cuttings increases the pressure. With basis in theory, observation and deduction of possible causes, plausible explanations can be found.

A close correlation between WOB and SPP is present in several cases, and an increased WOB could theoretically be the mechanism causing an SPP increase. In the 8 ½" section of both well K 470 and K 480, it is observed that WOB often increases as a hard stringer

is encountered, while the SPP decreases in correlation with ROP, as shown in figure 13. If an increase in WOB would be the cause of increased SPP, a pressure increase would be expected when encountering a hard formation where WOB increases. This is however not supported by observations, and the WOB alone is not likely to be the cause of the pressure increase in these sections. In the K 470 17 ½" section, it is not possible to exclude WOB as a causing factor, as no cases with hard formation are found. SPP increase is only observed during an operator induced ROP increase caused by increased WOB in this section.

Suspended cuttings in the mud may increase SPP, as the fluid density increases. Calculations in section 3.4.5 show that in order to observe a significant increase in SPP, a major part of the vertical section must contain suspended cuttings. This effect takes place over time as fluid in the wellbore is displaced. Axial dispersion prolongs this effect further and a pressure increase would be gradual. The rapid pressure changes observed in figure 13 - 15 can therefore not be explained by neither the additional hydrostatic nor friction pressure loss caused by suspended cuttings.

Suspended cuttings may increase the effective viscosity due to particle interaction. Minerals from formations such as clay may change the composition of the drilling fluid, increasing its viscosity further. Einstein's equation (33), describing effective viscosity in suspensions, is used in calculations in section 3.4.5. These calculations indicate that the combined effect from density and viscosity in friction pressure loss is not sufficient to explain the observed results. The vast majority of the cases shows a response in SPP to change in ROP within a couple of minutes, indicating that the change in SPP is likely to occur in the annulus around bit and BHA. The simulations in section 5.3 show pressure effects too low to explain the rapid changes observed in SPP. This may, however, indicate that Einstein's equation of effective viscosity is not a good description of viscosity changes during drilling.

Increase in viscosity and density is not sufficient to explain the observed pressure effects. The applied theory or its underlying assumptions may not be applicable to the conditions around the bit and BHA during drilling. Cuttings may accumulate in front of tight passages, such as the bit shoulder or stabilizers, where cuttings are prevented to pass at a high rate. This could cause a thick slurry of cuttings and mud to form in front of the bit shoulder, with a high density and particle interaction, causing the effective viscosity

to increase. Cuttings particles in this case would have a positive slip velocity, causing mud to pass through the accumulated cuttings in suspension. The cross sectional flow area through this highly permeable blockage would be low, whereas the wetted perimeter of the cross section would be high. This would result in a small hydraulic diameter and a high velocity of the mud, in addition to a higher density and viscosity, causing the friction pressure loss to increase.

This hypothetical cuttings "plug" would continuously be washed out in one end, while newly generated cuttings would be accumulated in the other, causing a slightly higher retention time of cuttings over the BHA. When the ROP is decreased, a lower feed rate of cuttings would cause the length of the plug or its concentration to decrease, causing a rapid decrease in the pressure loss over the bit, annulus and BHA.

As described in section 3.4.5, reduction of the cross sectional flow area will cause a significant pressure loss. In order for a pressure loss of the magnitude observed to be a result of bedding, the majority of the produced cuttings must be rapidly deposited, with a limited bed length and a significant bed height. Similarly, rapid erosion of beds must take place after a reduction in ROP, in order to explain the observed pressure decreases. The change in bed size must occur over a short period of time in accordance with the duration of the pressure change, typically 1-3 minutes. Simulation of cuttings deposition is not studied or performed in this thesis. Formation and erosion of cuttings beds related to change in ROP can therefore not be ruled out as a contributing cause of change in SPP.

6.4 Further work

In addition to using recorded drilling data, information about rheology, geology and cuttings should be considered implemented to a larger extent in the analysis. Geology is one of the areas where information has been limited during data analysis. Detailed geological information about the sections would strengthen the quality of the analysis and could contribute to a better understanding of the generation and transport of cuttings. This enables the possibility of studying whether the formation type affects the SPP response from change in ROP.

Data from sections where downhole pressure measurement equipment has been used

could offer valuable information about cuttings transport. It could also be used for correcting and calibrating the empirical models. The possibility for including the effect of WOB on SPP should also be considered when developing a prediction model.

Software for pattern recognition that identifies relevant intervals can be implemented to substitute the manual identification of intervals used in this thesis. Critical parameters and other conditions for distinguish interesting intervals from non-relevant data must be specified. Implementing such software is an essential step if real time drilling data is to be analysed live.

In order to investigate how cuttings are transported along the BHA and drill string, a lab experiment could provide valuable knowledge. Studies where cuttings transport is observed at various flow rates, rotational speeds, inclinations, cuttings size and concentrations, and BHA configuration could offer a better understanding of the actual conditions regarding cuttings transport and accumulation during drilling.

7 Conclusion

A correlation between changes in ROP and SPP is observed in all four sections. Moreover, an increase in ROP tends to result in a proportional increase in SPP, despite the change in WOB. This thesis sheds light on these effects.

An empirical equation on the form $\Delta\text{SPP} = a\Delta\text{ROP}$ is found for each section from curve fitting. Variations in the slope, a, between the fitted curves for the different sections are observed. A consistent correlation between variations in a and the respective section is not identified, and data from more wells is needed to investigate such a section-based dependency.

Theoretical calculations indicate that the pressure response to change in ROP is not solely caused by either a change in viscosity, density or cuttings weight in the inclined or vertical section. Based on analysis of data and simulations, other and unknown effects may be present in order to explain the observed pressure responses, or the presented theory around this topic is insufficient. The reason for the observed change in SPP, and especially the magnitude of the effect, is not fully understood.

The cause of the change in ROP, such as stringers, soft formation or an operator induced change in ROP, does not seem to affect the response in SPP unless a downhole mud motor is used. Analysis of additional data from other wells may contribute to verify this observation.

Nomenclature and Acronyms

Roman Symbols

A	Cross sectional area of the wellbore
A_{ann}	Cross sectional area of annulus
A^0_{ann}	Reference cross sectional area of annulus
A_b	Cross sectional area of cuttings bed layer
A_h	Cross sectional area of homogeneous layer
A_p	Cross sectional area of drill pipe
c	Cuttings concentration or cord length of cuttings bed layer
c_{inc}	Cuttings concentration in the inclined section
C_{RSS}	Constant for calculating pressure drop over RSS, specified by producer
c_{vert}	Cuttings concentration in the vertical section
c_{bit}	Cuttings concentration at the bit
d_{hyd}	Hydraulic diameter
d^*_{hyd}	Relative hydraulic diameter
d^0_{hyd}	Reference hydraulic diameter
d_c	Diameter of cuttings particle
d_i	Inner diameter of pipe or annulus
d_o	Outer diameter
d_p	Outer diameter of drill pipe
f	Darcy-Weisbach friction factor
F_b	Ratio of cross sectional cuttings bed area to wellbore area $\frac{A_b}{A}$
f_c	Flow resisting-factor for interaction between cuttings particles

g	Gravity of Earth
h_{inc}	Vertical height of inclined section
h_c	Cuttings bed height
K	Consistency index in Power law model
K_{bit}	Nozzle loss coefficient for calculating pressure loss over bit
L	Measured depth, length of wellbore segment
N	Number of nozzles in the bit
p_{hyd}	Hydrostatic pressure
p^*_{hyd}	Relative hydrostatic pressure
q_{cling}	Volume rate of mud clinging to the string
q_c	Cuttings influx
q_m	Mud flow rate
R_t	Transport ratio of cuttings in the vertical section
Re	Reynolds number
S	Perimeter of wellbore
s	Arc length of cuttings bed layer
S_{ann}	Wetted perimeter of annulus
S_h	Wetted perimeter of homogeneous layer
S_p	Perimeter of drill pipe
v^*	Relative average velocity
v_{ann}	Average fluid velocity in the annulus
v_{slip}	Slip velocity of a cuttings particle
z	True vertical depth

Greek Symbols

ΔL_b Length of cuttings bed

Δp_{bit} Pressure loss over bit

Δp_{RSS} Pressure loss through the RSS

Δp_f^* Relative hydraulic friction pressure loss

Δp_f^0 Reference hydraulic friction pressure loss

$\Delta p_{s\&s}$ Pressure loss caused by surge and swab

$\dot{\gamma}$ Shear rate

ϵ Absolute roughness of pipe or annulus

ϵ_{rel} Relative roughness of pipe or annulus

μ General fluid viscosity

μ_{eff} Effective viscosity of the wellbore fluid

μ_{pl} Plastic viscosity

μ_m Viscosity of mud

ρ_c Mass density of cuttings

ρ_m Mass density of mud

τ Shear stress

τ_y Yield point, minimum shear stress needed to enable flow.

Acronyms

BHA Bottom hole assembly

BHP Bottom hole pressure

ECD Equivalent circulating density

MPD Managed pressure drilling

PDM Positive displacement motor, downhole mud motor

ROP Rate of penetration

RSS Rotary Steerable System

SPP Standpipe pressure

SRWD Steerable ream while drilling

WOB Weight on bit

References

Ahmed, R. M. and Miska, S. Z. (2008). Experimental study and modeling of yield power-law fluid flow in annuli with drillpipe rotation. Paper SPE 112604 presented at the 2008 IADC/SPE Drilling Conference held in Orlando, Florida, U.S.A., 4–6 March 2008.

Cayeux, E., Mesagan, T., Tanripada, S., Zidan, M., and Fjelde, K. K. (2013). Real-time evaluation of hole cleaning conditions using a transient cuttings transport model. Paper SPE 163492 presented at the SPE/IADC Drilling Conference and Exhibition held in Amsterdam, The Netherlands, 5–7 March 2013.

Cho, H., Shah, S. N., and Osisanya, S. O. (2001). Effects of fluid flow in a porous cuttings-bed on cuttings transport efficiency and hydraulics. Paper SPE 71374 presented at the 2001 SPE Annual Technical Conference and Exhibition held in New Orleans, Louisiana, 30 September–3 October 2001.

Chowdhury, D., Skalle, P., and Rahman, M. M. (2009). Prediction of standpipe pressure using conventional approach. *Chemical Engineering Research Bulletin.* vol. 8, No 1, pp. 7-11.

Crespo, F. E., Ahmed, R. M., Saasen, A., Enfis, M., and Amani, M. (2012). Surge-and-swab pressure predictions for yield-power-law drilling fluids. Paper SPE 138938 presented at the SPE Latin American & Caribbean Petroleum Engineering Conference held in Lima, Peru, 1–3 December 2010.

Hemphill, T., Campos, W., and Pilehvari, A. (1993). Yield-power law model more accurately predicts mud rheology. *Oil and Gas Journal;(United States).* vol. 91, No 34.

Rommetveit, R. and Bjørkevoll, K. S. (1997). Temperature and pressure effects on drilling fluid rheology and ecd in very deep wells. Paper SPE 39282 presented at the 1997 SPE/IADC Middle East Drilling Technology Conference held in Bahrain, 23-25 November 1997.

Skalle, P. (2013). *Drilling Fluid Engineering.* BookBoon.com, third edition.

Schlumberger (2010). Product brochure: PowerDrive Xceed. `http://www.slb.com/~/media/Files/drilling/brochures/directional_drilling/powerdrivexceed.pdf`.

Woods, K., Board, N., Alter, A., and University, P. (1966). *Permafrost International Conference: Proceedings*. Publication (National Research Council (U.S.))). National Academy of Sciences-National Research Council.

Appendices

A Observed effects from change in critical parameters

A.1 Flow rate

The correlation between the flow rate and SPP is evident when reviewing the drilling data. Changes as low as 0.5% in circulation rate can be observed in SPP when plotting drilling data. **Figure A-1** illustrates how the flow rate impacts the SPP during drilling of a stand in an 8 ½" section of well K 480. This demonstrates that the flow rate is a parameter that has a large impact on the pressure loss through the well. It is therefore a critical parameter when selecting intervals for analysis, as described and predicted in section 3.1.

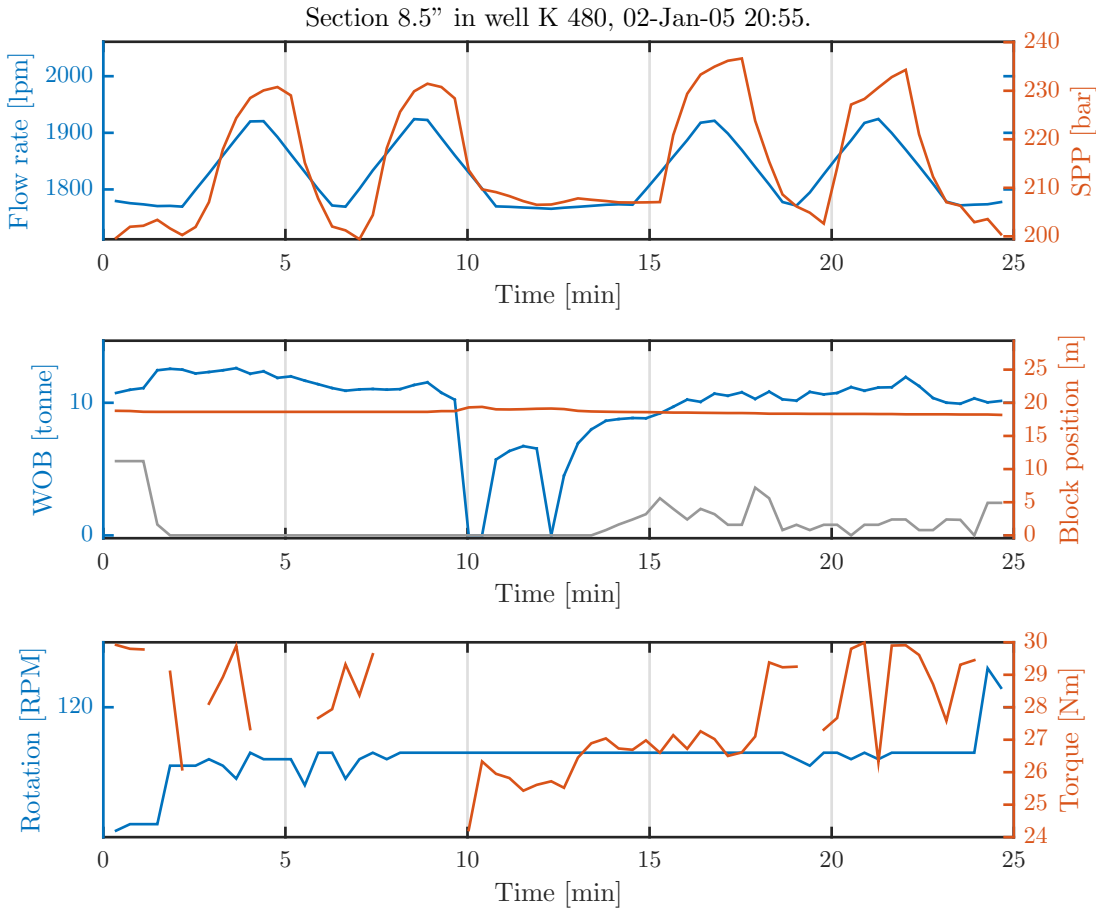

Figure A-1: Figure showing how the SPP immediately alters as the flow rate is changed. The pump rate is changed from approximately 1770 lpm to 1920 lpm at four occasions and the SPP increases with between 23-27 bar accordingly.

A.2 Rotation

Rotation will often influence the SPP, as described in section 3.2. Whether an increase in RPM leads to an increase or decrease in SPP depends on how the annular flow patterns changes. In order to find intervals of good quality to analyse it is necessary to determine how a change in a parameter like rotation will affect the SPP. When evaluating the different sections there were found several incidents of changes in RPM and how they seems to influence the pressure. **Figure A-2** and **A-3** are examples of such cases retrieved from the drilling data of the 17 ½" and 8 ½" section respectively.

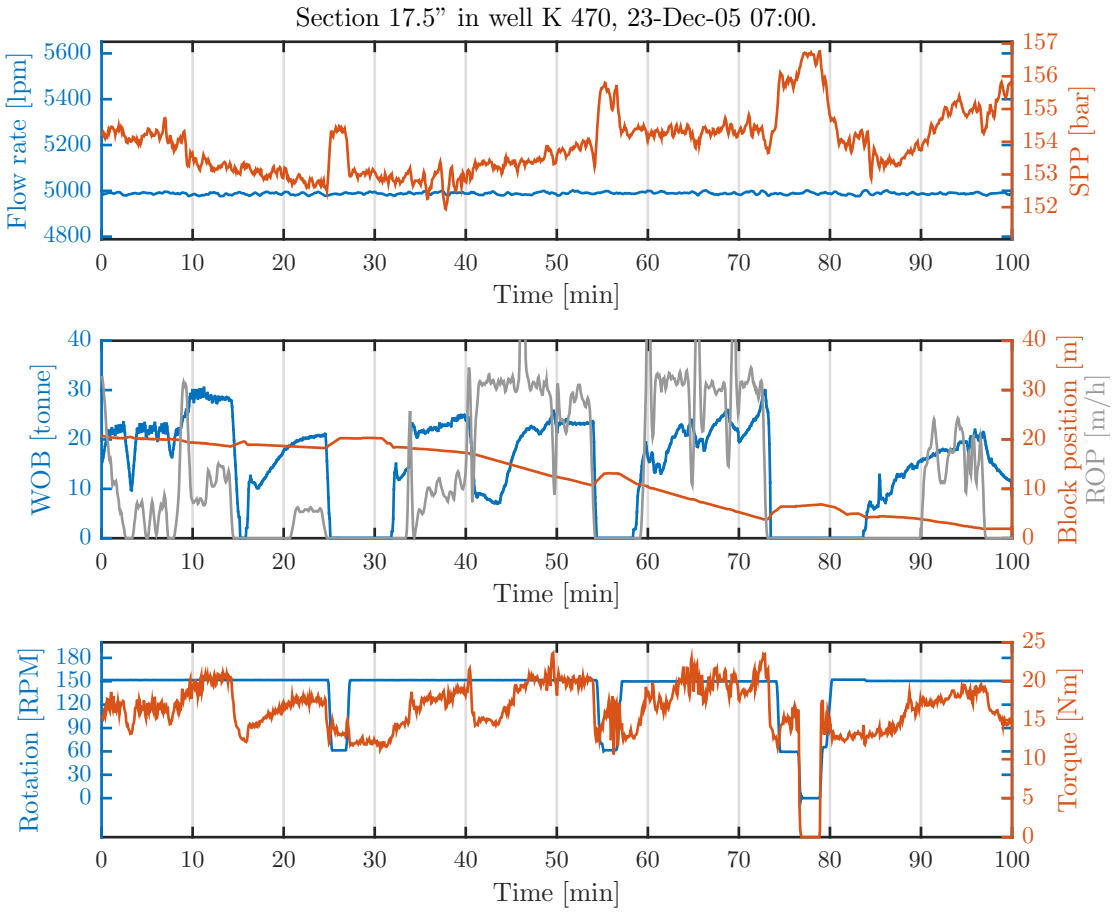

Figure A-2: 17 ½" section: SPP increases as the rotation speed is lowered from 150 to 60 RPM at 25 and 55 minutes into the interval. At 76 minutes the RPM in lowered to 0, giving an even higher pressure increase.

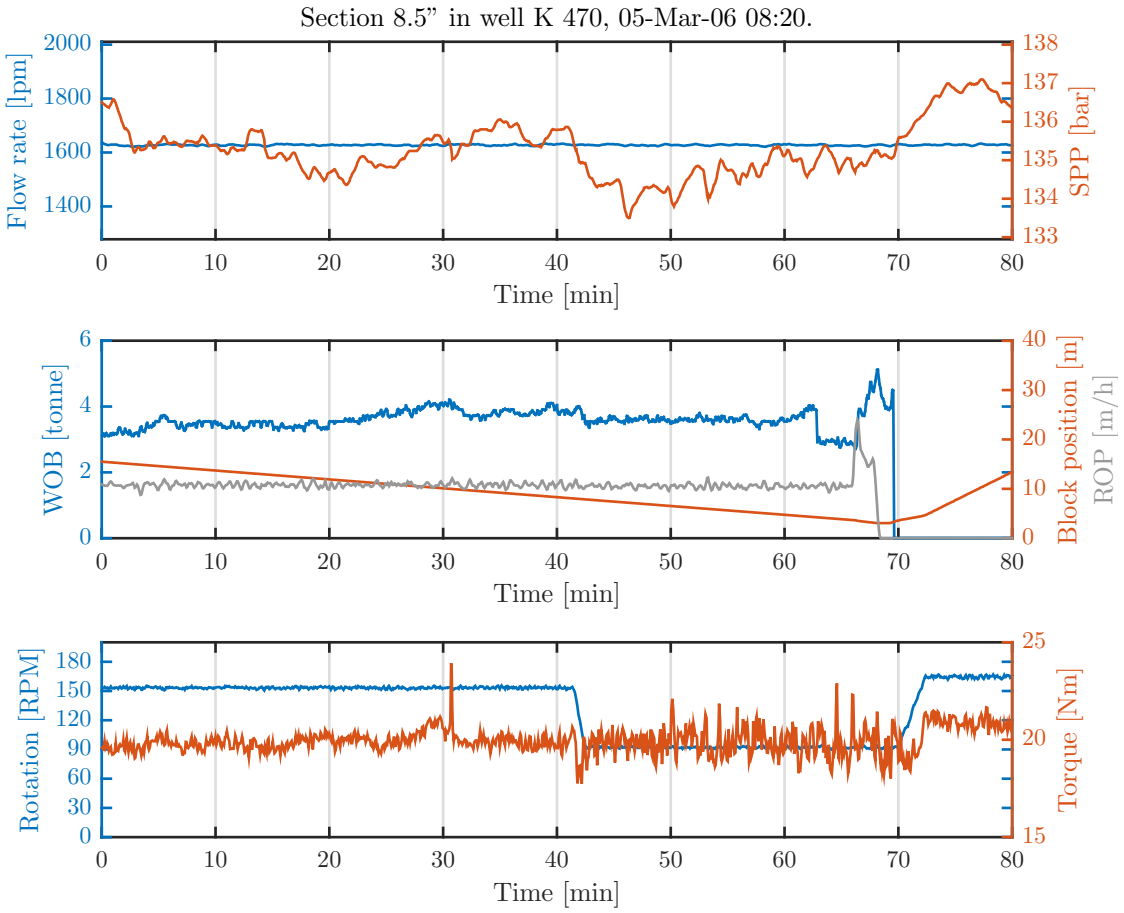

Figure A-3: K 470 8 ½" section: It can be observed that the SPP decreases as the RPM is lowered from 150 to 90 rpm at 41 minutes into the interval. SPP is slightly increasing 10 minutes after the RPM reduction, and seems to reach equilibrium at 60 minutes. This may be a result of increasing cuttings bed height, as string rotation is reduced.

Figure A-2 shows drilling data from the 17 ½" section where the RPM is lowered on three occasions, at 25, 55 and 76 minutes into the interval. Although there are changes in block position and WOB during the interval, the change in SPP clearly matches the alterations in rotational speed. The flow rate is kept constant through the interval. The pressure increase is approximately 1.7 bars on the two first increases where the rotational speed goes from 150 to 60 rpm. The SPP increases 2.3 bars on the third as the RPM decreases from 150 to 60. Figure A-3 plots drilling data from a 17 ½" section where the RPM is lowered from 150 to 90 rpm 42 minutes into the interval and adjusted up again at 70 minutes. As opposed to the interval from the 17 ½" section in figure A-2, the

SPP actually decreases in the interval where the RPM is lowered. In general, it appears to be a trend that the SPP decreases with a decreasing RPM in the 8 ½" section and increases with a decreasing RPM in the 17 ½" section.

There are several plausible explanations to these two different responses to RPM reduction, such as presence of helical flow patterns in the 17 ½" section, causing a lower SPP at high rotation speeds. Differences in rheology of the mud used in the two sections may be an important factor influencing the viscosity of the mud. The average fluid velocity is 0.63 and 1.13 m/s, with an estimated Reynolds number of 6400 and 4500 for the 17 ½" and 8 ½" section respectively, indicating turbulence in both sections.

A.3 Surge and swab

As described in section 3.3, the fastest pipe velocity relevant to analysed intervals in this thesis, is experienced during reaming. The effect of pipe movements from reaming has therefore been analysed in order to obtain an approximation of the alteration in SPP this can lead to. **Figure A-4** shows drilling data for a case of backreaming after drilling a stand in the 8 ½" section of well K 480.

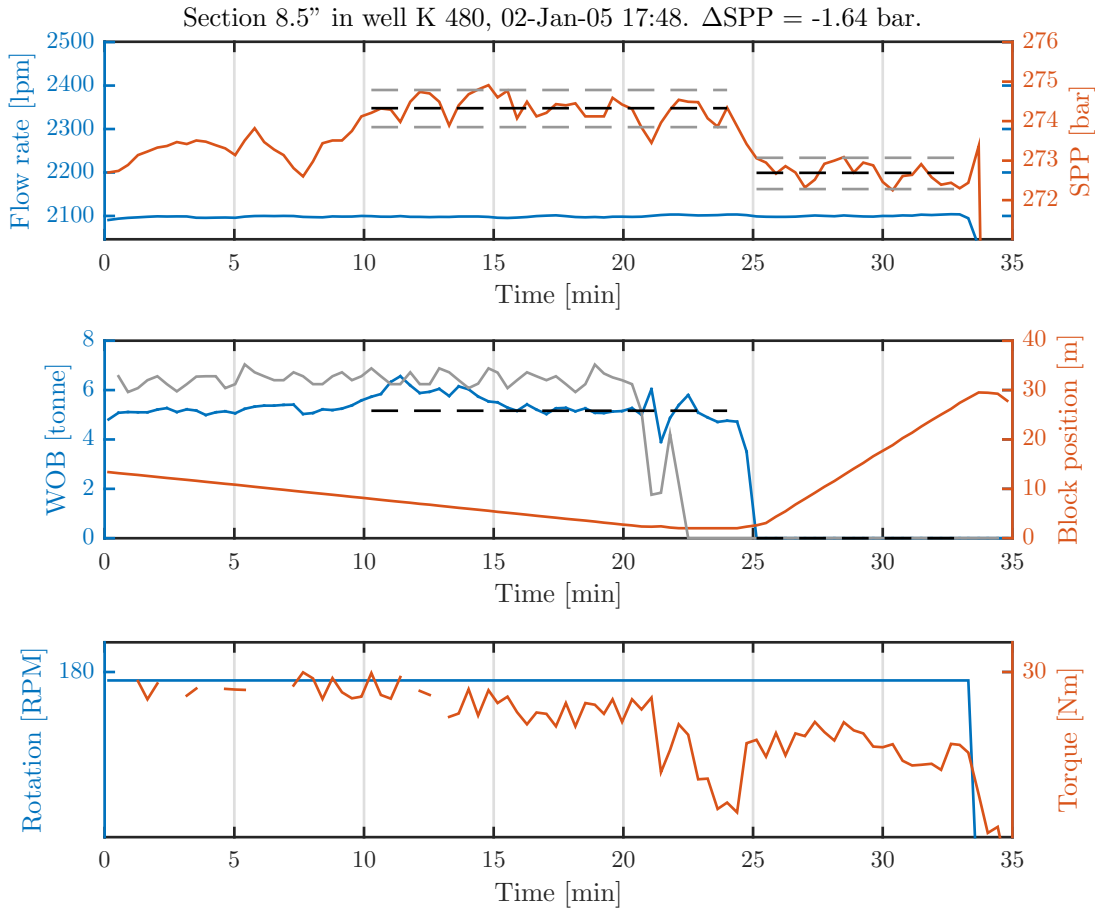

Figure A-4: Reduction in SPP as the drill string is pulled out of the hole at approximately 24 minutes into the displayed interval. The data is gathered during drilling from the 8 ½" section of well K 480. The black dotted line in the upper plot shows the average SPP for the evaluated interval, while the grey dotted line on each side shows the 5% and 95% percentile of the average.

From the plotted interval of drilling data in figure A-4 it can be observed that the average SPP, marked with black lines, decreases with 1.64 bar when pulling of the string is initiated. It can not be determined with certainty whether this pressure decrease is caused by swab from the drill string or some other effect. Examples of such effects might be the release of nozzle blockage as the bit is pulled of bottom. However, the pressure drop in figure A-4 occurs over period of around 2 minutes, indicating that the effect of any nozzle blockage does not account for the entire pressure decrease.

Theoretical calculations of the pressure change can be performed, which might support

that the swab effect causes this. The drill string is pulled with a velocity of approximately 0.029 m/s during the backreaming period, while the flow rate is kept constant at 2100 lpm along with a rotation of 180 RPM. The drilling fluid has a density of 1700 kg/m^3 and a plastic viscosity of 35 cP. According to the drilling report, The BHA is approximately 122 m long, and the drill string consists of 5" drill pipe. During the reaming activity plotted in figure A-4, the bit was at a MD of 5600 m, yielding a 5" drill pipe length of 5478 m. By taking this information into account, the pressure drop including surge or swab can be calculated by using equation 22.

By using the presented equations in section 3.3 and data for the backream situation plotted in figure A-4, the difference in friction pressure loss is calculated to be -0.1 bar. This is only 6% of the observed pressure loss in figure A-4 above. As previously mentioned, several simplifying assumptions have been made when calculating $\Delta p_{s\&s}$, including neglecting of the compressibility and elasticity effects, and the additional friction from tool joints and other geometrical inconsistencies in the hole. This, combined with the possibility of other contributing effects might explain why the theoretical approximation deviates from the observed effect. As mentioned in section 3.3, eccentricity can lower the pressure change from surge and swab by up to 40%. This would yield an even lower pressure change than calculated above, supporting the assumption that the pressure alteration in figure A-4 is not caused by swab effects.

The observed swab effect of pulling the pipe is relatively small. In addition to this, the change in pressure seems to occur only while the velocity of the pipe is changing, and stabilizes as the velocity is kept constant. If a surge and swab effect of considerable size were to occur in one of the analysed intervals, it would be in the pipe acceleration phase of a reaming or backreaming case. However, calculations show that pressure changes of significant size are unlikely to occur during reaming with normal pipe velocities.

A.4 Weight on bit

In most cases, a change in SPP is seen after the ROP has changed, which strengthens the suspicion that the pressure change is caused by a change in ROP. However, in a few cases it is observed that the WOB increases when ROP decreases or remains unchanged, while the SPP still increases. **Figure A-5** shows such an example, where the SPP increases at two occasions, corresponding to the increase in WOB. There is no alterations in ROP or

critical parameters during these two intervals, indicating that the WOB is what causing the pressure spikes.

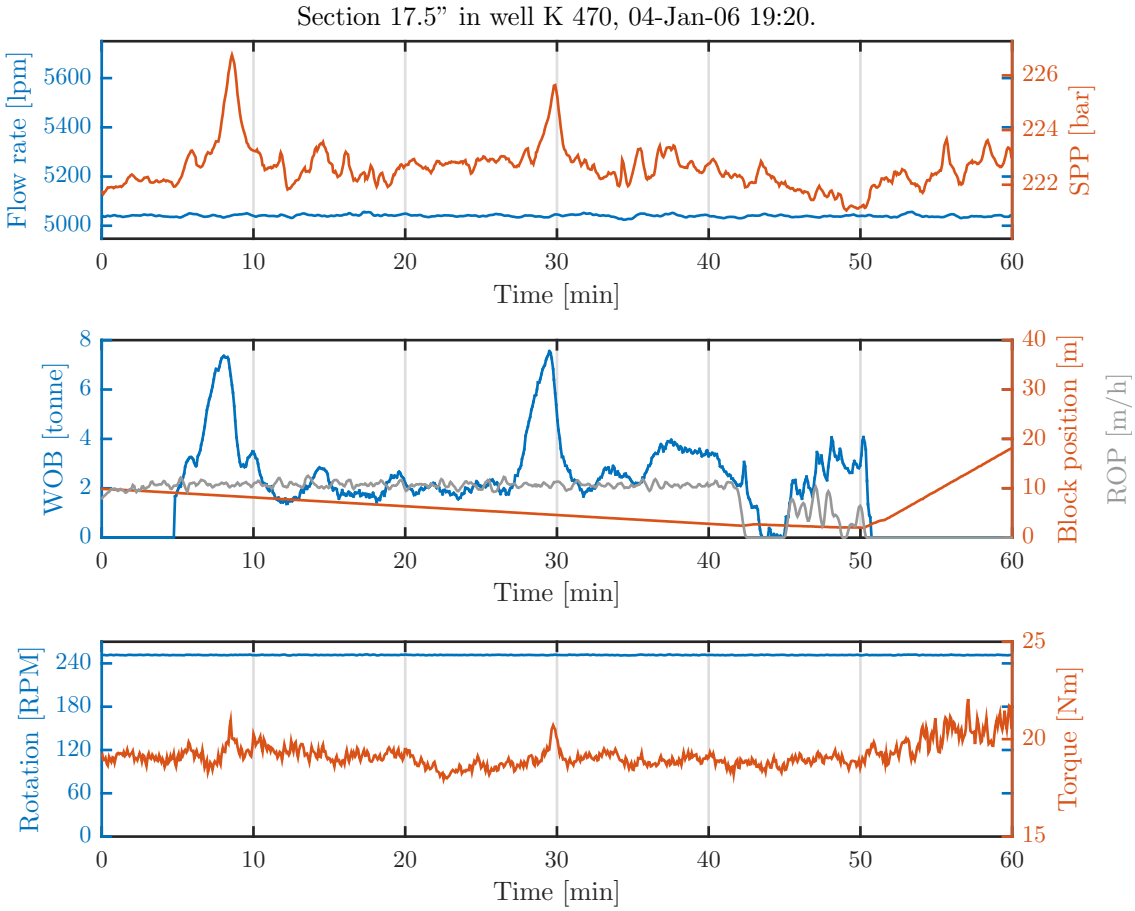

Figure A-5: During drilling of a stand in a 17 ½" section, the WOB is increased significantly. The SPP increases correspondingly with the WOB, but the ROP does not change during the pressure spikes. This indicates that the pressure increases at 8.5 and 29.5 minutes into the interval is caused by a WOB related effect and not by cuttings concentration.

B Pressure changes during backreaming

Reaming is defined as straightening and smoothing the borehole by rotating, pumping and moving the pipe without expanding the wellbore in axial direction. During backreaming, bedded cuttings are removed as the BHA, with a larger diameter and higher fluid velocity, is slowly pulled out of the hole, lifting bedded cuttings into suspension. In addition, small amounts of cuttings may be generated from the borehole walls as the hole is straightened and smoothed.

During backreaming, cuttings beds close to the BHA can be moved further back with the mud flow, forming higher cuttings beds. This can cause a reduction in flow area and subsequently a higher friction pressure loss. Also, if the cuttings beds are high and not immediately eroded by the flow around the tail of the BHA, the cuttings may partially block tight fluid passages around stabilizers and BHA components with a large external diameter.

If the mud velocity and pipe rotation is sufficiently high, beds may be eroded and even fully removed. This leads to a larger cross sectional flow area and subsequently a lower friction pressure loss, causing the standpipe pressure to decrease.

B.1 Observed SPP changes during backreaming

In order to investigate the pressure effect of cuttings during reaming, relative standpipe pressure is plotted against time. Relative SPP is a function of time t, given as $\frac{\text{SPP}(t)}{\text{SPP}(0)}$, where $t = 0$ is defined as the moment when reaming is initiated. **Figure B-1** shows relative SPP for all sections. A relative SPP of 1 indicates no change in SPP through time, whereas a relative SPP greater than 1 indicates a pressure increase.

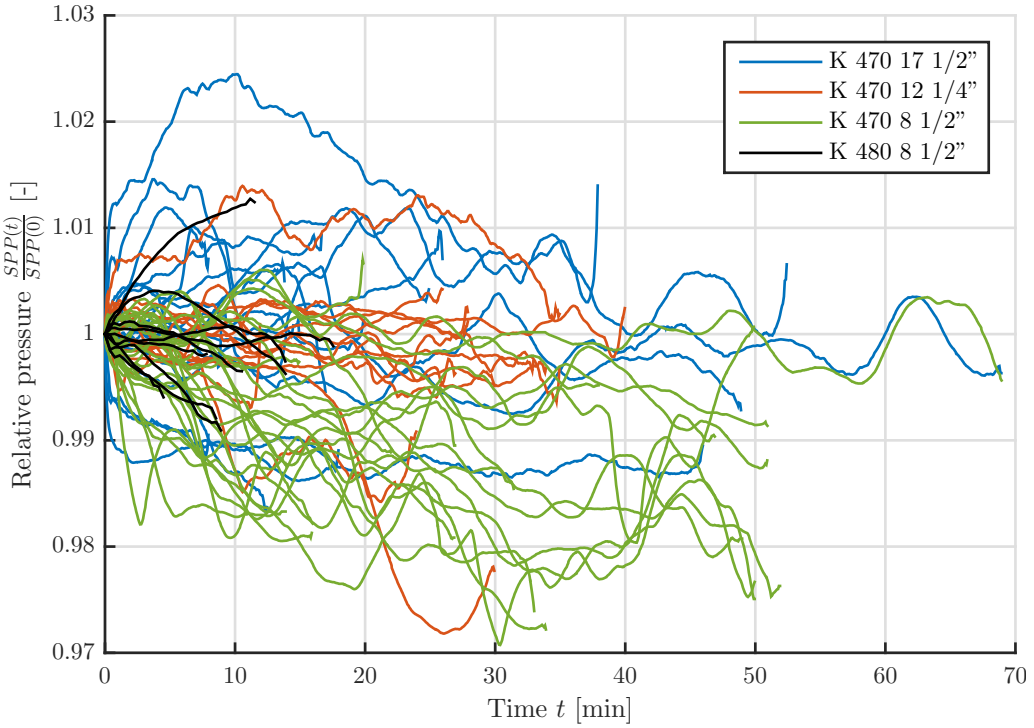

Figure B-1: Relative standpipe pressure vs. time during backreaming for all sections. No

SPP in the K 470 8 ½” section (green) is constant or decreasing over time for most reaming intervals, although some increases are seen within the first 15 minutes. Most of the examples from the K 470 12 ¼” section remains relatively constant in SPP through the interval, with some exeptions located both above and under the “neutral line” where $\frac{\text{SPP}(t)}{\text{SPP}(0)}$=1. The reaming intervals from both K 470 17 ½” section and the K 480 8 ½” section seems to have no distinct majority of intervals placed on either side of the neutral line.

In general it does not seem to be a trend in relative SPP vs. time during backreaming in any of the sections. In order to further analyse the development of SPP in backreaming intervals, the different sections must be evaluated against possible affecting parameters. There are several parameters that might have an effect on the SPP while backreaming, such as RPM, pipe velocity, and ROP prior to backream.

Influence of ROP on SPP during reaming

Relative SPP was plotted against time for each section and grouped by the average ROP before backream was initiated. The ROP was calculated by taking the average ROP greater than 0 over the last 20 minutes before the pipe is pulled. The data is divided into four groups of ROP, with intervals of ROP = 0 - 13 m/h, 13 - 23 m/h, 23 - 35 m/h, >35 m/h. A higher ROP may cause higher beds. This can lead to a higher concentration of suspended cuttings during backreaming and higher interference between BHA and beds. As beds are removed during reaming, the SPP should drop as a result of the increased annular flow area. However, reduction of flow area may occur, causing partial blockage of the annulus and a higher SPP. Because of this, beds may cause either an increase or a decrease during backreaming.

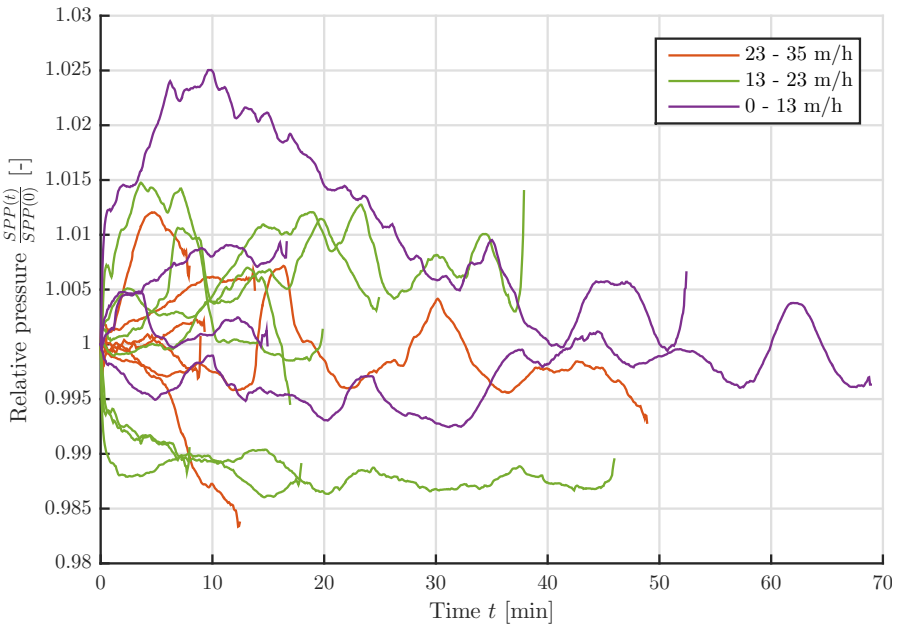

Figure B-2: Relative standpipe pressure during backreaming in K 470 17 ½" grouped by ROP.

Figure B-2 shows relative SPP in K 470 17 1/2" during backreaming grouped by ROP. Both cases where pressure increases, decreases or remains constant are represented in all three ROP groups, showing that there is no clear trend between SPP development vs. time and ROP prior to backreaming. Most cases have pressure change within ±1.5%. The greatest change in pressure seems to occur in the minutes after reaming is initiated,

whereas the pressure change seems to stabilize further into the time interval

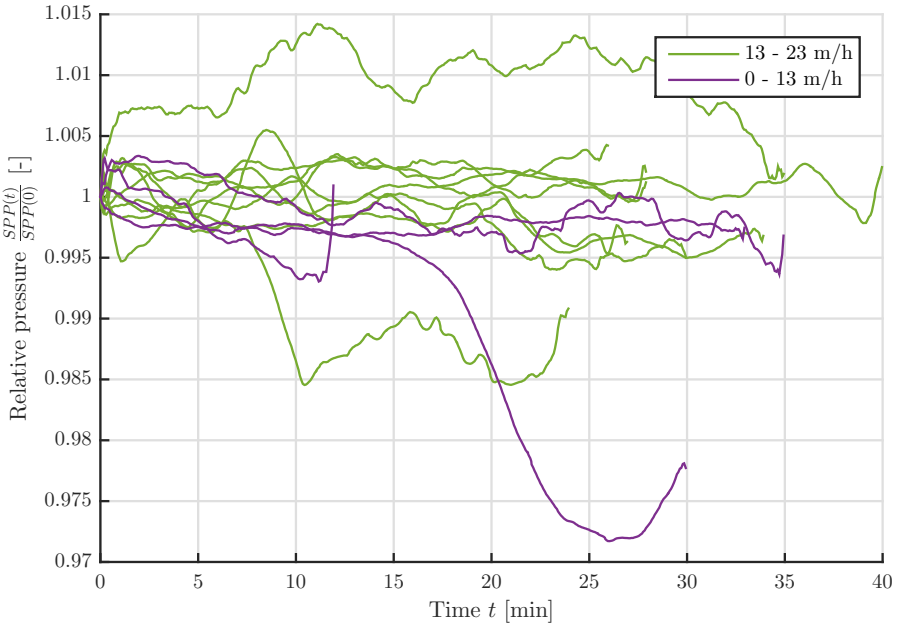

Figure B-3: Relative standpipe pressure during backreaming in K 470 12 ¼" grouped by ROP.

In section K 470 12 ¼", most cases of backreaming have a pressure change of ±0.5%, as shown in **figure B-3**. Only three cases have a pressure change of more than 1% of initial SPP. Cases with a previous ROP of 0 - 13 m/h seem to decrease more than those with ROP within 13 - 23 m/h. However, due to only four cases with ROP within 0 - 13 m/h, no clear pressure trend can be pointed out.

In **figure B-4**, showing relative SPP vs. time in section K 470 8 ⅛" grouped by ROP, all cases are on or below the neutral line $\frac{\text{SPP}(t)}{\text{SPP}(0)} = 1$, indicating constant or decreasing SPP during reaming. Every ROP group has cases representing constant or decreasing pressure, where both high and low ROP are represented in both ends of the pressure change sample.

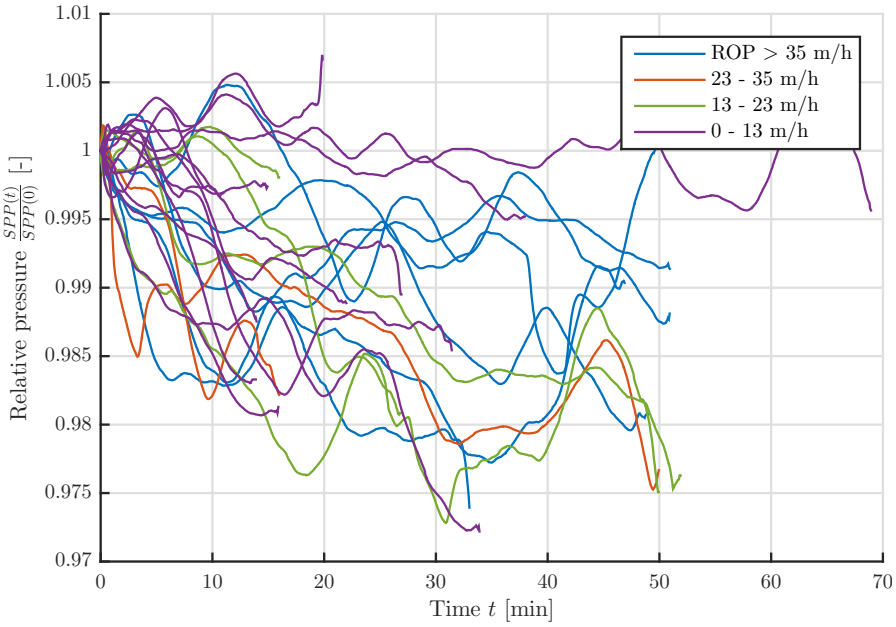

Figure B-4: Relative standpipe pressure during backreaming in K 470 8 ⅛" grouped by ROP.

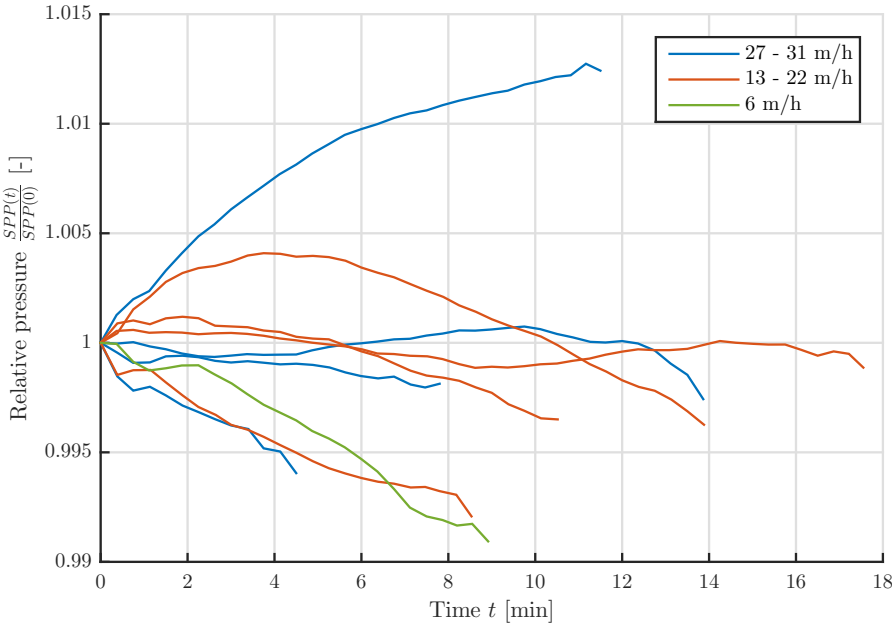

Figure B-5: Relative standpipe pressure during backreaming in K 480 8 ⅛" grouped by ROP.

Figure B-5 shows pressure during reaming in K 480 8 ½". No connection between SPP and ROP prior to backreaming can be seen, as both increasing, constant and decreasing

pressures are seen for the groups 27 - 31 m/h and 13 - 22 m/h.

Influence of rotation speed on SPP during reaming

A high rotation speed improves hole cleaning as rotation of the drill pipe may lift bedded cuttings into suspension and erod the cuttings beds. By grouping relative SPP vs. time during backreaming for rotation speeds, the effect of rotation can be investigated.

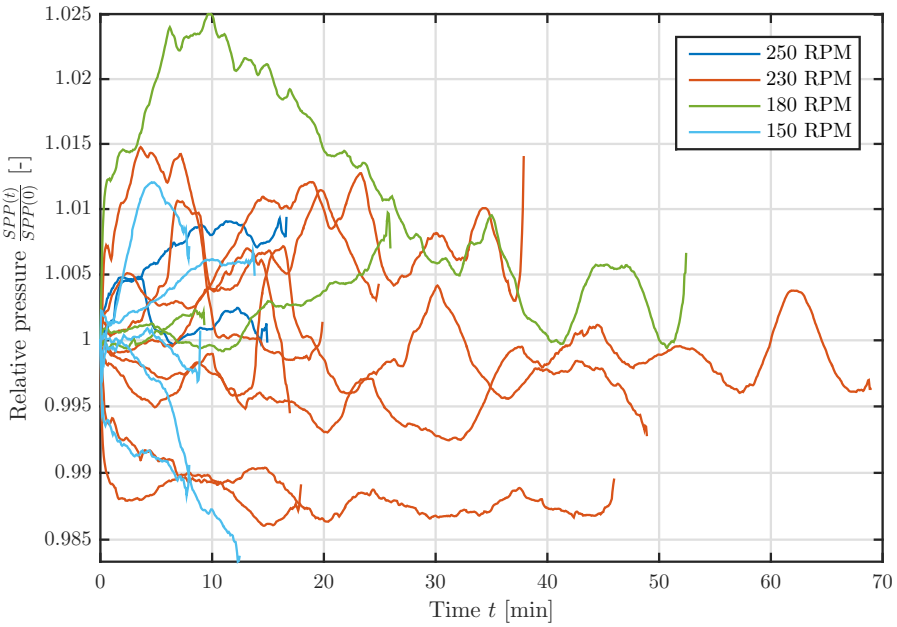

Figure B-6: Relative standpipe pressure during backreaming in K 470 17 ½" grouped by string rotation speed.

In **figure B-6** and **B-7** the relative SPP is plotted against time for sections K 470 17 ½" and K 470 8 ½", with the intervals divided into groups based on the RPM during the backream interval. Only sections K 470 17 ½" and K 470 8 ½" are represented, as the other two sections are backreamed with the same rotation speed throughout the section, offering little new information in regards to the effect of rotation on SPP. No clear connection between SPP and RPM can be seen from figure B-6 and B-7.

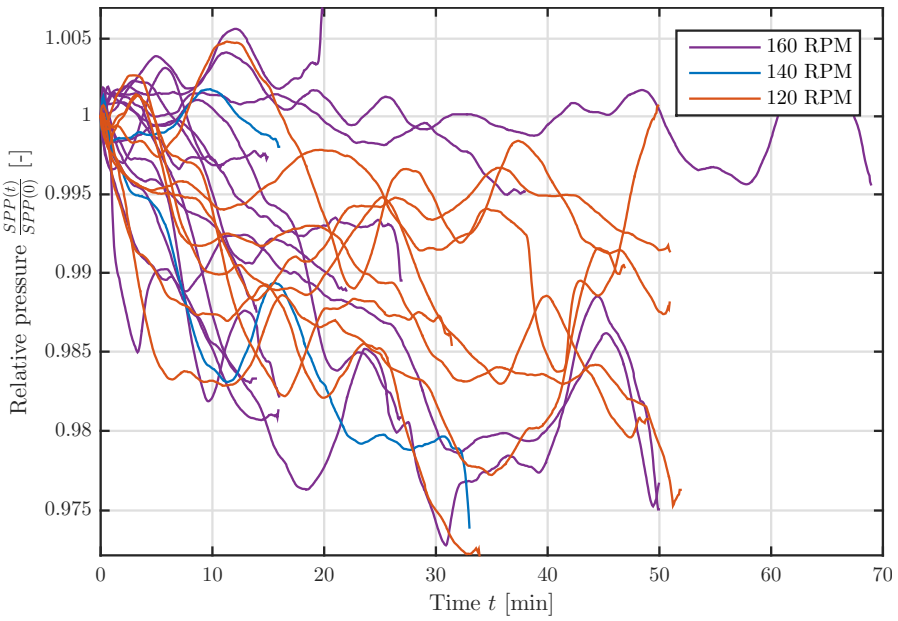

Figure B-7: Relative standpipe pressure during backreaming in K 470 8 ½" grouped by RPM.

Influence of pipe velocity on SPP during reaming

The pulling velocity of the pipe when backreaming may affect the pressure loss over annulus. A too high pipe velocity in comparison to the rate of bed erosion may result in cuttings blockage of the annulus around the BHA, causing an increased pressure loss. By grouping for pipe velocity when plotting relative standpipe pressure vs. time, the effect of pipe velocity on the pressure loss is shown.

All sections are plotted together in **figure B-8**. Naturally, as backreaming for most cases involves pulling one stand, the cases with a low pipe velocity have a longer time of reaming, whereas the cases with high pipe velocity have a short reaming period. All three pipe velocity groups include cases where the pressure either increases, decreases, stays constant or a combination of the three, not showing any correlation between the relative pressure and pipe velocity.

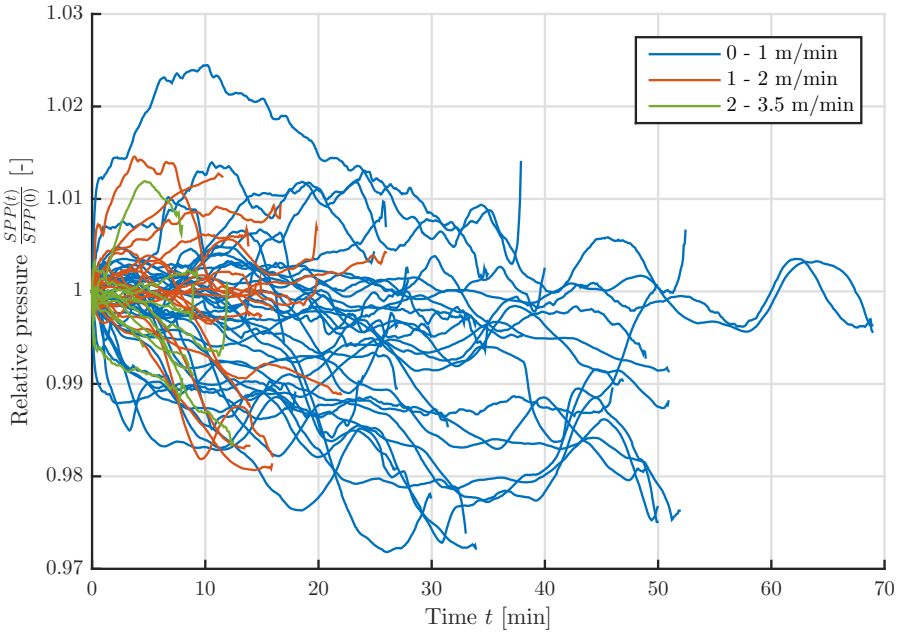

Figure B-8: Relative standpipe pressure vs. time during backreaming grouped by pipe velocity when pulling pipe for all sections.

For all sections, except K 480 8 ½", no correlation between pipe velocity and pressure during backreaming was seen. In **figure B-9**, however, a clear trend is seen, where cases with pipe velocity 2.5 - 3.5 m/min have decreasing pressures. For velocities 1 - 2 m/min the pressure is either increasing right after backreaming is initiated or remaining constant throughout the stand. This seems counter intuitive as a higher pressure loss is expected for higher pipe velocity. A possible explanation may be the driller intentionally pulling slower when the hole is believed to be dirty, and pulling fast when the hole seems clean and no cuttings beds are expected. The observed pattern could also be accidental, as the the number of cases is limited.

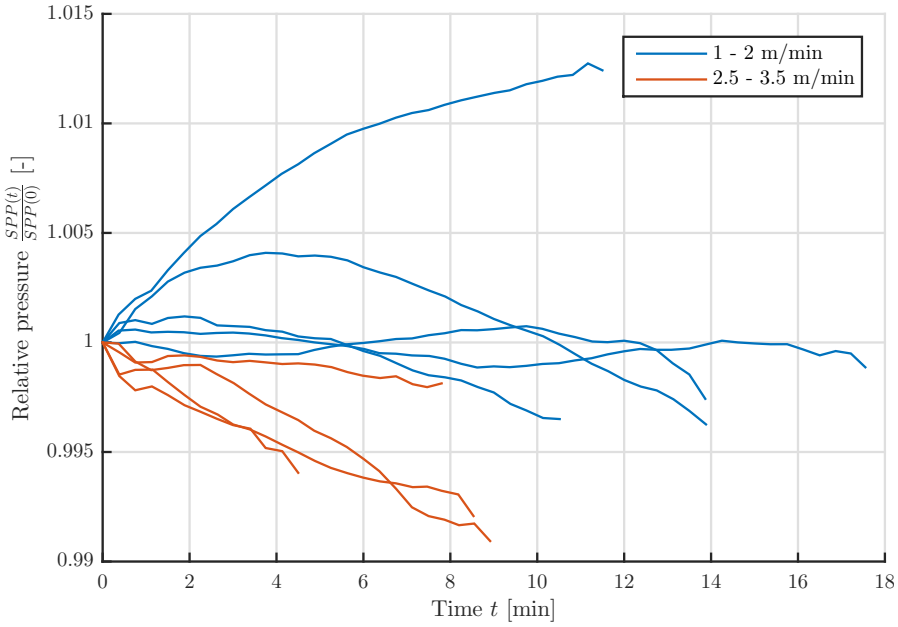

Figure B-9: Relative standpipe pressure vs. time during backreaming in K 480 8 ½" grouped by pipe velocity when pulling pipe.

B.2 Calculation of pressure changes during backreaming

As seen from figure B-4, showing relative standpipe pressure during reaming in the 8 ½" section in K 470, SPP may decrease with 1% within the first 10 minutes. A typical standpipe pressure for this section is 130 bar, giving an decrease in pressure loss of 1.3 bar. Calculations in section 3.4.5 indicate that such a pressure change is more than what can be caused by increased fluid density and viscosity.

A borehole with diameter 8 ½" has a cross sectional area $A = \frac{\pi}{4} d_{\text{bit}}^2 = 0.0366$ m^2, or 36.6 liters per meter. The total volume of cuttings drilled when drilling one stand is given as $V_c = AL_{\text{stand}} = 1$ m^3 for a length of a stand $L_{\text{stand}} = 27.4$ m. If no cuttings are transported to surface, but forming one long bed with a relative cuttings bed heigh $x \approx 10\%$, corresponding to $F_b = \frac{A_b}{A} = 5\%$ of the cross sectional wellbore area, the length of the bed is given as

$$F_b A L_b = \frac{V_{\text{stand}}}{\varepsilon_b} = \frac{A L_{\text{stand}}}{\varepsilon_b}$$
$$L_b = \frac{L_{\text{stand}}}{F_b \varepsilon_b} = 1096\text{m},$$

where V_{stand} is the volume of cuttings drilled from one stand, and ε_b is the packing efficiency of the bed, given as 50%.

The average pressure decrease in figure B-4 is approximately 1.7 bar after backreaming one stand. All cases from the section have a flow rate $q_m = 1600$ lpm. If only 27.4 meters of cuttings beds are removed, with a relative bed height is $x = 10\%$, the resulting decrease in SPP is

$$\begin{aligned}\Delta p_f^{\text{bed}} - \Delta p_f^0 &= \frac{f(x)}{2}\frac{L_b}{d_{\text{hyd}}(x)}\rho_m v(x)^2 - \frac{f^0}{2}\frac{L_b}{d_{\text{hyd}}^0}\rho_m (v^0)^2 \\ &= 0.3471 - 0.2654 = 0.0817 \text{ bar.}\end{aligned} \tag{56}$$

This is merely 5% of the decrease in SPP seen in section K 470 8 ½" after backreaming one stand.

Although some bedded cuttings may be suspended in the mud and transported up to surface during reaming, little new cuttings are generated. This leads to displacement of mud with relatively high concentration from drilling by mud with lower concentration. The K 470 8 ½" section has a measured depth of approximately 3500 m. With a flow rate $q_m = 1600$ lpm, the wellbore is displaced after 52 minutes. From section 3.4.5, the pressure loss from cuttings was calculated to 1.2 bar before displacement with a cuttings concentration of approximately 0.9%. After backreaming for 20-30 min, the pressure loss due to the remaining suspended cuttings may be 0.6 bar. Of the total decrease in SPP of 1.7 bar when backreaming, 1.1 bar may be caused by the removal of bedded cuttings.

As can be observed from figure B-4, SPP decreases with 1% or 1.3 bar for many cases within the first 10 minutes, which is close to the estimate of 1.1 bar in the previous paragraph. As bedded cuttings are expected to be removed in less time than displacing

the wellbore, this first rapid decline in figure B-4 is thought to be the pressure effect of removing bedded cuttings.

The result from equation 56 of 0.0817 bar is approximately 6% of the assumed 1.3 bar pressure decrease from cuttings bed removal. This indicates that the bed length, $L_b = 27.4$ m, is a too short, the bed height, $x = 10\%$, is a too low, or a combination of both, given that the estimate in (56) is fair. In order to decrease the pressure loss with 1.3 bar, the length of the removed cuttings bed must be between 400 and 450 m according to the model used in equation 56. This implies that beds are removed not only by the BHA but also by erosion from the rotating drill pipe on top of a cuttings bed.

A similar pressure decrease of 1.3 bar could be obtained by eroding a 1000 m long cuttings bed from $F_b = 6\%$ to $F_b = 4\%$, resulting in a decrease in relative bed height from $x = 11\%$ to $x = 8.4\%$.

Erosion of beds from BHA during backreaming is assumed to be complete, as the fluid velocity is high through the narrow annulus around the BHA. The erosion by the drill pipe may not be complete, as a larger flow area yields a low fluid velocity, allowing cuttings to go out of suspension. A combination of both erosion of beds and complete cuttings removal for parts of the wellbore during drilling seems plausible.

C Cases used in analysis

Intervals drilling

Table C-1: List of cases during drilling

Date	**Interval 1**	**Interval 2**	**Phenomenon**	**Section**	**ΔSPP**	**ΔROP**
dd/mm-yy	[min]	[min]			[bar]	m/h
25/12-04 17:18	35 - 47	48.6 - 57.5	Stringer	K 480 8 1/2”	-2.24	-18.78
25/12-04 17:18	48.6 - 57.5	58 - 62	Stringer	K 480 8 1/2”	2.44	22.18
25/12-04 17:18	58 - 62	62.5 - 67.5	Stringer	K 480 8 1/2”	-1.59	-20.79
25/12-04 19:15	49.4 - 58.5	60.4 - 64	Stringer	K 480 8 1/2”	-2.80	-27.74
25/12-04 19:15	10.5 - 32.5	33 - 34.5	Thin stringer	K 480 8 1/2”	-1.46	-13.33
25/12-04 19:15	33 - 34.5	35.6 - 46.5	Thin stringer	K 480 8 1/2”	2.25	13.52
25/12-04 19:15	35.6 - 46.5	47 - 48.5	Thin stringer	K 480 8 1/2”	-1.61	-20.28
25/12-04 19:15	47 - 48.5	49.4 - 58.5	Thin stringer	K 480 8 1/2”	1.83	21.10
01/01-05 22:10	46.5 - 49.5	50.8 - 53	Intentional	K 480 8 1/2”	2.95	28.00
01/01-05 22:10	27.5 - 29.6	31.5 - 35	Intentional	K 480 8 1/2”	1.80	24.39
01/01-05 22:10	20.5 - 21.5	21.5 - 23.6	Thin stringer	K 480 8 1/2”	1.47	12.78
02/01-05 02:10	11 - 18	19 - 28	Soft formation	K 480 8 1/2”	1.94	16.98
02/01-05 02:10	40 - 50	51 - 59	Soft formation	K 480 8 1/2”	2.99	24.70
02/01-05 04:00	113 - 130.5	131.9 - 145	Stringer	K 480 8 1/2”	-3.30	-26.26
04/01-05 05:15	20 - 27	34.5 - 37.7	Soft formation	K 480 8 1/2”	3.96	45.50
02/01-06 06:20	16.5 - 27	29 - 37	Intentional	K 470 17 1/2”	-2.45	-10.90
02/01-06 10:30	10 - 18	22 - 42.5	Intentional	K 470 17 1/2”	1.62	12.49
02/01-06 10:30	35 - 43	44.5 - 52	Intentional	K 470 17 1/2”	-3.19	-16.06
02/01-06 10:30	44.5 - 51	53.5 - 56	Intentional	K 470 17 1/2”	3.46	13.48
04/01-06 10:00	62 - 68	71 - 77.5	Intentional	K 470 17 1/2”	2.54	16.05
04/01-06 12:00	28 - 38	39 - 49	Intentional	K 470 17 1/2”	1.60	14.64
07/02-06 14:00	82 - 98	104 - 119	Soft formation	K 470 12 1/4”	1.10	4.96
07/02-06 16:42	10 - 13	14 - 16	Thin stringer	K 470 12 1/4”	-1.37	-16.88
08/02-06 00:00	24 - 34	36.5 - 40	Thin stringer	K 470 12 1/4”	-3.03	-15.70
08/02-06 00:00	35 - 40	40 - 50	Thin stringer	K 470 12 1/4”	3.56	13.96
08/02-06 06:00	85.5 - 93	98.5 - 106	Intentional	K 470 12 1/4”	2.21	3.06
08/02-06 06:00	98.5 - 106	114 - 123	Soft formation	K 470 12 1/4”	0.44	3.83
09/02-06 12:00	53 - 58	59 - 64	Intentional	K 470 12 1/4”	-1.27	-4.99
09/02-06 20:00	18 - 22	24.5 - 27	Intentional	K 470 12 1/4”	-3.37	-8.75

Continued on next page

Table C-1 – *Continued from previous page*

25/02-06 17:00	61 - 71	72 - 76.3	Thin stringer	K 470 8 1/2”	-2.39	-9.22
25/02-06 19:00	29.5 - 30.5	33 - 41	Thin stringer	K 470 8 1/2”	2.06	21.23
25/02-06 20:50	48 - 64	65 - 80	Stringer	K 470 8 1/2”	-2.02	-19.26
25/02-06 22:30	52 - 62	63 - 65	Thin stringer	K 470 8 1/2”	-3.05	-14.85
25/02-06 22:30	63 - 65	66 - 70	Thin stringer	K 470 8 1/2”	3.41	18.28
27/02-06 10:40	101 - 106	107 - 112	Thin stringer	K 470 8 1/2”	-1.99	-8.29
29/02-06 09:30	90 - 99	101 - 115	Stringer	K 470 8 1/2”	-2.42	-18.59
29/02-06 12:10	80 - 98	100 - 119	Soft formation	K 470 8 1/2”	2.96	13.54
30/02-06 21:30	33 - 39	39 - 50	Thin stringer	K 470 8 1/2”	-1.53	-14.76
30/02-06 21:30	39 - 49	50 - 58	Thin stringer	K 470 8 1/2”	2.71	9.90

Intervals backreaming

Table C-2: List of cases during backreaming

Date	**Duration**	**Interval**	**Section**
dd/mm-yy	[min]	[min]	
02/01-05 03:25	20	4 - 15	K 480 8 1/2”
02/01-05 06:25	14	0 - 14	K 480 8 1/2”
02/01-05 12:15	15	1.5 - 11	K 480 8 1/2”
02/01-05 16:20	15	6.3 - 11	K 480 8 1/2”
02/01-05 18:10	15	3.4 - 11.5	K 480 8 1/2”
02/01-05 19:45	20	1 - 15.2	K 480 8 1/2”
04/01-05 05:50	15	3.22 - 12	K 480 8 1/2”
04/01-05 07:20	40	10 - 28	K 480 8 1/2”
04/01-05 09:10	60	32 - 44	K 480 8 1/2”
27/02-06 12:00	140	57.5 - 89	K 470 8 1/2”
27/02-06 15:00	140	63 - 115	K 470 8 1/2”
27/02-06 18:00	140	75 - 108	K 470 8 1/2”
27/02-06 21:00	140	73 - 120	K 470 8 1/2”
28/02-06 02:00	140	39 - 88	K 470 8 1/2”

Continued on next page

Table C-2 – *Continued from previous page*

28/02-06 05:00	140	60 - 111	K 470 8 1/2”
28/02-06 07:00	140	63 - 114	K 470 8 1/2”
28/02-06 09:00	140	82 - 132	K 470 8 1/2”
28/02-06 15:00	140	80 - 114	K 470 8 1/2”
02/03-06 19:00	40	8 - 24	K 470 8 1/2”
03/03-06 23:00	160	81 - 150	K 470 8 1/2”
04/03-06 04:00	140	35 - 49	K 470 8 1/2”
04/03-06 08:00	140	19 - 33	K 470 8 1/2”
04/03-06 10:00	140	112 - 127	K 470 8 1/2”
04/03-06 16:00	140	63 - 83	K 470 8 1/2”
04/03-06 20:00	140	44 - 55	K 470 8 1/2”
05/03-06 00:00	140	63 - 79	K 470 8 1/2”
05/03-06 04:00	140	64 - 102	K 470 8 1/2”
05/03-06 08:00	140	93 - 115	K 470 8 1/2”
05/03-06 12:00	140	71 - 98	K 470 8 1/2”
05/03-06 19:40	140	34 - 50	K 470 8 1/2”
05/03-06 23:00	140	81 - 131	K 470 8 1/2”
06/03-06 02:00	140	72 - 122	K 470 8 1/2”
06/03-06 09:00	140	96 - 123	K 470 8 1/2”
23/12-05 05:00	140	36 - 45	K 470 17 1/2”
23/12-05 07:00	140	101 - 109	K 470 17 1/2”
23/12-05 10:00	140	80.5 - 88.5	K 470 17 1/2”
24/12-05 00:00	140	36 - 48.5	K 470 17 1/2”
24/12-05 02:00	140	112.1 - 126	K 470 17 1/2”
24/12-05 11:00	140	45.6 - 55	K 470 17 1/2”
31/12-05 05:00	140	104 - 130	K 470 17 1/2”
01/01-06 23:00	140	49 - 87	K 470 17 1/2”
02/01-06 01:00	140	61 - 110	K 470 17 1/2”
02/01-06 05:00	140	35 - 60	K 470 17 1/2”
02/01-06 07:00	140	47 - 116	K 470 17 1/2”
02/01-06 11:00	140	69 - 87	K 470 17 1/2”
04/01-06 02:00	140	99 - 116	K 470 17 1/2”

Continued on next page

Table C-2 – *Continued from previous page*

04/01-06 04:00	140	48 - 68	K 470 17 1/2”
04/01-06 07:00	140	89 - 135	K 470 17 1/2”
04/01-06 13:00	140	67.5 - 120	K 470 17 1/2”
04/01-06 19:00	140	70.3 - 87	K 470 17 1/2”
04/01-06 23:00	140	91 - 106	K 470 17 1/2”
07/02-06 18:00	140	49 - 79	K 470 12 1/4”
08/02-06 00:00	140	119 - 131	K 470 12 1/4”
08/02-06 04:00	140	67 - 91	K 470 12 1/4”
08/02-06 08:00	140	80 - 115	K 470 12 1/4”
08/02-06 14:00	140	58 - 85	K 470 12 1/4”
08/02-06 18:00	140	33 - 68	K 470 12 1/4”
08/02-06 22:00	140	55 - 83	K 470 12 1/4”
09/02-06 02:00	140	49 - 79	K 470 12 1/4”
09/02-06 06:00	140	46 - 80	K 470 12 1/4”
09/02-06 10:00	140	7 - 33	K 470 12 1/4”
09/02-06 12:00	140	107 - 135	K 470 12 1/4”
09/02-06 16:00	140	80 - 120	K 470 12 1/4”
09/02-06 20:00	140	72 - 105	K 470 12 1/4”

D Well data

This section presents key information from the wells being studied. For each section, short summarizing tables of well trajectory, BHA and bit specifications and mud properties is given. The most important events from the drilling operation relevant for this study, is also summarized. Unfortunately, complete information on all the sections is not available, and certain assumptions regarding mud rheology must be taken. Well K 470 consist of four sections (24", 17 ½", 12 ¼" and 8 ½"), where drilling data is available for all sections except for the 24" section. Any information regarding mud properties beyond density is not available. For well K 480, the 8½" is the only section where drilling data is available, but complete information on mud properties is provided. Well trajectories for both wells are plotted in **figure D-1** and **D-2**.

D.1 Well K 470

17½" section

Section geometry	
TVD interval	1316-1709 mTVD
MD interval	1508-2379 mMD
Interval length	871 m
Inclination start	60.8 °
Inclination end	60.4 °
Azimuth start	134.7 °
Azimuth end	99.1 °
BHA and bit	
Drill pipe	6⅝"
Length of BHA	107 m
Steering	PowerDrive
Bit	17½" milled tooth
Mud	water based
Mud weight	1300 kg/m^3
Average plastic viscosity	- mPas
Average yield point	- Pa
Average Power law exponent	- [-]
Average konsistensy index	- lb$_f$s^n/100ft^2

FIT++

- 17 1/2" BHA made up and RIH. Drilled shoe track, rat hole and 3 m new formation to 1511 mMD.

- Performed LOT, unsuccessful.
- Cement plug was set with cement stinger
- Drilled out cement. New LOT performed, unsuccessful
- Performed FIT. New cement plug set
- Drilled new hole to 1515.5 m. Performed FIT, successful

Drilling, first run

- Drilled from 1515,5 m. Several hard stringers were hit from 1556 m to 1587 m. Power Drive failed from 1593 m. Poor communication but drilling could proceed.
- Circulation and reaming was necessary from 1900 m due to torque and ECD reading
- Power Drive failed to turn left at 2070 m. POOH

Hole problems when POOH

- 4xBU with 5000 lpm 180 rpm, when pump pressure suddenly increased and hole partial packed off. Ten hours were spent to establish circulation in steps to 3800 lpm. ECD varied 1.692 – 1.714. After stable flow check it was pumped out of hole from 2025 with 200 lpm.
- Over pull and pack off tendencies at 1885 m, started circulate well clean. Circulation was established in steps to 5000 lpm and large amounts of cuttings were coming over the shakers. 33 hrs of circulation was necessary before backreaming could commence. The BHA was backreamed out of hole with from 1814 m to 135 m inside 20" casing!
- In total 96 hours were used to get out of hole. The BHA came out "encapsulated" in sticky cuttings. Prior to RIH with the new BHA, a BOP test was performed. A jet sub was used to wash the riser, BOP and wellhead, and large amounts of cuttings came over the shaker.
- Ultradrill mud had never been used in *the company* before. It was a water based mud system expected to have improved inhabitation properties. Ultradrill mud is designed to contain the polymer "UltraFree NS" which function is to prevent bit balling and be a ROP enhancer. The polymer consisted 80% of a synthetic oil "LAO" (linear alpha olefin) and was therefore not approved by *the company*, as it could not be defined and discharged as a water based mud. It was decided to use another polymer EMI 742 as a substitute. The EMI 742 polymer did not fulfil UltraFree NS's coating characteristics and prevention of bit balling. (More details can be found in Synergi 413135, see attachement.)
- In addition, by misconception, EMI-760 was mixed into the mud instead of UltraCap. The sticky cuttings was most likely caused by the use of EMI 769 instead of Ultracap, or a combination with a fluid formulated without UltraFree NS. It was decided to convert the mud system to Glydrill water based mud.

Drilling, second run

- Took weight when RIH at 1497 m inside 20" casing. Washed down to 1525 m and from 1915 to TD
- Drilled from 1915 m to 2116 m. BHA not able to follow well path, PowerDrive failed, POOH
- Circulated 3.5 hours and pulled to 1563 m when the string got 25 tons overpull
- Backreamed out of hole to 1497 m.

Drilling, third run

- Drilled from 2116 m to section TD at 2379 m with 5000 lpm, 180 rpm.
- Circulated 6xBU and pulled to 1908 m before string took weight
- Backreamed to 1495 and circulated 3xBU up before POOH

12¼" section

Section geometry		
TVD interval	2821-2895	mTVD
MD interval	2379-2787	mMD
Interval length	408	m
Inclination start	70.4	°
Inclination end	81.9	°
Azimuth start	81.5	°
Azimuth end	351.5	°

BHA and bit		
Drill pipe	5"	
Length of BHA	64	m
RSS	Motor and SRWD	
Bit	8½" PDC with 10⅝"×12¼" reamer wing	

Mud	oil based, MPD	
Mud weight	1300	kg/m^3
Average plastic viscosity	-	mPas
Average yield point	-	Pa
Average Power law exponent	-	[-]
Average konsistensy index	-	lb$_f$s^n/100ft^2

- Drilled from 2383 m with 3000 lpm 130 rpm. BHP was adjusted to 310 bars by the MPD choke.
- BHP was gradually increased at 2407 m while reaming one single to be prepared for max expected pressure when drilling into the high pressure zone.
- The pressure dropped after increasing BHP to 315 bars. 10 m3 mud was lost into formation. The losses were then stabilized by reducing BHP. A loss free rate was established with 2800 lpm and BHP at 311 bar (ECD 1.82 SG EMW).
- A Versa pack pill was tried set and squeezed into formation at 2225 m. A dynamically FIT was performed to 1.88 SG EMW, but 17 m3 mud was lost at 1.854 SG EWM. A 6 m3 Forma plug was then mixed and squeezed into formation. A new dynamically FIT was performed after the plug had set up, but the pressure leaked off at 1.86 SG EMW.
- The hole was then logged again to find the loss area. It was expected to find a resistivity peak due to the Forma plug, but no resistivity change was seen. A total of 100 m3 mud was lost to formation, and a drawdown test was performed to see if the mud was filled in a fracture. Only 400 litres came in return. Pressure levelled out at 1,786 SG EMW.

Squeezing cement into loss zone

- It was decided to kill the well by displacing to 1.88 SG Paratherm kill mud. The string was POOH, the low pressure riser installed and a 3 1/2" cement stinger made up.
- RIH w/cement stinger to 2470m. A 20.2 m3 cement plug was set, and 12 m3 was squeezed into formation. A hesitation squeeze of 3 m3 in two steps was performed with a max pressure of 49 bar.

Drilling, second run

- Drilled in MPD mode from 2407 with 2820 lpm, 90 rpm and 1.86 ECD (318 -32 bar BHP). At 2447 m it was lost mud to formation. 7m3 mud was lost with 1.86 – 1.87 SG EMW. Bottom hole pressure was reduced to 1.84 SG EMW(316,8 bar) to stabilize losses.
- Since Top Shetland could be confirmed on logs at 2411 m MD it was continued drilling with ECD readings of 1.76 SG – 1.79 SG EMW. A drawdown test was performed when Shetland was confirmed on logs.
- - Formation pressure 1.74 SG in top Shetland at 2411 m MD / xx m TVD
- Choke operators managed to operate choke within a window of 3 points on ECD. The window increases some when more cuttings came in return.
- TD was set at 2787 m MD (1906 m TVD), 1.15 m left and 2.15 m low of plan. It was decided to run the liner conventional since the pore pressure in Shetland was lower than max expected. The well was circulated 2.5 time bottoms up and then displaced to 1.77 SG kill mud before string was pulled out of hole.
- The BHA was pulled to 2366 and hung in the LPR. The RAS equipment was rigged down and the LP riser installed. The string was again retrieved and pulled out of hole.

8½" section

Section geometry		
TVD interval	1911-2072	mTVD
MD interval	2787-4399	mMD
Interval length	1512	m
Inclination start	63°	
Inclination end	94°	
Azimuth start	105°	
Azimuth end	180°	
BHA and bit		
Drill pipe	5"	
Length of BHA	39	m
RSS	PowerDrive Xceed	
Bit	8½" PDC	
Mud		
Mud weight	1700	kg/m^3
Average plastic viscosity	-	mPas
Average yield point	-	Pa
Average Power law exponent	-	[-]
Average konsistensy index	-	$lb_f s^n/100ft^2$

Drilling

- Section drilled in one run. Drilling was initiated with parameters according to LEDO technique, in this case ROP of 10-15 m/h, flow rate of 100 lpm, and 140-160 rpm.
- ECD was increased from 1.760-1.769 at 2900 m, and losses occured at 3003 mMD. Losses stabilized at 5-6 m^3/h after reducing flow rate to 1600 lpm, and the mud wheight was reduced to 1.69 at 3100 mMD.
- The low ROP made it difficult to obtain the desired dogleg. This was solved by steering and reaming in intervalls, with 70% WOB during steering and reaming 30% of the time.
- The well plan was changed and inclination dropped from 91° to 81° in order to find the Statfjord formation. By doing this, the well path dropped 14 m from 2080 mTVD at 3735 mMD, and the Statfjord formation was encountered as planned.
- PowerDrive Xceed failed at 4109 mMD, but drilling continued to true depth at 4399 mMD followed by four bottoms up before POOH.

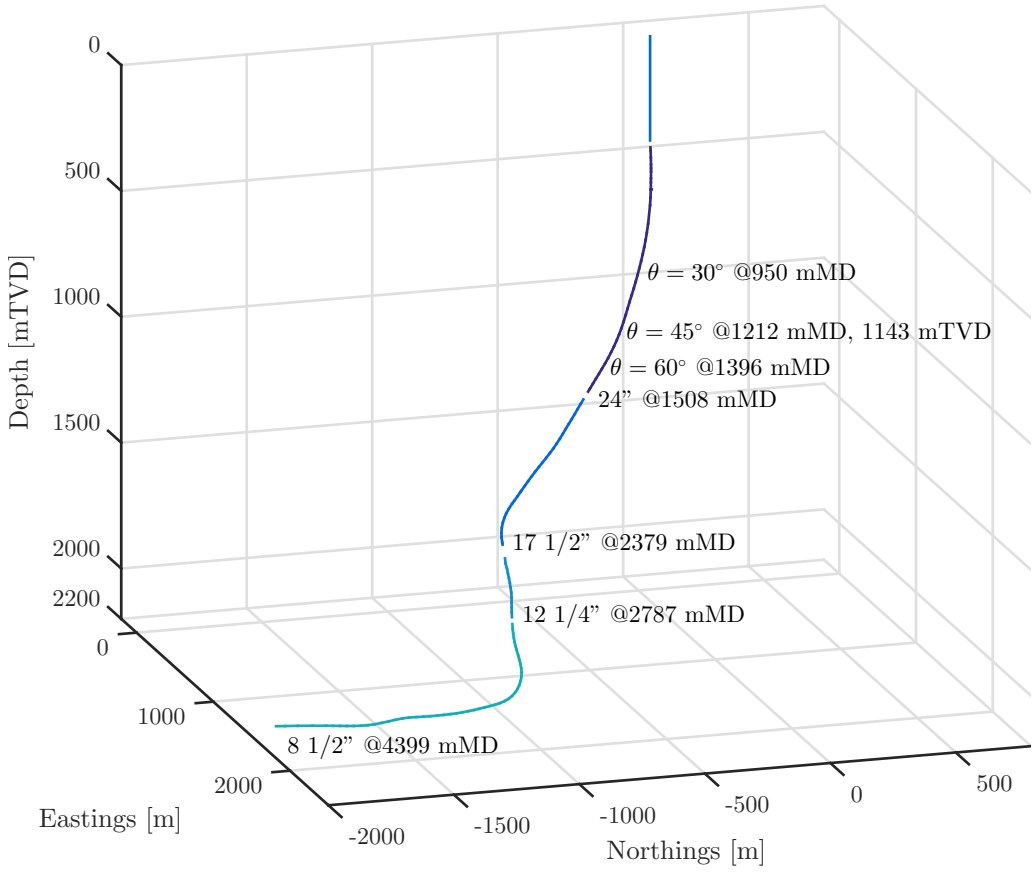

Figure D-1: Survey of well K 470

D.2 Well K 480

8½" section

Section geometry

TVD interval	2821-2895	mTVD
MD interval	5091-6203	mMD
Interval length	1112	m
Inclination start	70.4	°
Inclination end	81.9	°
Azimuth start	81.5	°
Azimuth end	351.5	°

BHA and bit

Length of BHA		
RSS	PowerDrive Xceed	
Bit	8½" PDC	

Mud

Mud weight	1570	kg/m^3
Average plastic viscosity	36.1	mPas
Average yield point	12.4	Pa
Average Power law exponent	0.68	[-]
Average konsistensy index	4.85	$lb_f s^n/100ft^2$

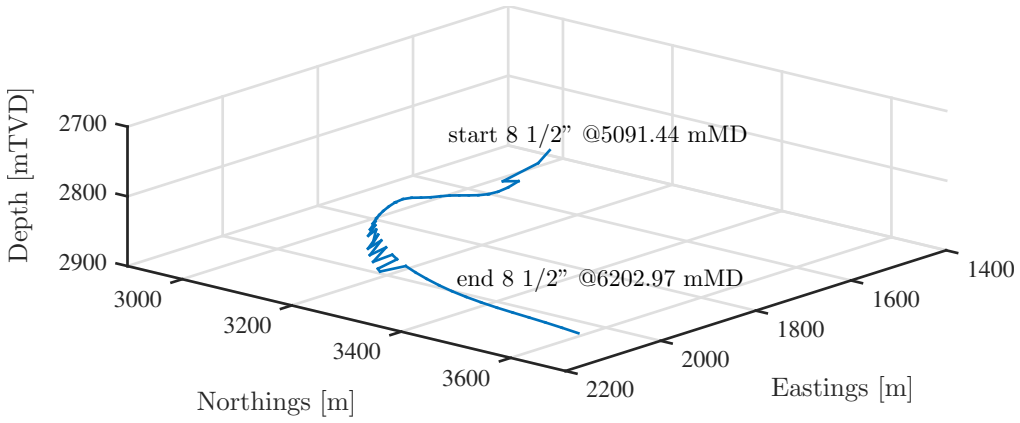

Figure D-2: Survey of well K 480

E BHA data

K 470 17 ½”

Table E-1: BHA data for K 470 17 ½”

Component	OD [in]	ID [in]	Length [m]	Acc. length [m]
BIT	17.5		0.45	0.45
POWERDRIVE	9.5		4.61	5.06
NM STRING STAB	17.375		1.82	6.88
NM FLEX WATE	6.625		2.89	9.77
POWER PULSE MWD	9.625		8.25	18.02
CDR W/APRS	9.625		7.1	25.12
NM STRING STAB	17.25	3.5	1.88	27
DRILL COLLAR, NM	9.5	3	7.95	34.95
DRILL COLLAR, NM	9.5	3	8.08	43.03
X-OVER	9.5	2.688	0.67	43.7
8” DRILL COLLAR	8	2.813	26.62	70.32
JAR	8.25	2.75	9.63	79.95
8” DRILL COLLAR	8	3	26.87	106.82
X-OVER	7.813	2.813	0.4	107.22
6 5/8” HWDP	6.625	5	84.47	191.69
DP 6 5/8”	6.625	5	10	201.69

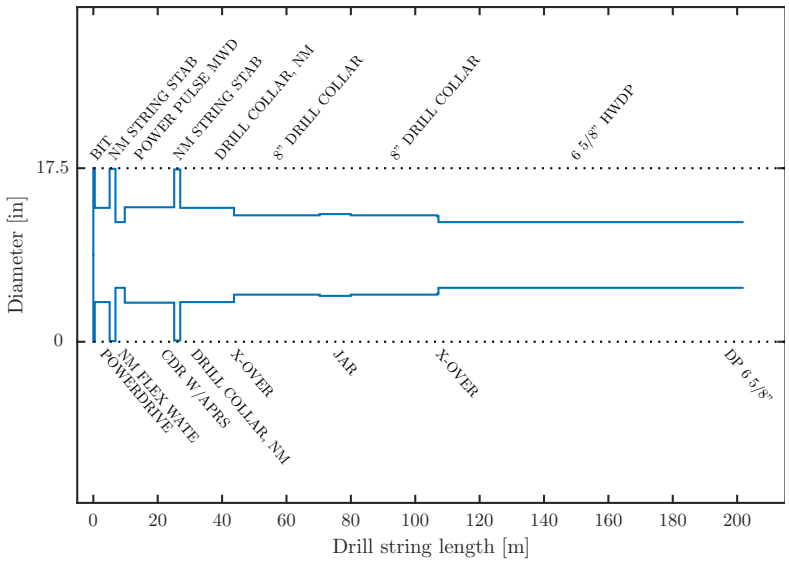

Figure E-1: Outline of the BHA in K 470 17 ½”

K 470 12 ¼”

Table E-2: BHA data for K 470 12 ¼”

Component	OD [in]	ID [in]	Length [m]	Acc Length [m]
BIT	8.5	2.25	0.24	0.24
REAMERWING	12.25	2	0.7	0.94
MUD MOTOR	8.19	0	8.28	9.22
FLOAT SUB	8.25	2.813	0.85	10.07
NM STRING STAB	10.625	2.813	2.17	12.24
VISION825	9.313	5.688	5.94	18.18
MWD	8.438	5.688	8.43	26.61
FLOAT SUB	8	2.75	1.99	28.6
NM DRILL COLLAR	7.938	2.813	24.24	52.84
JAR	7.875	3	9.55	62.39
X-OVER	7.875	3	1.2	63.59
5” HWDP	5	4	80.25	143.84
5” DP	5	4	10	153.84

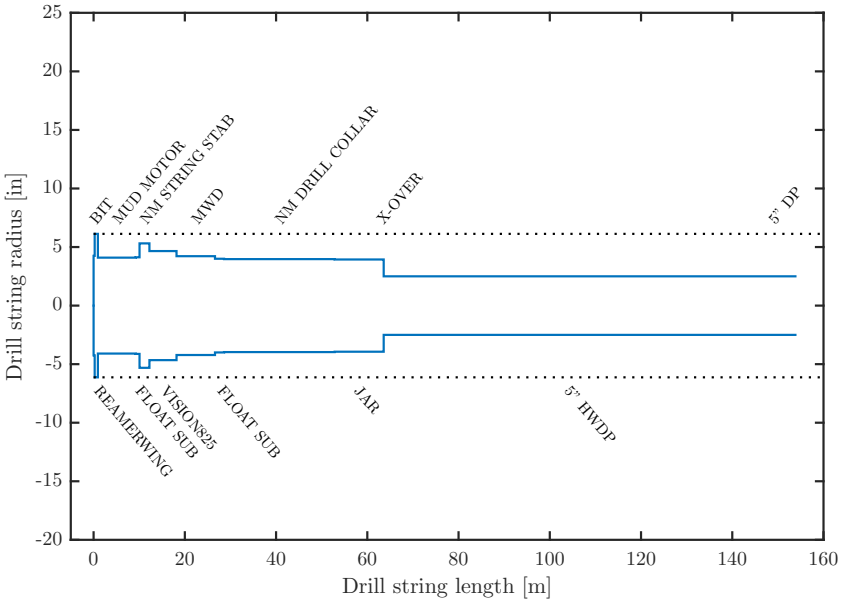

Figure E-2: Outline of the BHA in K 470 12 ¼”

K 470 8 ½”

Table E-3: BHA data for K 470 8 ½”

Component	OD [in]	ID [in]	Length [m]	Acc Length [m]
BIT, PDC	8.5	2.25	0.27	0.27
POWERDRIVE, XCEED	6.813	2.5	7.67	7.94
ARC	6.75	2.81	5.62	13.56
POWER PULSE MWD	6.75	5.11	8.36	21.92
STETHESCOPE W/8 ¼” STAB	6.75	2.25	10.13	32.05
ADN-6 W/8 ¼” STABILIZER	6.75	2.25	6.48	38.53
5” HWDP	5	3	26.77	65.3
JAR	6.44	2.75	9.69	74.99
5” HWDP	5	3	53.48	128.47
5” DP	4.93	4.28	10	138.47

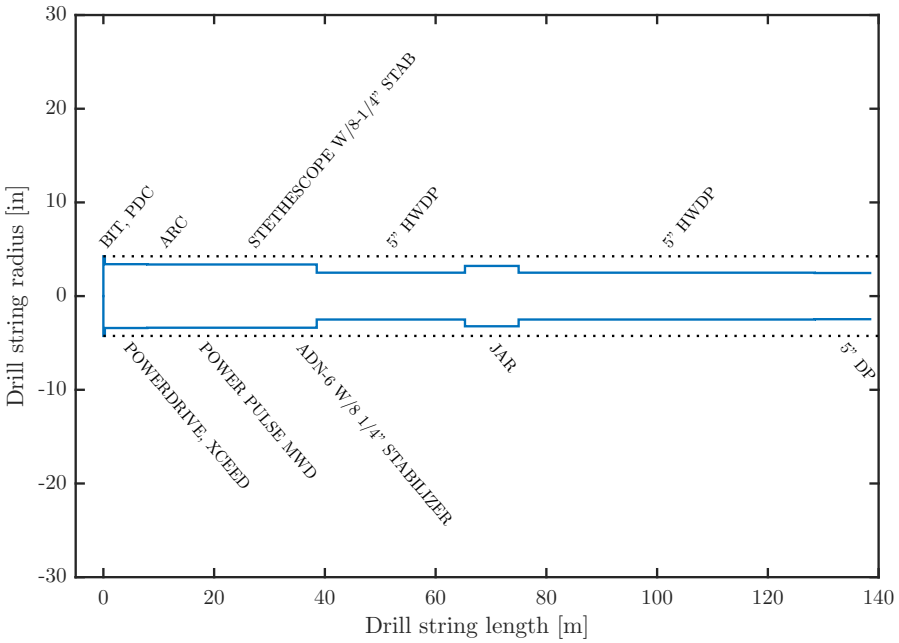

Figure E-3: Outline of the BHA in K 470 8 ½”

K 480 8 ½”

Table E-4: BHA data for K 480 8 ½”

Component	OD [in]	ID [in]	Length [m]	Acc Length [m]
BIT	8.5		0.26	0.26
POWERDRIVE XCEED	6.813		7.66	7.92
VISION675	6.875		5.7	13.62
POWER PULSE MWD	6.75		8.36	21.98
FPWD	6.75		10.2	32.18
ADN-6 W /8 1/4” STABILIZER	6.875		6.48	38.66
FLOAT SUB	6.563	2.813	1.21	39.87
NM HW DRILL PIPE	5	2.813	27.78	67.65
HYDRAULIC JAR	6.5	2.5	9.52	77.17
HWDP 5”	5	3	44.28	121.45
DRIFT SUB	6.625	2.25	1	122.45
DP 5”	5	4.275	10	132.45

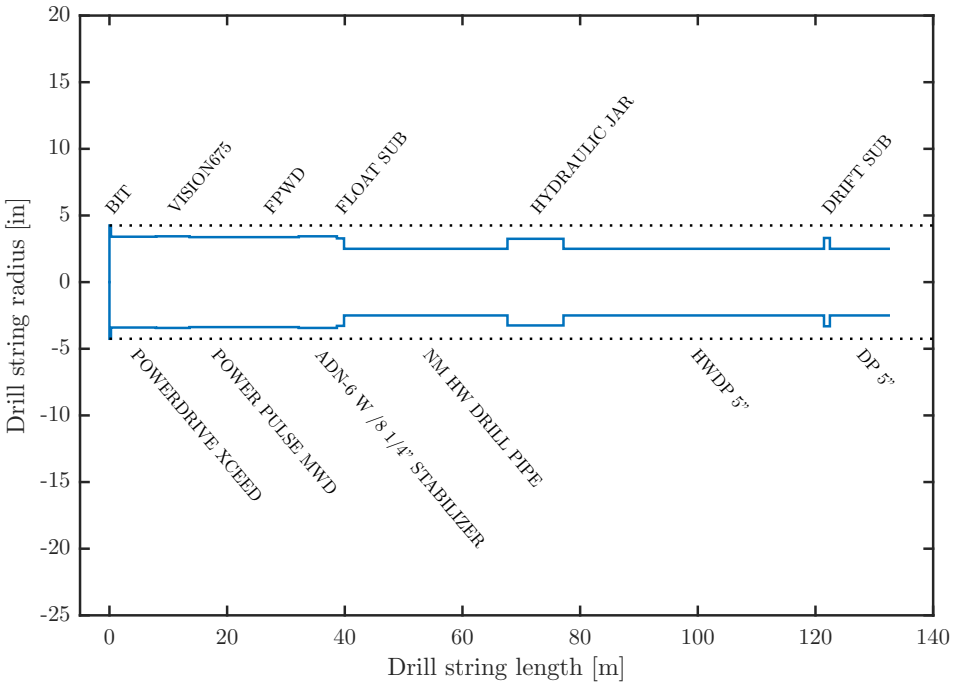

Figure E-4: Outline of the BHA in K 480 8 ½”

F Moody chart

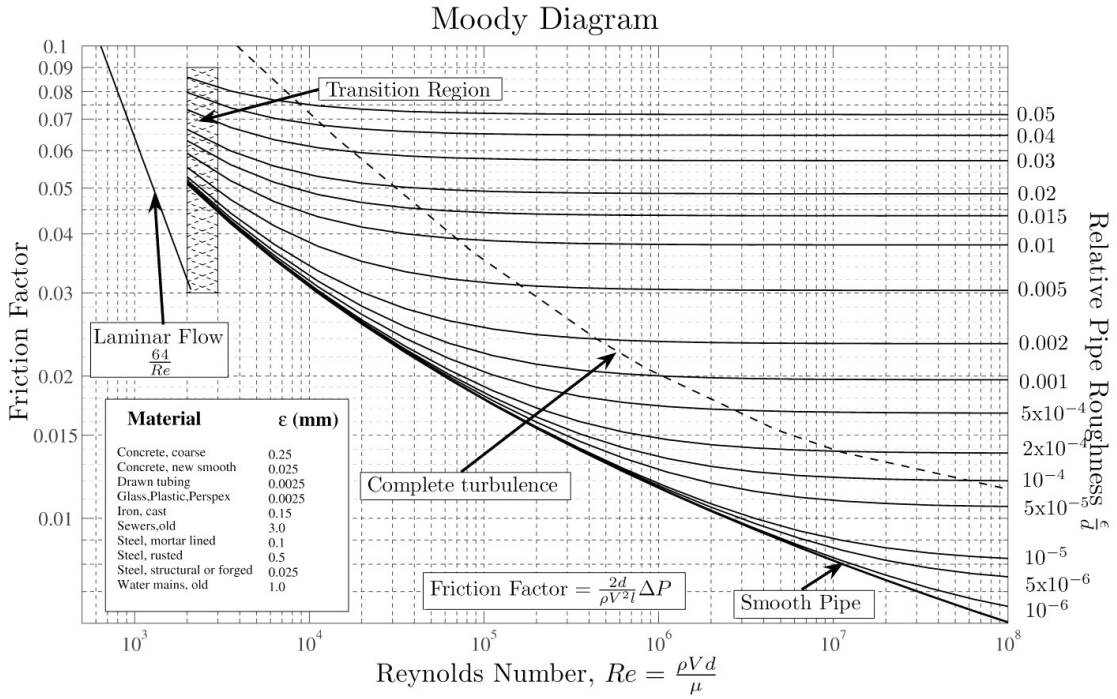

Figure F-1: Moody chart showing the relationship between the Reynolds Number, relative roughness and the Darcy-Weisbach friction factor. Courtesy of Wikipedia.org.